SAPIENZA
UNIVERSITÀ DI ROMA

Two-loop massive corrections for collider phenomenology

Department of Physics
PhD in Physics - cycle XXXVII

Federico Ripani
ID number 1869845

Advisor
Prof. Roberto Bonciani

Co-Advisor
Dr. Matteo Becchetti

Academic Year 2023/2024

Abstract

In this thesis two-loop massive corrections for two relevant processes at hadron colliders are presented.

The first part illustrates the Next-to-next-to-leading order QCD massive corrections to diphoton production at LHC. This process is an important test of the Standard Model and an interesting framework to evaluate the size of massive corrections at NNLO. All the relevant partonic subprocesses are taken into account. In particular, the two-loop amplitude in quark annihilation channel involves elliptic Master Integrals, which have been evaluated through differential equations. A semi-analytical approach to the solution, based on generalised power series expansions, has been adopted. A phenomenological study of the impact of these corrections on the invariant mass distribution is also presented.

The second part of the thesis is about the two-loop mixed QCD-Electroweak corrections to $qg \to Hq$ and its crossed channels, $\bar{q}g \to H\bar{q}$ and $q\bar{q} \to Hg$, considering the light-quark contribution and the exact dependence on the electroweak boson mass. Also for this process the relevant master integrals have been computed by means of the differential equation method, finding a solution as generalised power series expansions. Compared to the analytical formulae available in literature, our semi-analytical result allows to reduce the evaluation time of the relevant scattering amplitudes of one order of magnitude.

Contents

Chapter 1

Introduction

The Standard Model (SM) of particle physics is, so far, the most accurate model we have to describe nature, namely its building blocks and how do they interact at high-energy scales, or equivalently at short-distances. The discovery of the Higgs boson [1] in 2012 has been one of the main success of the SM. Furthermore, the SM describes with a very high accuracy a number of experimental results obtained at hadron and lepton colliders, with few exceptions, which, however, are not statistically significant. Nevertheless, experimental facts and theoretical arguments suggest that the SM is incomplete.

The requirement for fine tuning of some parameters in the strong CP and hierarchy problem is an indication that there is something we have not yet understood. The Flavour puzzle is an other longstanding unresolved problem: while the SM describes very well the generation of fermion masses and quark-mixing, it does not explain the origin of the observed hierarchy between the masses and between the mixing angles. We do not even know why there are three generations of fermions. It is not clear which is the mechanism which generates neutrino masses, which are different from zero, since neutrinos oscillate. Are strong and electroweak interactions low-energy realizations of a unified more fundamental force? Which is the UV completion of gravity? Then, there are experimental observations from the universe: Standard Model does not explain the nature of dark matter and dark energy as well as the origin of the asymmetry matter-antimatter. The list continues ... what it is certain is that hints of New Physics beyond Standard Model already exist and a better model is needed. Such a model should solve one or more of the problems aforementioned and, hopefully, predict unknown features of New Physics.

One thing that we can do is to test up to which scales the Standard Model is valid. To this aim, collider experiments are performing measurements with an unprecedented precision, and in the next years a statistic ten times greater than the current one will be achieved. To exploit such a level of precision, theoretical predictions must be carried out with the same accuracy. Increasing both theoretical and experimental precision leads to enhance the sensitivity to possible discrepancies with the Standard Model predictions, constraining models of New Physics.

A theoretical prediction, namely a cross-section computation, consists of several parts, each of them requiring a dedicated and an in-depth study. This thesis concerns mainly the

calculation of scattering amplitudes, which capture the hard dynamics part. Amplitudes are a bridge between theory and phenomenology since they embed information about the microscopic world. In the Standard Model they can be computed only through perturbation theory in the couplings and can be expressed as sums of Feynman diagrams. The theoretical uncertainty comes though from the truncation of the perturbative series and can be reduced considering more terms. Next-to-next-to leading order (NNLO) QCD corrections are now the standard along with the Next-to leading order (NLO) electroweak corrections. For some processes also the Next-to-next-to-next-to leading order (N^3LO) QCD corrections and mixed QCD-electroweak corrections are becoming relevant (see for instance [2] and ref.s therein). At higher-orders in perturbation theory amplitudes have an increasing number of legs and loops, and consequently the complexity of the calculation rapidly increases. Nowadays two-loop $2 \to 3$ processes as well as three-loop $2 \to 2$ processes are the challenge.

In scattering amplitude computations often happens that, despite highly complicated intermediate steps, the final result is simpler than one could have expected. Sometimes incredibly simple (an emblematic example is given by [3]). This has inspired the development of a number of modern techniques, such as on-shell methods, which allow to compute amplitudes, or part of them, without Lagrangian, assuming only unitarity and Lorentz invariance. So, scattering amplitudes, besides being fundamental ingredients to improve the accuracy of the theoretical predictions, turn out to represent a portal to study the role of physical principles in observable quantities.

So far, in most of the cases higher-order corrections have been computed with massless internal particles, which capture the most sizable part. However, to reach an accuracy of $\sim 1\%$, required by the experimental precision, also massive corrections have to be taken into account. Massive particles in the loops are only recently being considered at NNLO accuracy. Masses introduce more complex structures in the amplitudes, whose understanding is only just beginning. In QCD, massive corrections are mainly originated from the top quark, sometimes also corrections due to the masses of bottom and charm turn out to be appreciable (see introduction to chapter 4 for details). When electroweak corrections are considered several scales appear due to the presence of W and Z bosons. Moreover, for lepton collider processes, lepton masses, and in particular the muon mass, can be relevant.

This thesis describes the computation of two-loop massive corrections for two relevant processes at hadron colliders. In chapter 2 we review some modern techniques for the computation of Feynman integrals. In chapter 3 we present the diphoton production at NNLO with top quark mass dependence. In particular, in section 3.1 we describe the computation of the two-loop form factors for diphoton production in the $q\bar{q}$ channel, where Feynman diagrams with a loop of top quark have been considered [4]. In section 3.2 we present a phenomenological study for diphoton production at NNLO which fully takes into account the dependence on the top quark mass in all the relevant channels [5]. In chapter 4 we present the two-loop mixed QCD-Electroweak corrections to $qg \to Hq$ and its crossed channels, $\bar{q}g \to H\bar{q}$ and $q\bar{q} \to Hg$, considering the light-quark contribution and the exact dependence on the electroweak boson mass.

Chapter 2

Computational methods for Feynman integrals

Nowadays, thanks to a variety of modern techniques, tree-level and one-loop calculations can be carried out with a number of automated programs [6–9], that have strongly boosted the field of precision phenomenology. Such tools allowed us to reach NLO accuracy for highly non-trivial multi-particle processes. A similar level of automation has not yet been achieved for NNLO calculations. Despite significant progress has been made recently in computing multiloop scattering amplitudes, a tool that allows for the generation and evaluation of two-loop amplitudes is still lacking. However, a number of techniques and programs have been developed in the past few years to address different tasks in higher-loop computations. In this chapter, we describe some of these methods, emphasizing the ones used for the processes studied in this thesis.

In quantum field theory, when calculating perturbative scattering amplitudes, two distinct challenges typically arise, both of which become increasingly complex as the number of loops and legs increases. The first challenge is to express the loop integrand for the given scattering process in an appropriate form, and the second is to efficiently evaluate the resulting integrals, either through analytical or numerical methods.

For the first of the two problems, the standard approach consists in expressing the scattering amplitude in terms of Feynman diagrams and performing for each diagram a series of algebraic manipulations to separate the overall Lorentz structures (combinations of spinors and polarization vectors) from the scalar Feynman integrals. Although initially this procedure may seem straightforward, it can become highly difficult in practice for multiloop and multileg scattering amplitudes. A more efficient widely used approach for decomposing any scattering amplitude into scalar Feynman integrals is the projector method. By exploiting the symmetries of the scattering amplitudes, starting from Poincaré and gauge invariance, one can express any amplitude as a sum of Lorentz tensors, each multiplied by a scalar form factor. This decomposition is non-perturbative and, fixed the process, valid for any loop order, since it relies on symmetry arguments. From this decomposition, projector operators can be constructed, which, when applied to the scattering amplitude expressed as sum of Feynman diagrams, isolate the corresponding form factors.

The second problem we have to address is the calculation of scalar Feynman integrals. It has long been known that not all the scalar integrals contributing to a given process are independent. Indeed, they satisfy a number of identities called integration-by-parts identities (IBPs) [10, 11]. The solution of these identities, usually achieved through the Laporta's algorithm [12], lead to express every scalar integral in the amplitude as linear combination of a finite basis of integrals, which are called Master Integrals (MIs). Different processes can share a same subset of MIs. The reduction of a scattering amplitude to a linear combination of MIs is a bottleneck for some state-of-the-art computations due to the huge size of the IBPs.

The last problem that has to be addressed is the computation of the MIs, either analytically or numerically. Direct integration relies mostly on Feynman parametrization as well as Mellin-Barnes representation. Another widely used method to compute master integrals is based on differential equations [13–20], adopted also for the processes investigated in this thesis. Exploiting both the integration techniques, it has been found that a large set of MIs, contributing to phenomenologically relevant multiloop scattering amplitudes, admit an analytical expression in terms of Multiple Polylogarithms (MPLs), also called Goncharov Polylogarithms (GPLs) [21–24]. They are a class of special functions defined as iterated integrals over rational kernels, and represent a generalization of the classical Polylogarithms Li_n. MPLs form a Hopf algebra, and a systematic way to generate all possible functional identities among them is known. Codes to perform algebraic manipulations with MPLs are available [25, 26], as well as a public routine, `Ginac` [27], for their efficient numerical evaluation.

While a considerable number of multiloop amplitudes, that have been computed so far, are expressed in terms of MPLs, an increasing number of cases, especially when massive particles are considered, are known to show a more complicated mathematical structure. A first example dates back to '50s, at the beginning of QED, when the electron two-loop self-energy was found to involve elliptic integrals. Not surprisingly, also several amplitudes involving massive states, computed recently, show analytic structures characterised by the presence of elliptic functions, some of them [28, 29], included the two-loop heavy-quark contribution to diphoton production [4], studied in the next chapter of this thesis. In addition, even more complex geometries, beyond the elliptic case, have been found to appear in perturbative scattering amplitudes [30].

In recent years, a big effort has been devoted to the understanding of the analytic structure of Feynman integrals which do not admit an expression in terms of MPLs. However, in most cases, the numerical evaluation of the functions associated to such solution can be extremely challenging for phenomenological applications. Notably, there exist semi-analytical and numerical methods which allows for an efficient evaluation of Feynman integrals even in the cases where a knowledge of the class of special functions (and its properties) connected to the solution is missing. The program `pySecDec` [31], for example, combines sector decomposition, contour deformation and direct numerical Monte Carlo integration, to evaluate Feynman integrals. A different, semi-analytical method consists instead in finding the solution as generalized power series expansions around several points of the phase-space [32]. This technique relies on the differential equation system, satisfied by a basis of MIs, and has been implemented in a number of codes [33, 34].

We did not carry out a full-analytical study of the MIs contributing to the processes described in chapters 3 and 4 since our main goal is studying the phenomenological impact of the computed scattering amplitudes. Instead, we have done an extensive use of power series expansions, which, unlike other numerical techniques, allow to reach a very high number of significant digits.

This chapter is organised as follows: we describe the Integration-by-part identities in 2.1, while in 2.2 we review the differential equation method along with a discussion of the canonical basis, which particularly simplifies the differential equation system, and a description of the generalized power expansion technique.

2.1 Integration by Parts identities

Feynman integrals are in general divergent in four dimensions, so they have to be regulated, as usual we adopt dimensional regularization with $D = 4 - 2\epsilon$ the dimension of the space-time. A generic scalar Feynman integral has the following form:

$$\int \prod_{j=1}^{L} d^D k_j \, \frac{\prod_{k=1}^{P} N_k^{b_k}}{\prod_{i=1}^{E} D_i^{a_i}}, \tag{2.1}$$

where L is the number of loops, k_j are the loop momenta, E is the number of propagators and P the number of irreducible scalar products. The exponents a_i can assume any integer value, while b_i are non-negative. A generic denominator has the form $D_i = q_i^2 - m_i^2 + \mathrm{i}\varepsilon$, where q_i is the momentum flowing in the associated leg and m_i is the mass. The set of denominators $\{D_i\}$ defines the topology of the integral. Let $n-1$ be the number of independent external momenta, then the sum of the number of denominators and the number of numerators is fixed to $P + E = \frac{L(L+1)}{2} + (n-1)L$.

A certain topology contains an infinite number of integrals, obtained varying the exponents a_i and b_i. However, every integral can be expressed, exploiting integration-by-parts identities, as a linear combination of a finite basis of MIs. The IBPs are a realization of the invariance of the loop integration measure under space-time translations. All of them can be derived from a $D-$dimensional generalization of Gauss theorem:

$$\int \prod_{j=1}^{L} d^D k_j \, \frac{\partial}{\partial k_l^\mu} \left(v^\mu \frac{\prod_{k=1}^{P} N_k^{b_k}}{\prod_{i=1}^{E} D_i^{a_i}} \right) = 0, \tag{2.2}$$

where v^μ is either an external or a loop momentum. It can be easily checked that IBPs are relations between integrals of the same topology since derivatives do not introduce new denominators. We refer to a subset of integrals which have the same denominators as a sector, i.e. two integrals of a given topology belong to the same sector if and only if the positive denominator exponents a_i are the same for both integrals.

The solution to the IBPs consists of expressing every integral of a given topology as linear combination of a finite basis of Master Integrals. An algorithm to find such solution, and so determine the basis of MIs, is called Laporta's algorithm [12]. The algorithm is based on a bottom-up approach, starting from sectors with few denominators. Once the sector is given,

the algorithm consider all the integrals with fixed values of $M_d = \sum_i (a_i - 1)$ and $M_p = \sum_i b_i$. For each of these integrals the IBPs are generated, and all the integrals already known are substituted into them. If an IBP identity is independent w.r.t. all the ones considered before, it is used to reduce an integral. When all the IBPs have been analyzed, the algorithm increases M_d and M_p and generates new IBPs. Once M_d and M_p have reached predefined limits, the reduction of a new sector starts. The final result is the reduction of all the integrals, which appear in the selected IBPs, in terms of a finite basis of MIs. The choice of the MIs is arbitrary, The Laporta algorithm tends to prefer MIs with the lowest a_i, and eventually numerators if a sector has more than one master integral, although it is not the most convenient choice, especially for setting up a differential equation system.

To better illustrate the concepts introduced, we will apply them to a simple example, the massless one-loop box. The definition of the topology is:

$$I\left(a_1, a_2, a_3, a_4\right) = \int \mathcal{D}^D k \frac{1}{D_1^{a_1} D_2^{a_2} D_3^{a_3} D_4^{a_4}},$$

where the inverse propagators are defined as,

$$\begin{aligned} D_1 &= k^2, & D_2 &= \left(k - p_1\right)^2, \\ D_3 &= \left(k + p_2\right)^2, & D_4 &= \left(k - p_1 + p_3\right)^2, \end{aligned}$$

where we have dropped the $+\mathrm{i}\varepsilon$ for the sake of simplicity. The external massless particles are on-shell, $p_i^2 = 0$ and $\left(p_1 + p_2 - p_3\right)^2 = 0$, while there are two independent kinematics variables, $\left(p_1 + p_2\right)^2 = s$ and $\left(p_1 - p_3\right)^2 = t$. The exponents of the denominators a_i can be any integer numbers.
Applying (2.2) with the integrand of (2.1) and $v^\mu = \{k^\mu, \left(k - p_1\right)^\mu, \left(k + p_2\right)^\mu, \left(k - p_1 + p_3\right)^\mu\}$, the following IBPs are obtained:

$$\begin{aligned} &a_4 I\left(a_1 - 1, a_2, a_3, a_4 + 1\right) + a_3 I\left(a_1 - 1, a_2, a_3 + 1, a_4\right) + a_2 I\left(a_1 - 1, a_2 + 1, a_3, a_4\right) \\ &+ \left(2a_1 + a_2 + a_3 + a_4 - D\right) I\left(a_1, a_2, a_3, a_4\right) - a_4 t I\left(a_1, a_2, a_3, a_4 + 1\right) = 0, \end{aligned} \tag{2.3}$$

$$\begin{aligned} &a_4 I\left(a_1, a_2 - 1, a_3, a_4 + 1\right) + a_3 I\left(a_1, a_2 - 1, a_3 + 1, a_4\right) + a_1 I\left(a_1 + 1, a_2 - 1, a_3, a_4\right) \\ &+ \left(a_1 + 2a_2 + a_3 + a_4 - D\right) I\left(a_1, a_2, a_3, a_4\right) - a_3 s I\left(a_1, a_2, a_3 + 1, a_4\right) = 0, \end{aligned} \tag{2.4}$$

$$\begin{aligned} &a_4 I\left(a_1, a_2, a_3 - 1, a_4 + 1\right) + a_2 I\left(a_1, a_2 + 1, a_3 - 1, a_4\right) + a_1 I\left(a_1 + 1, a_2, a_3 - 1, a_4\right) \\ &+ \left(a_1 + a_2 + 2a_3 + a_4 - D\right) I\left(a_1, a_2, a_3, a_4\right) - a_2 s I\left(a_1, a_2 + 1, a_3, a_4\right) = 0, \end{aligned} \tag{2.5}$$

$$\begin{aligned} &a_3 I\left(a_1, a_2, a_3 + 1, a_4 - 1\right) + a_2 I\left(a_1, a_2 + 1, a_3, a_4 - 1\right) + a_1 I\left(a_1 + 1, a_2, a_3, a_4 - 1\right) \\ &+ \left(a_1 + a_2 + a_3 + 2a_4 - D\right) I\left(a_1, a_2, a_3, a_4\right) - a_1 t I\left(a_1 + 1, a_2, a_3, a_4\right) = 0. \end{aligned} \tag{2.6}$$

Let us consider the sector $I(0, 1, 1, 0)$, then equations (2.4) and (2.5), with $a_1 = a_4 = 0$

and $a_2 = a_3 = 1$, read

$$(3-D)I(0,1,1,0) - s\,I(0,1,2,0) = 0, \tag{2.7}$$
$$(3-D)I(0,1,1,0) - s\,I(0,2,1,0) = 0, \tag{2.8}$$

which allow to reduce $I(0,1,2,0)$ and $I(0,2,1,0)$ to $I(0,1,1,0)$, which can be chosen as a master integral. Indeed one can show that all the integrals of this sector can be reduced to the bubble in the $s-$channel $I(0,1,1,0)$. Similarly, the $t-$channel bubble $I(1,0,0,1)$ can be chosen as a master integral for the corresponding sector. Other bubble sectors with one on-shell leg are zero for dimensional regularization, as well as tadpoles. Let us consider now a triangle sector, for example $I(1,1,1,0)$, then equation (2.3), with $a_1 = a_2 = a_3 = 1$ and $a_4 = 0$, reads

$$I(0,1,2,0) + I(0,2,1,0) + (4-D)I(1,1,1,0) = 0, \tag{2.9}$$

which, together with (2.7) and (2.8), allows to reduce the triangle to the bubble:

$$I(1,1,1,0) = -\frac{2(3-D)}{s(4-D)} I(0,1,1,0). \tag{2.10}$$

It is not difficult to show that there are no master integrals in the triangle sectors, since they can all be reduced to one of the two bubble MIs. Finally, the box sector can be shown to have one master integral which can be chosen as $I(1,1,1,1)$. So, in this case we have three master integrals that, as usual, we organise in a vector,

$$\begin{pmatrix} I(0,1,1,0) \\ I(1,0,0,1) \\ I(1,1,1,1) \end{pmatrix}. \tag{2.11}$$

For state-of-the-art computations the scalar part of an amplitude can contain tens of thousands Feynman integrals, which are reduced to a basis of hundreds of master integrals. In these cases the analytical solution to IBPs is recovered starting from multiple numerical solutions, which are obtained by means of finite fields reconstruction technique. IBP solution methods have been implemented recently in a number of public codes [35–44]. Recently a package for the generation, inspired by algebraic geometry, of very compact sets of IBPs has been developed [45]. Reducing an amplitude to a linear combination of master integrals, with rational coefficients expressed in a suitable form for an efficient numerical evaluation, is one of the main bottlenecks for higher-order predictions for collider observables.

2.1.1 Lorentz identities

Lorentz invariance generates a set of identities between Feynman integrals, called Lorentz identities (LIs), which can be shown to be linear dependent to IBPs. However, LIs can be useful in practice to find the solution and often are added into IBP linear systems.
Let us consider an infinitesimal Lorentz transformation on the external momenta,

$$p_i^\mu \to p_i^\mu + \delta p_i^\mu = p_i^\mu + \omega^{\mu\nu} p_{i\nu}, \tag{2.12}$$

where $\omega^{\mu\nu}$ is an antisymmetric tensor. A scalar Feynman integral $I(p_i)$ is Lorentz invariant, which means

$$I(p_i) = I(p_i + \delta p_i). \tag{2.13}$$

Expanding the right-hand side of (2.13),

$$I(p_i + \delta p_i) \simeq I(p_i) + \sum_j \frac{\partial}{\partial p_j^\mu} I(p_i)\, \delta p_j^\mu, \tag{2.14}$$

and making the antisymmetry of $\omega^{\mu\nu}$ explicit, we obtain the following identity,

$$\omega^{\mu\nu} \sum_j \left(\frac{\partial}{\partial p_j^\mu} I(p_i)\, p_{j\nu} - \frac{\partial}{\partial p_j^\nu} I(p_i)\, p_{j\mu} \right) = 0. \tag{2.15}$$

We can generate LIs from the last expression by replacing the Lorentz transformation parameters $\omega^{\mu\nu}$ with antisymmetric combinations of the external momenta.
Once the integral is given, equation (2.15) can generate up to 6 identities. However, the number of independent external momenta constraints the number of antisymmetric tensors. For example, no LIs exist for the bubble, which has only one independent external momentum, while for the triangle the only choice is $\omega^{\mu\nu} = p_1^\mu p_2^\nu - p_1^\nu p_2^\mu$, and so on.

There also many symmetry relations among different sectors which simplify considerable the IBP equation system.

2.2 Differential equations

The last problem that has to be addressed is the calculation of the master integrals. To this aim the differential equation method has turned out to be very effective. Given a basis of MIs, it is possible, using IBPs, to set up a system of linear differential equations. Thus the problem of integrating over loop momenta is moved to the integration of a differential equation. In this section we will describe this method.

Scalar Feynman integrals are functions of the independent kinematic invariants and the masses of external and internal particles. If n is the number of the external particles, there are $3n - 10$ independent kinematic invariants, which can be parametrized by momentum twistor variables or, in the case of four particles, by the Mandelstam invariants s and t. To derive an integral w.r.t. the independent kinematic variables some algebraic manipulations are needed since denominators and numerators are expressed in terms of momenta.

Let us consider n external outgoing particles with momenta p_i, $i = 1, ..., n$, which satisfy momentum conservation $\sum_i p_i = 0$ and on-shell conditions $p_i^2 = 0$ (generalization to $p_i^2 = m_i^2$ is straightforward). We define the differential operator

$$\mathcal{O}_{jk} = p_j^\mu \frac{\partial}{\partial p_k^\mu}, \tag{2.16}$$

which, introducing the Mandelstam invariants $(p_i + p_j)^2 = s_{ij}$, can be expressed as

$$\mathcal{O}_{jk} = s_{ji} \frac{\partial}{\partial s_{ik}}, \tag{2.17}$$

where the sum over dummy indices is implied. We will refer to the set of the independent kinematic variables as $\{x_i\}$. The Mandelstam s_{ij} can be expressed as combinations of the x_i, then the derivative with respect to x_i can be obtained using the chain rule,

$$\frac{\partial}{\partial x_i} = \sum_{j<k} \frac{\partial s_{jk}}{\partial x_i} \frac{\partial}{\partial s_{jk}}. \tag{2.18}$$

By inverting equation (2.17), we can finally express the derivative (2.18) w.r.t. x_i in terms of momentum derivatives,

$$\frac{\partial}{\partial x_i} = \sum_{j<k} \frac{\partial s_{jk}}{\partial x_i} \left(\mathcal{G}^{-1}\right)_{jl} \mathcal{O}_{lk}, \tag{2.19}$$

where $\mathcal{G}_{ij} = s_{ij}$. In general $\mathcal{G}^{-1}$ is singular since s_{ij} are not all independent, however the combination in (2.19) is finite.

Since the differential operators (2.19) do not introduce new denominators, the derivatives of a basis of master integrals can be reduced, using IBPs, to linear combinations of the same starting MIs. Let $\vec{f}(\vec{x}, \epsilon)$ be the vector of the elements of a basis of MIs, then it satisfies the following linear systems of differential equations,

$$\partial_{x_i} \vec{f}(\vec{x}, \epsilon) = A_i(\vec{x}, \epsilon) \vec{f}(\vec{x}, \epsilon), \tag{2.20}$$

where the matrices $A_i(\vec{x}, \epsilon)$ are rational functions of ϵ and the x_i. Setting up the systems (2.20) requires the reduction of top-sector integrals with one of the denominators raised to the power of two, which normally do not appear in the amplitude. However, reducing derivatives demands the solution of a smaller set of IBPs than the one which is needed for amplitude reduction.

From Schwarz Lemma for partial derivatives, we deduce the integrability conditions for the matrices A_i,

$$\partial_{x_i} A_j - \partial_{x_j} A_i - [A_i, A_j] = 0. \tag{2.21}$$

By performing a change of basis $\vec{g}(\vec{x}, \epsilon) = T(\vec{x}, \epsilon) \vec{f}(\vec{x}, \epsilon)$ (the choice of the MIs is arbitrary), the matrices A_i change according to the following,

$$A_i \to \tilde{A}_i = T A_i T^{-1} + \left(\partial_{x_i} T\right) T^{-1}, \tag{2.22}$$

while differential equations become

$$\partial_{x_i} \vec{g}(\vec{x}, \epsilon) = \tilde{A}_i(\vec{x}, \epsilon) \vec{g}(\vec{x}, \epsilon). \tag{2.23}$$

Defining $dA = \sum_i A_i dx_i$, we can write (2.20) in a more compact form,

$$d\vec{f} = dA \vec{f}, \tag{2.24}$$

where $d\vec{f} = \sum_i \partial_{x_i} \vec{f} dx_i$ is the usual notation for the differential of a multivariate function.

We will explicitly derive the differential equation system for the MIs of the one-loop massless box. We have two independent kinematic invariants s and t, however we can derive and solve differential equations with respect to the ratio $x = \frac{t}{s}$ and reconstruct the dependence on s through dimensional analysis. This can be achieved in practise by making the substitutions $s \to 1$ and $t \to x$. The derivative with respect to x can be written as a linear combination of derivatives with respect to the Mandelstam invariants,

$$\frac{d}{dx} = \frac{\partial}{\partial s_{13}} - \frac{\partial}{\partial s_{23}}, \tag{2.25}$$

where we used the notation $s_{12} = (p_1+p_2)^2$, $s_{13} = (p_1-p_3)^2$, $s_{23} = (p_2-p_3)^2$ and the fact that, after the substitutions, $s_{12} = 1$, $s_{13} = x$, $s_{23} = -1-x$. Applying (2.17) with $j = k = 1, 2, 3$, we obtain the rules,

$$p_3 \cdot \frac{\partial}{\partial p_3} = x \frac{\partial}{\partial s_{13}} - (1+x) \frac{\partial}{\partial s_{23}}, \tag{2.26}$$

$$p_2 \cdot \frac{\partial}{\partial p_2} = \frac{\partial}{\partial s_{12}} - (1+x) \frac{\partial}{\partial s_{23}}, \tag{2.27}$$

$$p_1 \cdot \frac{\partial}{\partial p_1} = \frac{\partial}{\partial s_{12}} + x \frac{\partial}{\partial s_{13}}, \tag{2.28}$$

which allow us to reduce the differential operator with respect to x in terms of momentum derivatives,

$$\frac{d}{dx} = \frac{1}{2}\left[\left(\frac{1}{x} + \frac{1}{1+x}\right) p_3 \cdot \frac{\partial}{\partial p_3} + \left(\frac{1}{x} - \frac{1}{1+x}\right)\left(p_1 \cdot \frac{\partial}{\partial p_1} - p_2 \cdot \frac{\partial}{\partial p_2}\right)\right]. \tag{2.29}$$

Using the IBPs (2.3–2.6) with the substitutions $s \to 1$ and $t \to x$, it is possible to express the derivatives of the MIs in closed form:

$$\frac{d}{dx}\vec{g}(x,\epsilon) = A(x,\epsilon)\vec{g}(x,\epsilon) \qquad A(x,\epsilon) = \begin{pmatrix} 0 & 0 & 0 \\ 0 & -\frac{\epsilon}{x} & 0 \\ \frac{2(2\epsilon-1)}{x(1+x)} & \frac{2(1-2\epsilon)}{x^2(1+x)} & -\frac{1+x+\epsilon}{x(1+x)} \end{pmatrix}, \tag{2.30}$$

where $\vec{g}(x,\epsilon)$ is the vector of MIs (2.11).

2.2.1 Canonical basis

Differential equations (2.20) can simplify considerably when a good choice of basis is made. To this aim, in [46] the concept of canonical basis was introduced. A set of master integrals f_i is in canonical form if: *i*) the integration of the corresponding system of differential equations is given directly by iterated integrals in the ϵ expansion; *ii*) f_i have uniform transcendentality according to the definition given in [46]. More concretely, a basis of master integrals f_i is a canonical basis if it satisfies the following two conditions:

- the ϵ dependence of the differential equation matrix factorizes as,

$$d\vec{f}(x,\epsilon) = \epsilon d\tilde{A}(x)\vec{f}(x,\epsilon); \tag{2.31}$$

- the matrix $d\tilde{A}(x)$ is a dlog form:

$$d\tilde{A}_{ij}(x) = \sum_k c_{kij} d\log\left(l_k(x)\right) \quad c_{kij} \in \mathbb{Q}, \tag{2.32}$$

  where c_{kij} are rational numbers and $l_k(x)$ are the letters of the solution and are algebraic functions of the kinematics variables.

As far as the initial conditions are known, the solution to (2.31) is immediately reached in terms of Chen's iterated integrals [47],

$$\vec{f}(x,\epsilon) = \mathbb{P}\left[\exp\left(\epsilon \int_\gamma d\tilde{A}(x)\right)\right] \vec{f}(x_0,\epsilon)\,, \tag{2.33}$$

where γ is a path in the space of the kinematics variables which connects the initial point x_0 with the end point x. The canonical master integrals f_i are normalized so that they have a Taylor expansion in the regulator parameter,

$$\vec{f}(\vec{x},\epsilon) = \sum_{k=0}^{\infty} \epsilon^k \vec{f}^{(k)}(\vec{x}). \tag{2.34}$$

The first condition (2.31) is essential for a simple perturbative solution in ϵ. The equation (2.32) is a sufficient, not necessary, condition for the integral basis f_i to be uniform transcendental. All the integrals that can be expressed in terms of GPLs admit a dlog form, however the contrary is not true, in [48] an example of a double integral of dlog forms which is not polylogarithmic is shown. In the elliptic case, while a procedure to cast the system in $\epsilon-$factorised form has been provided by [49], it is not clear in a complete general case what should be a uniform transcendental form equivalent to Eq. (2.32).

A number of techniques have been developed to find the canonical basis for a basis of master integrals [50]. For the processes studied in this thesis we used a semi-algorithmic top-bottom approach proposed in [51] and structured in the following steps:

- The first step consists of searching for the precanonical basis, which proceeds by trial and constitutes the non-algorithmic part of the method.
  Let us consider master integrals of a given sector. Since we adopt a top-bottom approach, we assume that the canonical MIs $f_a(x,\epsilon)$ for the subsectors have already been found. Differential equations read,

$$dT_i = dH_{ij} T_j + dS_{ia} f_a \tag{2.35}$$

  where we reserve the indices $i, j, k, ...$ for the sector considered, while the indices $a, b, c, ...$ are used for the subsectors. T_i are precanonical if the matrix of the corresponding homogeneous system depends linearly on ϵ and decouple as soon as $\epsilon = 0$,

$$dH = dH_0(x) + \epsilon dH_1(x), \tag{2.36}$$

  where dH_0 is triangular up to a reordering of the T_i.

- The second step is about finding the canonical form of the homogeneous part of (2.35).

The following change of basis is considered,

$$g_i = h_{0ij}(x) T_j, \tag{2.37}$$

where $h_0(x)$ is an invertible solution of the equation,

$$dh_0 + h_0 dH_0 = 0. \tag{2.38}$$

Differential equations in the new basis $\{g_i\}$ are:

$$dg_i = d\tilde{S}_{ia} f_a + \epsilon d\tilde{H}_{1ij} g_j, \tag{2.39}$$

where $d\tilde{S}_{ia} = h_{0ik} dS_{ka}$ and $d\tilde{H}_1 = h_0 dH_1 h_0^{-1}$.

- The third and final step consists of rotating to the canonical form the inhomogeneous terms. In most cases[1], it happens that $d\tilde{S}$ has only simple poles in ϵ,

$$d\tilde{S} = d\tilde{S}_0 + \sum_\alpha \frac{d\tilde{S}_\alpha}{(\epsilon - r_\alpha)}, \tag{2.40}$$

where r_α are rational numbers. The canonical basis is constructed through the following Ansatz,

$$f_i = g_i + \left(\Omega_0 + \sum_\alpha \frac{\Omega_\alpha}{(\epsilon - r_\alpha)} \right)_{ib} f_b, \tag{2.41}$$

where Ω_0 and Ω_α have to be determined. Writing differential equations for f_i and imposing that only the term proportional to ϵ survives, one obtains the conditions which fix the Ωs,

$$d\tilde{S} - r_\alpha d\tilde{H}_1 \Omega_\alpha + d\Omega_\alpha + r_\alpha \Omega_\alpha dG = 0, \tag{2.42}$$

$$d\tilde{S}_0 - d\tilde{H}_1 \sum_\alpha \Omega_\alpha + d\Omega_0 + \sum_\alpha \Omega_\alpha dG = 0, \tag{2.43}$$

where we used $df_a = \epsilon dG_{ab} f_b$. Finally, the canonical differential system reads

$$df_i = \epsilon d\tilde{H}_{1ij} f_j + \epsilon \left(\Omega_0 dG - d\tilde{H}_1 \Omega_0 \right)_{ia} f_a. \tag{2.44}$$

As prove of concept we describe the canonical basis of the one-loop massless box topology, starting from the system of differential equations (2.30). We choose the following basis for the three master integrals:

$$f_1 = \epsilon(1 - 2\epsilon) g_1 \tag{2.45}$$

$$f_2 = \epsilon(1 - 2\epsilon) g_2 \tag{2.46}$$

$$f_3 = \epsilon^2 x g_3, \tag{2.47}$$

where g_i are given in (2.11). The normalization was chosen such that all f_i admit a Taylor

[1] We stress that we are not describing a complete general algorithm but rather an empiric method which works for several phenomenologically relevant cases.

expansion in ϵ. This basis satisfies the system of differential equations,

$$d\vec{f}(x,\epsilon) = \epsilon d\tilde{A}(x)\vec{f}(x,\epsilon), \tag{2.48}$$

with

$$d\tilde{A}(x) = \begin{pmatrix} 0 & 0 & 0 \\ 0 & -1 & 0 \\ 0 & 2 & -1 \end{pmatrix} d\log(x) + \begin{pmatrix} 0 & 0 & 0 \\ 0 & 0 & 0 \\ -2 & -2 & 1 \end{pmatrix} d\log(1+x). \tag{2.49}$$

The result at any order in ϵ can be written as a linear combination of harmonic polylogarithms [52] of argument x, with indices in the set $\{0,-1\}$. In particular, the symbol alphabet in this case is $\{x, 1+x\}$. The last information we need to completely determine the solution are the boundary conditions. The bubble integrals f_1 and f_2 are known in closed form:

$$f_1 = \frac{\Gamma^2(1-\epsilon)}{\Gamma(1-2\epsilon)}(-s)^{-\epsilon} \tag{2.50}$$

$$f_2 = \frac{\Gamma^2(1-\epsilon)}{\Gamma(1-2\epsilon)}(-s)^{-\epsilon}x^{-\epsilon}, \tag{2.51}$$

where we reconstructed the dependence on s by dimensional analysis and used the integration measure:

$$\mathcal{D}^D k = \frac{d^D k}{i\pi^{\frac{D}{2}}\Gamma(1+\epsilon)}. \tag{2.52}$$

Furthermore, the requirement that the planar integrals be finite at $x=-1$ (which corresponds to $u=0$) turns out to fix the boundary for f_3:

$$f_3(-1) = 2\frac{\Gamma^2(1-\epsilon)}{\Gamma(1-2\epsilon)}(-s)^{-\epsilon-2}(1+e^{-i\pi\epsilon}). \tag{2.53}$$

This completely solves this family of Feynman integrals, to all orders in ϵ. For example f_3 up to ϵ^4 reads

$$\begin{aligned} f_3 = 2\frac{\Gamma^2(1-\epsilon)}{\Gamma(1-2\epsilon)}(-s)^{-\epsilon-2}\Bigg\{ & 2 - \epsilon G(0,x) - \frac{\pi^2}{2}\epsilon^2 + \\ & \epsilon^3\left[-\frac{1}{2}\pi^2 G(-1,x) + \frac{1}{2}\pi^2 G(0,x) - G(-1,0,0,x) + G(0,0,0,x) - \zeta(3)\right] + \\ & \epsilon^4\Bigg[-\zeta(3)G(-1,x) + \zeta(3)G(0,x) - \frac{1}{2}\pi^2 G(-1,-1,x) + \frac{1}{2}\pi^2 G(-1,0,x) + \\ & \frac{1}{2}\pi^2 G(0,-1,x) - \frac{1}{2}\pi^2 G(0,0,x) - G(-1,-1,0,0,x) + 2G(-1,0,0,0,x) + \\ & G(0,-1,0,0,x) - 2G(0,0,0,0,x) - \frac{\pi^4}{30}\Bigg]\Bigg\}, \end{aligned} \tag{2.54}$$

where G are multiple polylogarithms [21–24], defined as,

$$G(a_1,a_2,...,a_n;z) = \int_0^z \frac{dt}{t-a_1}G(a_2,...,a_n;t) \qquad G(;z) = 1 \tag{2.55}$$

$$G(\underbrace{0,...,0}_{n};z) = \frac{1}{n!}\log^n z, \tag{2.56}$$

where a_i are complex numbers and are called weights. Multiple polylogarithms with weights only in the set $\{0,1,-1\}$ are called harmonic polylogarithms (HPL or H), as the ones in Eq. (2.54). We see that all the basis elements f_i have uniform degree of transcendentality, to all orders in ϵ.

2.2.2 Generalized power series expansions

While massless corrections can be usually expressed in terms of GPLs, higher-order massive corrections have in general a more complicated mathematical structure. This is for instance the case of the two MIs of the equal-mass two-loop sunrise. The related system of first-order linear differential equations cannot be decoupled and it admits solutions in terms of complete elliptic integrals of the first and second kind. Despite a lot of progress being made in understanding classes of special functions beyond GPLs, such as iterated integrals over elliptic kernels, we still do not have a sufficient analytic control required for their efficient numerical evaluation, with the exception of a small number of cases.

In this contest, the generalized power series expansion method allows to efficiently evaluate Feynman integrals without knowing the analytical solution. The method consists in finding series solutions for Feynman integrals starting from their systems of differential equations. The advantage is that series representation is already suitable for an efficient numerical evaluation inside the radius of convergence.

In order to clearly describe the method we apply it to find series solutions to the two MIs of the equal-mass two-loop sunrise. The system of first-order linear differential equations that involves the two coupled MIs $\mathcal{F}_1$ and $\mathcal{F}_2$ at $\mathcal{O}(\epsilon^0)$ is

$$\frac{d\mathcal{F}_1}{dx} = \frac{1}{x}\mathcal{F}_1 - \frac{3}{x}\mathcal{F}_2 - \frac{9}{x} \tag{2.57}$$

$$\frac{d\mathcal{F}_2}{dx} = \frac{2(x+3)}{(x+9)(x+1)x}\mathcal{F}_1 - \frac{10x+18}{(x+9)(x+1)x}\mathcal{F}_2 - \frac{x^2+31x+108}{2(x+9)(x+1)x}, \tag{2.58}$$

where $x = -\frac{p^2}{m^2}$ with p the momentum injected in the diagram and m the internal mass. This system corresponds to a single second-order linear differential equation for one of the two MIs involved. In the case of $\mathcal{F}_1$ we find

$$\frac{d^2\mathcal{F}_1}{dx^2} + p(x)\frac{d\mathcal{F}_1}{dx} + q(x)\mathcal{F}_1 = \Omega(x), \tag{2.59}$$

with

$$p(x) = \frac{10x+18}{x(x+9)(x+1)} \tag{2.60}$$

$$q(x) = -\frac{4}{x(x+9)(x+1)} \tag{2.61}$$

$$\Omega(x) = -\frac{2x^2+13x+141}{4x(x+1)(x+9)}. \tag{2.62}$$

The method consists in finding multiple series solutions to (2.59) around a set of points which allow us to cover the phase-space region we want to have access. The starting observation is that Feynman integrals satisfy Fuchsian differential equations. Given a general linear differential equation of the $p-$th order of the form of (2.59),

$$\frac{d^p\mathcal{F}}{dx^p} + \sum_{l=1}^{p} q_l(x) \frac{d^{p-l}\mathcal{F}}{dx^{p-l}} = 0, \tag{2.63}$$

and being x_0 a singular point for a subset of the coefficients $q_l(x)$, (2.63) is Fuchsian if and only if $(x - x_0)^l q_l(x)$ is analytical in x_0 with $l = 1, ..., p$. This condition ensures that every singular point for the differential equation is either a regular point or a regular singular point for the solution. Consequently the solution to (2.63) can be expressed, in the vicinity of x_0, as a generalized power series with terms of the form,

$$(x - x_0)^{w+m} \log^n(x - x_0), \tag{2.64}$$

where m and n are positive integer numbers, and w is in general a rational number either positive or negative. Not all the linear differential equations are Fuchsian, indeed if we consider the following,

$$\frac{df}{dx} + f = 0, \tag{2.65}$$

it cannot be associated to any Feynman integral since the singular point $x = \infty$ does not satisfy the Fuchsian condition. To confirm this, we observe that the solution e^{-x} has en essential singular point at $x = \infty$ and does not admit an expansion with terms of the form of (2.64).

Going back to the sunrise example, we start to find the solution around $x = 0$. We first consider the corresponding homogeneous equation of (2.59). Since $x = 0$ is a singular regular point, we make an Ansatz for the solution of the form:

$$\mathcal{F}_1^{(0)} = x^\alpha \sum_{n=0}^{\infty} a_n x^n, \tag{2.66}$$

where a_n are numerical coefficients determined from the differential equation and from the boundary conditions. Substituting the solution (2.66) in the homogeneous version of (2.59) and picking the first term of the expansion, we obtain the indicial equation for the determination of α:

$$\alpha(\alpha + 1) = 0, \tag{2.67}$$

with two solutions $\alpha = 0$ and $\alpha = -1$. Since the MIs must be regular at $x = 0$, we keep only the solution with $\alpha = 0$. Therefore, the general solution of the homogeneous differential equation is

$$\mathcal{F}_1^{(0)} = \sum_{n=0}^{\infty} a_n x^n, \tag{2.68}$$

which converges in a circle of radius r = 9, i.e. up to the nearest singular point. Considering the following terms in the expansion of the homogeneous differential equation, we can fix all the coefficients of the series in terms of the first one, a_0.

We now look for a particular solution of Eq. (2.59) in $x = 0$ of the form:

$$\tilde{\mathcal{F}}_1 = \sum_{n=0}^{\infty} p_n x^n. \tag{2.69}$$

Substituting eq. (2.69) in the second-order differential equation expanded around $x = 0$ we obtain, as in the case of the general solution of the homogeneous equation, terms p_n that depend on p_0. However, in this case we can choose to set $p_0 = 0$. The general solution of the complete equation is therefore:

$$\mathcal{F}_1 = \sum_{n=0}^{\infty} c_n x^n, \tag{2.70}$$

where $c_n = a_n + p_n$. The first few coefficients are:

$$c_0 = a_0 \tag{2.71}$$

$$c_1 = \frac{2}{9}a_0 - \frac{47}{24} \tag{2.72}$$

$$c_2 = \frac{17}{108} - \frac{2}{81}a_0 \tag{2.73}$$

$$c_3 = \frac{2}{243}a_0 - \frac{37}{648}. \tag{2.74}$$

Matching with boundary conditions, the coefficient a_0 is found to be:

$$a_0 = \frac{21}{2} - 3\sqrt{3}\left(\frac{\mathrm{Li}_2(l_+) - \mathrm{Li}_2(l_-)}{2i}\right), \qquad l_\pm = \frac{-1 \pm i\sqrt{3}}{2}. \tag{2.75}$$

In order to cover the whole physical region we have to expand around singular branch points[2]. In the sunrise example the branch point is $x = -9$, which corresponds to the three particle production threshold. From unitarity we expect the solution to develop a branch cut for $x < -9$. The Ansatz for the solution around $x = -9$ is:

$$\mathcal{F}_1^{(0)} = (x+9)^\alpha \sum_{n=0}^{\infty} a_n (x+9)^n, \tag{2.76}$$

which, substituted in the homogeneous second-order differential equation, leads to the indicial equation,

$$\alpha(\alpha - 2) = 0. \tag{2.77}$$

For the sake of simplicity the numerical coefficients have the same symbols of the ones in the series solution around $x = 0$, even though they are different. The solutions of (2.77) constraint the general homogeneous solution, which reads[3]:

$$\mathcal{F}_1^{(0)} = \sum_{n=0}^{\infty} a_n (x+9)^n + \log(x+9) \sum_{n=2}^{\infty} b_n (x+9)^n. \tag{2.78}$$

[2] An alternative would be expanding around complex values of the kinematics variables as implemented in the program `SeaSyde` [34].

[3] See [32] for a detailed discussion on how to build the homogeneous solution starting from roots of the indicial polynomial.

We can fix all the coefficients of the series in terms of the two coefficients a_0 and a_2. We look for the particular solution of Eq. (2.59) around $x = -9$ of the same form of the homogeneous one, with the difference that we can now set to zero the two free constants. The general solution of (2.59) is therefore:

$$\mathcal{F}_1 = \sum_{n=0}^{\infty} c_n (x+9)^n + \log(x+9) \sum_{n=2}^{\infty} d_n (x+9)^n, \tag{2.79}$$

where the first few coefficients are:

$$c_0 = a_0 \tag{2.80}$$

$$c_1 = \frac{31}{48} - \frac{1}{18} a_0 \tag{2.81}$$

$$c_2 = a_2 \qquad\qquad d_2 = \frac{1}{432} a_0 + \frac{5}{384} \tag{2.82}$$

$$c_3 = \frac{17}{93312} a_0 + \frac{1}{12} a_2 - \frac{107}{82944} \qquad d_3 = \frac{1}{5184} a_0 + \frac{5}{4608}. \tag{2.83}$$

The coefficients a_0 and a_2 are determined by matching with the solution around $x = 0$. The matching is performed by imposing that the two solutions, centered at $x = 0$ and $x = -9$, assume the same value in the region where both series converge. In practice one can choose an intermediate point, such as $x = -4.5$, and match the solutions for both the MIs. The solution for $\mathcal{F}_2$ can be obtained from the solution for $\mathcal{F}_1$ and Eq. (2.57).

To evaluate the solution (2.79) on its branch-cut we use the Feynman prescription, which attributes to x a small negative imaginary part. Consequently the logarithm, for $x < -9$, has the following analytic continuation:

$$\log(x+9) \to \log(s-9) - i\pi, \tag{2.84}$$

where $s = -x$. One can continue this procedure, for example expanding around the point $x = \infty$ and matching with the solution in $x = -9$. To reach the wanted number of significant digits one has to find the right compromise between the number of expansions and the number of terms in the series used for the numerical matching, considering that lowering one of them means increasing the other.

For multi-scale problems, for which there is a set of kinematics invariants $\{s_i\}$, one usually defines a path $\gamma(x) = (\gamma_{s_1}(x), \gamma_{s_2}(x), ...)$, where x is the line parameter. The differential equation along the path is:

$$\frac{d}{dx}\vec{f}(x,\epsilon) = A_x(x,\epsilon)\vec{f}(x,\epsilon) \qquad A_x(x,\epsilon) = \sum_i \frac{d\gamma_i(x)}{dx} A_{s_i}(\gamma(x),\epsilon). \tag{2.85}$$

In the series expansion method, one considers multiple one-dimensional series solutions to (2.85). A solution centered in a branch point or singularity (x_0) has the following general form:

$$f_j^{(i)}(x) = \sum_{w \in W} \sum_{l=0}^{N_{i,j}} \sum_{k=k_0}^{\infty} c_{ijkl;w} (x - x_0)^{w+k} \log^l(x - x_0), \tag{2.86}$$

where $f_j^{(i)}$ is the coefficient of ϵ^i of the $j-$th master integral, and W is a finite set of algebraic numbers, in almost all the applications $W = \{0, \frac{1}{2}\}$. A detailed description on how to determine (2.86) starting from the differential equation system in a complete general case can be found in [32, 33]. The analytic continuation of (2.86) can be performed by assigning an imaginary part to the line parameter, in accordance with the Feynman prescription.

The method has been implemented in a number of codes [33, 34, 53], and succesfully applied in several phenomenological applications [5, 54–56].

Chapter 3

Heavy quark contribution to diphoton production at hadron colliders

The production of photon pairs (diphotons) at the Large Hadron Collider (LHC) is a very relevant process for phenomenological studies in the context of the Standard Model (SM) [57–60] and in the search for new physics [61–66]. In particular, diphoton final states are highly relevant for Higgs boson studies [67–74] (and played a crucial role in its discovery [75,76]), as they constitute an irreducible background for a Higgs boson decaying into two photons.

Due to its physical relevance, the study of diphoton production requires dedicated and accurate theoretical calculations, in particular including QCD radiative corrections at high perturbative orders. The state of the art for diphoton production is represented by the *next-to-next-to-leading order* (NNLO) accuracy (taking into account five light quark flavours) [77–80] in perturbative QCD. Massless NNLO corrections enhance the NLO prediction for the invariant mass spectrum of $\sim 40\%$ for $m_{\gamma\gamma} > 50\,\text{GeV}$, turning out to be important. The relevant scattering amplitudes in the completely massless case have been known in the literature for some time [81–91].

More recently, scattering amplitudes belonging to higher orders in the strong coupling α_s (i.e. beyond the NNLO) have become available (in the massless case): the three-loop matrix element [92]; the two-loop scattering amplitudes for a photon pair in association with one jet in the leading colour approximation [93–95], and, very recently, the full colour case [96,97]. The two-loop scattering amplitudes for diphoton production in gluon fusion [98] together with the recent computation of diphoton production in association with one jet [97,99] at NNLO emphasise that all the building blocks are in place for the *next-to-next-to-next-to-leading order* (N^3LO) *massless* calculation. However, the implementation of slicing subtraction methods to reach the N^3LO accuracy could be challenging in this case, due to the presence of a high number of particles in the final state and the use of a photon isolation prescription. More clearly, the NNLO calculation of the diphoton cross section in association with one jet at small diphoton transverse momentum could be very CPU demanding. First-order electroweak/QED corrections are also known [100,101].

Regarding the diphoton background in Higgs boson production, it is possible to constrain the Higgs boson width from interference effects of the continuum $gg \to \gamma\gamma$ spectrum with the signal $gg \to H \to \gamma\gamma$. The phenomenology behind this process has therefore been studied in detail in the literature, with effective calculations at NLO (and beyond) [83, 102–109].

The small transverse momentum region of the diphoton pair is also of interest in SM and Higgs boson studies, in the determination of the Higgs boson width, etc. The transverse momentum (q_T) resummation for diphoton production is known at next-to-next-to-leading logarithmic accuracy (NNLL) [110] and at N^{3}LL [111] in association with fixed-order NNLO results.

The possibility of measuring the top quark mass has been pointed out in the literature [112, 113], if massive scattering amplitudes in diphoton production are taken into account (via loop corrections). These threshold effects of top quark pair production are manifested in the diphoton-invariant mass spectrum around two times the value of the top quark mass.

In the massive case, the first non-trivial corrections appear at the NNLO, through the inclusion of top quark loops and top quark radiation[1]. The mass effects of the so-called *box* contribution ($gg \to \gamma\gamma$) were discussed in ref. [78] (together with partial N^{3}LO contributions). Due to the large gluon luminosity at the LHC, the size of the box contribution is of the order of the Born subprocess $q\bar{q} \to \gamma\gamma$. It is therefore of interest to calculate the corrections of the following perturbative order to gluon fusion channel (formally N^{3}LO contributions). Regarding the gluon fusion channel only, the simplest approach (which captures very sizable components) is to consider the NLO QCD corrections to the box contribution. In this context, two recent papers have shown the impact of massive NLO QCD corrections on the gluon fusion channel [114, 115]. In the gluon channel the effective NLO top-quark correction turned out to enhance the effective NLO massless prediction of $\sim 7\%$ for $m_{\gamma\gamma} > 400\,\text{GeV}$.

Considering the full NNLO accuracy, with the top-quark mass dependence, there are still three missing ingredients that were not available or not presented together in previous phenomenological studies in the literature: i) the massive one-loop real-virtual contribution ($q\bar{q} \to \gamma\gamma g$ and $q(\bar{q})g \to \gamma\gamma q(\bar{q})$), the double real radiation of top quarks ($q\bar{q} \to \gamma\gamma t\bar{t}$ and $gg \to \gamma\gamma t\bar{t}$) and the two-loop virtual corrections to the Born sub-process $q\bar{q} \to \gamma\gamma$.

In section 3.1 we report on the computation of the two-loop amplitude for diphoton production in the quark annihilation channel, where the full dependence on the heavy quark mass, which appear in the loops, is retained. This is the last missing ingredient needed to a full phenomenological study of diphoton up to NNLO in QCD. This work is presented also in [4].

In section 3.2 we consider a phenomenological study of diphoton production at NNLO, taking into account the full top quark mass dependence. This work has been presented for the first time in [116]. We include all NNLO massive scattering amplitudes: i) the box contribution in the gluon fusion channel [78], ii) the two-loop scattering amplitude $q\bar{q} \to \gamma\gamma$ presented in section 3.1, and the real radiation contributions (double real and real-virtual).

[1]The inclusion of the massive b-quark contribution it is also possible in this context but it is often not considered in the literature.

3.1 Two-loop heavy quark QCD corrections to $q\bar{q} \to \gamma\gamma$

To perform the computation described in this section we employed a number of techniques for scattering amplitude calculations. We considered the partonic process $q\bar{q} \to \gamma\gamma$ and the relative two-loop Feynman diagrams, which contain a massive heavy quark loop, as shown in figure 3.1. The associated amplitude is decomposed into a combination of tensors multiplied by scalar form factors, as described in [117], and the scalar integrals appearing in the expressions of the form factors are written in terms of a basis of master integrals (MIs). The decomposition in terms of MIs is performed using Integration-by-Parts (IBPs) identities [10, 11], via the Laporta Algorithm [12], implemented in the computer code[2] `KIRA` [35, 36]. The MIs relevant for this process have been computed by means of the differential equations method [13–20]. While for the integrals associated to the planar topologies analytic expressions are available in the literature [51, 118–123], the non-planar ones have been computed numerically in [114, 115]. Indeed, while the planar MIs admit an analytic solution in terms of Multiple Polylogarithmic functions (MPLs) [25, 124–128], it is known that the functional space for the analytic solution of the non-planar double-box family [129] contains elliptic integrals [49, 130–140]. In recent years, a big effort has been devoted to the understanding of the analytic structure of Feynman integrals which do not admit an expression in terms of MPLs. However, even in the cases in which an analytic solution in closed form is available, the numerical evaluation of the functions associated to such solution can be extremely challenging for phenomenological applications [141, 142]. In order to be able to overcome the issues previously described, we choose to exploit the generalised power series method [32, 143–148] to solve the system of differential equations associated to the MIs. This technique, currently implemented in two public computer codes [33, 34], has recently attracted a lot of interest due to its wide range of applicability and it has been successfully employed in several phenomenological applications [5, 54–56]. Specifically, in the calculation reported in this work, we used the software `DiffExp` [33] to obtain a semi-analytic solution for the MIs.

In 3.1.1 we describe the general setup for the computation and we set the context in which the two-loop amplitudes are relevant. We discuss the form factors computation along with their UV singularity structure and the renormalisation procedure. In 3.1.2 we report on the MIs calculation, describing the approach that we used to solve the differential equations, along with a brief analysis on the geometry underlying the actual analytic solution.

3.1.1 Computational setup and amplitude structure

We consider the two-loop form factors for diphoton production in the quark annihilation channel with a heavy quark loop. At the partonic level, the scattering amplitude proceeds as the Born subprocess:

$$q(p_1) + \overline{q}(p_2) + \gamma(p_3) + \gamma(p_4) \to 0, \tag{3.1}$$

[2] Other available implementations are described in [37–43]

where all the momenta of the particles are incoming. The kinematics for this process is described by the Mandelstam variables

$$s = (p_1 + p_2)^2,\ t = (p_1 + p_3)^2,\ u = (p_2 + p_3)^2,\ \text{with } s + t + u = 0, \tag{3.2}$$

where the external particles are on-shell, i.e. $p_i^2 = 0$, and we indicate with m_t^2 the heavy-

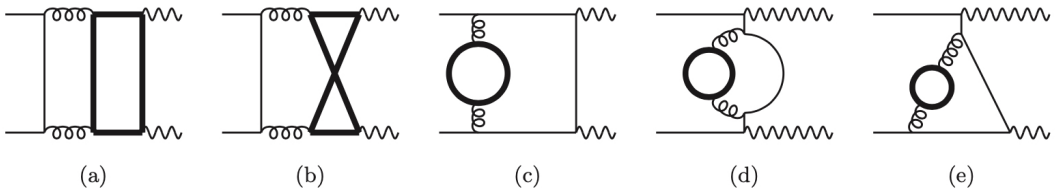

Figure 3.1. Representative set of two-loop diagrams with internal heavy-quark loops, which contribute at NNLO QCD corrections to diphoton production in the quark annihilation channel. Thin black lines represents light quarks, thick black lines heavy quarks, curly lines gluons and wavy lines photons.

quark squared mass[3]. In order to obtain the scattering amplitude, we generated the relevant Feynman diagrams using the `FeynArts` package [149]. We found a total number of 14 diagrams contributing to the amplitude, the representative ones are shown in fig. 3.1. We write the scattering amplitude in terms of form factors, which are decomposed into a basis of 63 MIs exploiting IBPs reduction [10–12, 35, 38–44], as implemented in the software `Kira` [35].

The Feynman diagrams contributing to this process can be mapped into 5 different scalar integral families: NPA, PLA, PLAx12, PLAx124 and PLAx1234, reported in appendix A. After the reduction, the whole set of MIs is described only by the families NPA, PLA and PLAx12, and there are 5 top-sectors, shown in fig. 3.7.

Out of the 63 MIs, 57 admit an analytical expression in terms of Multiple Polylogarithms and they have been studied in [51, 122, 123, 145, 150, 151], the remaining 6, belonging to the non planar topology NPA, are elliptic. Specifically, the non-planar triangle sector, which contains 2 MIs, has been solved analytically in [152] in terms of elliptic Multiple Polylogarithms (*e*MPLs), a class of special functions which are a generalisation, in the elliptic case, of the standard MPLs. On the other hand, the 4 double-box MIs of the non-planar top-sector (shown in fig. 3.6) have been computed numerically in [114, 115]. Moreover, the homogeneous solution of the non-planar double-box has been studied analytically in [153]. In the work described in [4] and presented also in this section, we performed an independent calculation of all the MIs by means of the differential equations method [13–20]. In particular we solved the system of differential equations semi-analytically exploiting the generalised power series expansion technique, as described in [32] and implemented in the software `DiffExp` [33].

The two-loop amplitude computed in this work constitutes a necessary ingredient of the recently presented full massive NNLO QCD corrections to diphoton production at hadron

[3]For the rest of this paper we will refer to the heavy quark as top quark. We note however that our formulas are general and they can be evaluated with a different value of the heavy quark mass.

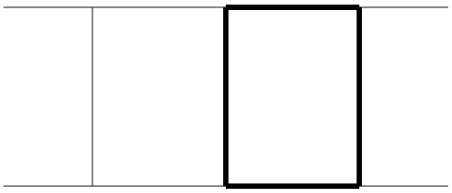

Figure 3.2. PLA$(1,1,1,1,0,1,1,0,1)$

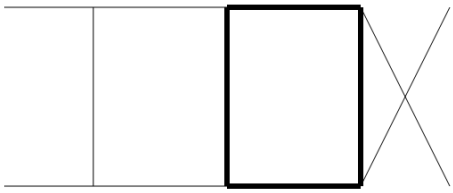

Figure 3.3. PLAx12$(1,1,1,1,0,1,1,0,1)$

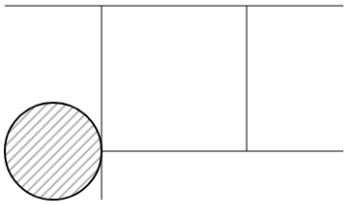

Figure 3.4. PLA$(1,1,0,1,0,1,0,1,0)$

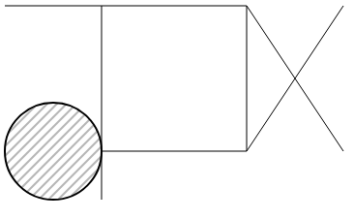

Figure 3.5. PLAx12$(1,1,0,1,0,1,0,1,0)$

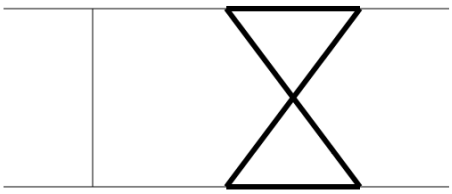

Figure 3.6. NPA$(1,1,1,1,0,1,1,1,0)$

Figure 3.7. The 5 top-sectors for the master integrals are shown: subfigures 3.2 and 3.3 are respectively a planar double-box topology and its crossed one, 3.4 and 3.5 are respectively the massless box, times the tadpole, and its crossed, while 3.6 is a non-planar double-box topology. Thin black lines represents massless particles, thick black lines heavy particles.

colliders [5], which will be the topic of section 3.2. We anticipate that our two-loop form factors, taking into account the full dependence on the top quark mass, are finite after UV renormalization. Therefore, they can be included directly (without the use of any IR regularization prescription) in any numerical implementation of the NNLO cross section. Below we will illustrate the precedent statement with a specific example based on the q_T-subtraction method [154, 155] (which can easily be extended to any other subtraction method).

To this end, we consider the following scattering process,

$$h_1 + h_2 \to \gamma\gamma + X \tag{3.3}$$

where h_1 and h_2 are the colliding hadrons, and X denotes any additional radiation, we are indeed considering the inclusive process. At the NNLO, the cross-section for this process can

be computed using the q_T-subtraction method [154–156] as follows

$$d\sigma^{\gamma\gamma}_{\rm NNLO} = \mathcal{H}^{\gamma\gamma}_{\rm NNLO} \otimes d\sigma^{\gamma\gamma}_{\rm LO} + \left[d\sigma^{\gamma\gamma+\rm jets}_{\rm NLO} - d\sigma^{CT}_{\rm NLO} \right]. \tag{3.4}$$

The terms inside the square brackets $d\sigma^{\gamma\gamma+jets}_{\rm NLO}$ and $d\sigma^{CT}_{\rm NLO}$ represent the cross section for diphoton plus jet production at NLO [91] and the corresponding counterterm, needed to cancel the associated singularities in the small-q_T limit. The coefficient function $\mathcal{H}^{\gamma\gamma}_{\rm NNLO}$ (defined in [156]) is the so-called hard-virtual function and it includes the one-loop and two-loop corrections to the Born subprocess. This object admits a perturbative expansion in terms of the strong coupling α_S:

$$\mathcal{H}^{\gamma\gamma} = 1 + \frac{\alpha_S}{\pi}\mathcal{H}^{\gamma\gamma}_{\rm NLO} + \left(\frac{\alpha_S}{\pi}\right)^2 \mathcal{H}^{\gamma\gamma}_{\rm NNLO} + \cdots . \tag{3.5}$$

In our particular case (diphoton production) the one-loop contribution to eq. (3.5) was calculated in [88], while the massless two-loop contribution was first calculated in [90] and later in [92]. The explicit expressions of the hard virtual factor (computed with the previous massless one- and two-loop amplitudes) in the hard scheme (see [155] for more details) are given in Appendix A of ref. [155]. The inclusion of the new two-loop massive form factors proceeds by simple addition to that of the massless case [90]. After regularising the IR divergences [155] present in the massless two-loop amplitude [90], our massive two-loop contribution can be added directly to the massless finite remainder.

After generating all the relevant Feynman diagrams for the process, the amplitude $\mathcal{A}_{q\bar{q},\gamma\gamma}$ has been decomposed in terms of form factors [117], and the UV singularities have been regularised in dimensional regularisation. The expression obtained has been used to compute the NNLO corrections to the hard function $\mathcal{H}^{\gamma\gamma}$ coming from two-loop diagrams which involve a massive top quark loop. Specifically, from the knowledge of the finite remainder $\mathcal{A}^{(\rm fin)}_{q\bar{q},\gamma\gamma}$ of the amplitude, we can obtain the hard function from the all-orders relation [155]:

$$\mathcal{H}^{\gamma\gamma} = \frac{|\mathcal{A}^{(\rm fin)}_{q\bar{q},\gamma\gamma}|^2}{|\mathcal{A}^{(0)}_{q\bar{q},\gamma\gamma}|^2}, \tag{3.6}$$

where $\mathcal{A}^{(0)}_{q\bar{q},\gamma\gamma}$ is the Born-level amplitude for this process:

$$|\mathcal{A}^{(0)}_{q\bar{q},\gamma\gamma}|^2 = 128\,\pi^2\,\alpha^2_{em}\,Q^4_q\,N_c\left(\frac{t}{u}+\frac{u}{t}\right), \tag{3.7}$$

where α_{em} is the QED coupling, Q_q is the electric charge of the incoming quarks and N_c is the number of colours. We also performed a sum over initial and final polarisations and initial colours.

This massive hard-virtual coefficient represents the last missing ingredient necessary to perform a NNLO phenomenological study, for diphoton production at the LHC, which takes into account the complete dependence on the top quark mass [5].

Form factors

The bare scattering amplitude can be written[4] as

$$\mathcal{A}_{q\bar{q},\gamma\gamma} = \alpha_{em}\, \delta_{ij}\, \epsilon^{\mu}_{\lambda_3}(p_3)\epsilon^{\nu}_{\lambda_4}(p_4)\overline{v}_{s_2}(p_2)\mathcal{A}_{\mu\nu}(s,t,u,m_t^2)u_{s_1}(p_1), \tag{3.8}$$

where δ_{ij} is the Kronecker delta function with i and j the color indices of the incoming $q\bar{q}$ pair, $\epsilon^{\mu}_{\lambda_3}(p_3)$ and $\epsilon^{\nu}_{\lambda_4}(p_4)$ are external photon polarisation vectors and $\overline{v}_{s_2}(p_2)$, $u_{s_1}(p_1)$ the quark spinors.

We decomposed the amplitude in tensor structures, which embed the dependence on external particle polarisations, and scalar form factors. In our computation we adopt the 't Hooft-Veltman scheme, where the external momenta and polarisations are four-dimensional objects while internal momenta and gamma matrices are D-dimensional. As outlined in [117], in this scheme there is a correspondence between the number of independent helicity amplitudes in the process and the number of tensor structures that remain independent when four-dimensional external states are considered. For the process we are considering there are four possible helicity configurations:

$$\mathcal{A}\left(q^-_{p_1},\overline{q}^+_{p_2},\gamma^+_{p_3},\gamma^+_{p_4}\right) \qquad \mathcal{A}\left(q^-_{p_1},\overline{q}^+_{p_2},\gamma^+_{p_3},\gamma^-_{p_4}\right) \tag{3.9}$$

$$\mathcal{A}\left(q^-_{p_1},\overline{q}^+_{p_2},\gamma^-_{p_3},\gamma^+_{p_4}\right) \qquad \mathcal{A}\left(q^-_{p_1},\overline{q}^+_{p_2},\gamma^-_{p_3},\gamma^-_{p_4}\right). \tag{3.10}$$

Right-handed quark configurations can be obtained by charge-conjugation transformation. Therefore the amplitude (3.8) can be decomposed in terms of a set of four independent tensors which are built using external momenta and polarisation vectors:

$$\mathcal{A}_{q\bar{q},\gamma\gamma} = \sum_{k=1}^{4} \mathcal{F}_k\, T_k, \tag{3.11}$$

where the T_k are chosen as [117]:

$$\begin{aligned}
T_1 &= \overline{v}_{s_2}(p_2)\not{\epsilon}_{\lambda_3}(p_3)u_{s_1}(p_1)\epsilon_{\lambda_4}(p_4)\cdot p_2,\\
T_2 &= \overline{v}_{s_2}(p_2)\not{\epsilon}_{\lambda_4}(p_4)u_{s_1}(p_1)\epsilon_{\lambda_3}(p_3)\cdot p_1,\\
T_3 &= \overline{v}_{s_2}(p_2)\not{p}_3 u_{s_1}(p_1)\epsilon_{\lambda_3}(p_3)\cdot p_1\epsilon_{\lambda_4}(p_4)\cdot p_2,\\
T_4 &= \overline{v}_{s_2}(p_2)\not{p}_3 u_{s_1}(p_1)\epsilon_{\lambda_3}(p_3)\cdot \epsilon_{\lambda_4}(p_4).
\end{aligned} \tag{3.12}$$

The decomposition (3.11) has been achieved also by enforcing the physical transversality conditions $\epsilon_{\lambda_i}\cdot p_i = 0$ for the polarisation vectors, and by choosing as gauge fixing the conditions $\epsilon_{\lambda_3}\cdot p_2 = \epsilon_{\lambda_4}\cdot p_1 = 0$, which imply for the photons the polarization sums:

$$\sum_{\lambda_3}\epsilon^{\mu}_{\lambda_3}\epsilon^{*\nu}_{\lambda_3} = -g^{\mu\nu} + \frac{p_2^{\mu}p_3^{\nu}+p_3^{\mu}p_2^{\nu}}{p_2\cdot p_3}, \qquad \sum_{\lambda_4}\epsilon^{\mu}_{\lambda_4}\epsilon^{*\nu}_{\lambda_4} = -g^{\mu\nu} + \frac{p_1^{\mu}p_4^{\nu}+p_4^{\mu}p_1^{\nu}}{p_1\cdot p_4}, \tag{3.13}$$

where $g^{\mu\nu} = \mathrm{diag}(1,-1,-1,-1)$. The coefficients of T_k are the so-called scalar form factors, $\mathcal{F}_k$. These objects are functions of the kinematic invariants of the process, and of the space-time

[4] For the sake of simplicity we are omitting color indices on the left side of Eq. (3.8)

dimension D, and they can be written in terms of scalar Feynman integrals. Their expression can be obtained by applying a set of projectors, $\{\mathcal{P}_k\}$, to the amplitude $\mathcal{A}_{q\bar{q},\gamma\gamma}$ and summing over polarizations:

$$\mathcal{F}_k = \sum_{s_1,s_2,\lambda_3,\lambda_4} \mathcal{P}_k \, \mathcal{A}_{q\bar{q},\gamma\gamma}. \tag{3.14}$$

The projectors are

$$\mathcal{P}_i = \sum_{j=1}^{4} \left(M^{-1}\right)_{ij} T_j^\dagger, \qquad M_{ij} = \sum_{pol} T_i^\dagger T_j, \tag{3.15}$$

where M_{ij} is called the projector matrix and it depends in general on the dimension D. The inverse of M is smooth when $D = 4$, confirming that the tensors 3.12 are independent in four dimensions. For completeness we give here the explicit expressions for the set of projectors $\{\mathcal{P}_k\}$ with $k = 1, ..., 4$,

$$\mathcal{P}_1 = \frac{1}{(D-3)t}\left[\frac{u}{2s^2}T_1^\dagger - \frac{u}{2s^2 t}T_3^\dagger\right], \tag{3.16}$$

$$\mathcal{P}_2 = \frac{1}{(D-3)t}\left[\frac{u}{2s^2 t}T_3^\dagger + \frac{u}{2s^2}T_2^\dagger\right], \tag{3.17}$$

$$\mathcal{P}_3 = \frac{1}{(D-3)t}\left[\frac{(Du^2-4st)}{2s^2ut^2}T_3^\dagger - \frac{u}{2s^2t}T_1^\dagger + \frac{u}{2s^2t}T_2^\dagger - \frac{(t-s)}{2sut}T_4^\dagger\right], \tag{3.18}$$

$$\mathcal{P}_4 = \frac{1}{(D-3)t}\left[-\frac{(t-s)}{2sut}T_3^\dagger + \frac{1}{2u}T_4^\dagger\right]. \tag{3.19}$$

We stress that the independent four-dimensional tensors 3.12 span the space of the helicity amplitudes of the process we are considering. In [117] bases of four-dimensional tensors for most of the processes relevant for collider phenomenology are built, and some of them have been applied for recent multiloop multileg scattering amplitude computations, in particular the basis 3.12 was already successfully applied in the computation of the three-loop massless scattering amplitudes for the production of a pair of photons in quark-antiquark annihilation [157].

The form factors $\mathcal{F}_k$ admit the following perturbative expansion:

$$\mathcal{F}_k = \mathcal{F}_k^{(0)} + \left(\frac{\alpha_S}{\pi}\right)\mathcal{F}_k^{(1)} + \left(\frac{\alpha_S}{\pi}\right)^2 \mathcal{F}_k^{(2)} + \cdots, \tag{3.20}$$

where α_S is the strong coupling constant. At leading order we have:

$$\mathcal{F}_1^{(0)} = 4\pi\alpha_{em}\delta_{ij}Q_q^2\frac{-1}{t}, \tag{3.21}$$

$$\mathcal{F}_2^{(0)} = 4\pi\alpha_{em}\delta_{ij}Q_q^2\frac{1}{t}, \tag{3.22}$$

$$\mathcal{F}_3^{(0)} = 4\pi\alpha_{em}\delta_{ij}Q_q^2\frac{2}{tu}, \tag{3.23}$$

$$\mathcal{F}_4^{(0)} = 4\pi\alpha_{em}\delta_{ij}Q_q^2\frac{(t-u)}{tu}. \tag{3.24}$$

The massive corrections, we are interested in, appear starting from the two-loop order. Therefore, they affect only the term $\mathcal{F}_k^{(2)}$. From now on we will focus just on this contribution, which we will refer to as $\mathcal{F}_{k,\texttt{top}}^{(2)}$. We generated all the relevant Feynman diagrams for this

contribution using `FeynArts` [149], and we found 14 different two-loop Feynman diagrams, the representative ones are depicted in fig. 3.1. We used `FORM` [158, 159] to apply the projectors to the Feynman diagrams and perform the Dirac algebra. The form factors, then, were expressed as linear combinations of 63 MIs, which are defined in appendix A.

We find the following structure for the form factors $\mathcal{F}^{(2)}_{k,\texttt{top}}$:

$$\mathcal{F}^{(2)}_{k,\texttt{top}} = \mathcal{F}^{(2)}_{k,\texttt{top};0} + \mathcal{F}^{(2)}_{k,\texttt{top};2}\,, \tag{3.25}$$

$$\mathcal{F}^{(2)}_{k,\texttt{top};0} = 4\pi\alpha_{em}\delta_{ij}\,C_F Q_q^2\,\mathcal{B}_k \qquad \mathcal{F}^{(2)}_{k,\texttt{top};2} = 4\pi\alpha_{em}\delta_{ij}\,C_F Q_t^2\,\mathcal{C}_k, \tag{3.26}$$

where $\mathcal{B}_k$ and $\mathcal{C}_k$ depend only on the kinematic variables and the dimension D, $C_F = \frac{N_c^2-1}{2N_c}$ is the Casimir of the fundamental representation of $SU(N_c)$ and Q_t is the electric charge of the top quark running in the loop. The two contributions $\mathcal{F}^{(2)}_{k,\texttt{top};0}$ and $\mathcal{F}^{(2)}_{k,\texttt{top};2}$ are related to different powers of the top electric charge Q_t. The first contribution $\mathcal{F}^{(2)}_{k,\texttt{top};0}$ is associated to the diagrams of the type (c), (d) and (e) in fig. 3.1 in which the top quark does not couple to the external photons, while the second contribution $\mathcal{F}^{(2)}_{k,\texttt{top};2}$ comes from the diagrams of the type (a) and (b) where the top quark actually couples with the photon.

We perform our computations in the context of dimensional regularisation. As a consequence, potential ultraviolet (UV) and infrared (IR) singularities can appear in the form factors as poles in the dimensional regulator $\epsilon = (4-D)/2$. However, since the diagrams with a top loop start contributing to the $q\bar{q}$ channel at the two-loop order, $\mathcal{F}^{(2)}_{k,\texttt{top}}$ does not have IR singularities and therefore all the ϵ poles are of UV origin. Furthermore, $\mathcal{F}^{(2)}_{k,\texttt{top};2}$ is also free of UV divergences because the top electric charge does not appear at previous orders, then the UV poles come only from the contribution $\mathcal{F}^{(2)}_{k,\texttt{top};0}$.

Helicity amplitudes

For the construction of the helicity amplitudes we followed [157], and we report here the main steps. We can obtain the helicity amplitudes from our form factors by evaluating the tensor structures T_i for well-defined helicity states. We write for left-handed spinors $\bar{v}_L(p_2) = \langle 2|$ and $u_L(p_1) = |1]$ and for the the photon j of momentum p_j:

$$\epsilon^{\mu}_{j,-}(q_j) = \frac{\langle q_j|\gamma^{\mu}|j]}{\sqrt{2}\langle q_j j\rangle}\,, \quad \epsilon^{\mu}_{j,+}(q_j) = \frac{\langle j|\gamma^{\mu}|q_j]}{\sqrt{2}[j q_j]}\,.$$

With these definitions and denoting with λ_q the helicity of the quark, we can compute the helicity amplitudes $\mathcal{A}_{\lambda_q\lambda_3\lambda_4}$. For a left-handed quark, these are:

$$\begin{aligned} \mathcal{A}_{L--} &= \frac{2[34]^2}{\langle 13\rangle[23]}\alpha\,, \quad \mathcal{A}_{L-+} = \frac{2\langle 24\rangle[13]}{\langle 23\rangle[24]}\beta\,, \\ \mathcal{A}_{L+-} &= \frac{2\langle 23\rangle[41]}{\langle 24\rangle[32]}\gamma\,, \quad \mathcal{A}_{L++} = \frac{2\langle 34\rangle^2}{\langle 31\rangle[23]}\delta\,, \end{aligned} \tag{3.27}$$

with

$$\begin{aligned}
\alpha &= \frac{t}{2}\left(\mathcal{F}_2 - \frac{t}{2}\mathcal{F}_3 + \mathcal{F}_4\right), \\
\beta &= \frac{t}{2}\left(\frac{s}{2}\mathcal{F}_3 + \mathcal{F}_4\right), \\
\gamma &= \frac{s\,t}{2u}\left(\mathcal{F}_2 - \mathcal{F}_1 - \frac{t}{2}\mathcal{F}_3 - \frac{t}{s}\mathcal{F}_4\right), \\
\delta &= \frac{t}{2}\left(\mathcal{F}_1 + \frac{t}{2}\mathcal{F}_3 - \mathcal{F}_4\right).
\end{aligned} \tag{3.28}$$

Note that the remaining amplitudes for a right-handed quark can be obtained by a charge-conjugation transformation as follows,

$$\mathcal{A}_{R\lambda_3\lambda_4} = \mathcal{A}_{L\overline{\lambda}_3\overline{\lambda}_4}\left(\langle ij\rangle \leftrightarrow [ji]\right), \tag{3.29}$$

where $\overline{\lambda}_i$ indicates $-\lambda_i$.

UV Renormalisation

We renormalise the bare form factors in a mixed scheme. The external quark fields are renormalised on shell; the strong coupling constant is renormalised in a scheme in which the massless contribution, coming from light quarks and gluons, is treated in $\overline{\text{MS}}$, while the heavy-quark contribution is renormalised on shell (at zero momentum). No renormalisation is needed for the top quark mass m_t at this order in perturbation theory and the same occurs for the external photon field.

We have, then

$$\overline{\mathcal{F}}_k = Z_q\,\mathcal{F}_k\left(\alpha_S = \mu^{2\epsilon} Z_{\alpha_S}\overline{\alpha}_S\right), \tag{3.30}$$

where the overlined objects $\overline{\mathcal{F}}_k$, $\overline{\alpha}_S$ are the renormalised ones and μ is the renormalisation scale. The renormalisation factors Z_q and Z_{α_S} admit a perturbative expansion in the strong coupling constant [160–163]:

$$Z_q = 1 + \left(\frac{\overline{\alpha}_S}{\pi}\right)\delta Z_q^{(1)} + \left(\frac{\overline{\alpha}_S}{\pi}\right)^2 \delta Z_q^{(2)} + \mathcal{O}(\overline{\alpha}_S^3), \tag{3.31}$$

$$Z_{\alpha_S} = 1 + \left(\frac{\overline{\alpha}_S}{\pi}\right)\delta Z_{\alpha_s}^{(1)} + \mathcal{O}(\overline{\alpha}_S^2). \tag{3.32}$$

In our renormalisation scheme, we have

$$\delta Z_q^{(1)} = 0, \tag{3.33}$$

$$\delta Z_q^{(2)} = \pi^{-2\epsilon}\Gamma^2(1+\epsilon)\left(\frac{\mu^2}{m_t^2}\right)^{2\epsilon} C_F N_h T_F\left(\frac{1}{16\epsilon} - \frac{5}{96}\right), \tag{3.34}$$

$$\delta Z_{\alpha_s}^{(1)} = \delta Z_{\alpha_s,\overline{\text{MS}}}^{(1)} + \delta Z_{\alpha_s,N_h,\text{OS}}^{(1)}, \tag{3.35}$$

where $\delta Z^{(1)}_{\alpha_s,\overline{\text{MS}}}$ contributes only to the renormalisation of the massless amplitude, while $\delta Z^{(1)}_{\alpha_s,N_h,\text{OS}}$, proportional to the number of heavy quarks N_h, renormalizes exclusively the

massive contribution to the amplitude. The expression of $\delta Z^{(1)}_{\alpha_s,N_h,\text{OS}}$ is given by

$$\delta Z^{(1)}_{\alpha_s,N_h,\text{OS}} = \pi^{-\epsilon}\Gamma(1+\epsilon)\left(\frac{\mu^2}{m_t^2}\right)^{\epsilon}\frac{N_h}{6\epsilon}\,. \tag{3.36}$$

In our case we consider only the top-quark, so $N_h = 1$, and we used $T_F = \frac{1}{2}$.

Putting all together, the renormalised form factors read

$$\overline{\mathcal{F}}^{(2)}_{k,\texttt{top};2} = \mathcal{F}^{(2)}_{k,\texttt{top};2}\,, \tag{3.37}$$

$$\overline{\mathcal{F}}^{(2)}_{k,\texttt{top};0} = (\mu^2)^{2\epsilon}\,\mathcal{F}^{(2)}_{k,\texttt{top};0} + \mu^{2\epsilon}\,\delta Z^{(1)}_{\alpha_s,N_h,\text{OS}}\,\mathcal{F}^{(1)}_k + \delta Z^{(2)}_q\,\mathcal{F}^{(0)}_k\,. \tag{3.38}$$

The merely two-loop contribution of the renormalised finite form factors, $\overline{\mathcal{F}}^{(2)}_{k,\texttt{top};2}$ and $\overline{\mathcal{F}}^{(2)}_{k,\texttt{top};0}$, is written as a linear combination of ϵ-expanded master integrals of the precanonical basis, given in A, where the coefficients are rational functions of the Mandelstam, while the UV counter term contribution is written in terms of harmonic polylogarithms (HPL). The analytic expressions of the counter terms $\mu^{2\epsilon}\,\delta Z^{(1)}_{\alpha_s,N_h,\text{OS}}\,\mathcal{F}^{(1)}_k + \delta Z^{(2)}_q\,\mathcal{F}^{(0)}_k$ are given in appendix B.

3.1.2 Master Integrals Computation

In this subsection we discuss the details of the MIs computation. The MIs are computed through the differential equations method. The system of differential equations associated to the MIs is solved semi-analytically employing the generalised power series expansion technique, as described in [32] and implemented in the software `DiffExp` [33]. We also show that some of the MIs that appear in the computation admit an analytic solution in terms of elliptic functions.

We provide a single system of differential equations which includes all the MIs appearing in the amplitude. This system is in canonical form just for the sectors whose analytic solution could be given in terms of MPLs. We notice that the basis of MIs in which we solve the differential equations, which we will refer in the following as $\vec{f}$, and the one in which we write the form factors are different. We choose this approach in order to avoid square roots of the kinematic invariants in the expressions of the form factors. In appendix A, along with the definition of the precanonical basis $\mathcal{T}_i$, we provide the rotation to the basis f_i.

The system of differential equations

The three integral families to which the MIs belong are defined as follows:

$$I_{\texttt{topo}}(n_1,...,n_9) = \int \frac{\mathcal{D}k_1\mathcal{D}k_2}{D_1^{n_1}D_2^{n_2}D_3^{n_3}D_4^{n_4}D_5^{n_5}D_6^{n_6}D_7^{n_7}D_8^{n_8}D_9^{n_9}}\,, \tag{3.39}$$

where $\texttt{topo} \in \{\text{PLA}, \text{PLAx12}, \text{NPA}\}$ labels the families and the corresponding propagators $D_1,...,D_9$ are given in appendix A. The computation is done in dimensional regularization with $D = 4-2\epsilon$ dimensions, and our convention for the integration measure is

$$\mathcal{D}k = \frac{\mathrm{d}^D k}{i\pi^{2-\epsilon}\Gamma(1+\epsilon)}m_t^{2\epsilon}\,. \tag{3.40}$$

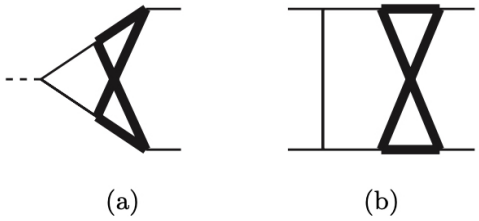

Figure 3.8. Diagrams representing the two elliptic sectors in the non planar topology NPA. Thin lines represent massless particles, while thick lines massive particles.

The number of MIs appearing in the form factors is 63. The system of differential equations can be divided in two different subsets:

- **(I) Canonical logarithmic**: the subset of MIs whose differential equations are in canonical logarithmic form;
- **(II) Elliptic sectors**: this subset contains MIs whose analytic solution involves elliptic functions and it is not written in ϵ-factorized form.

We refer to the basis used to solve the system as $\vec{f}(\vec{x}, \epsilon)$, where

$$\vec{x} = \{s, t\}\,, \quad s = \frac{2\,p_1 \cdot p_2}{m_t^2},\ t = \frac{2\,p_1 \cdot p_3}{m_t^2} \tag{3.41}$$

is the vector of the kinematic invariants with respect to which we derived the differential equations[5]. The subset (II) contains two sectors: the first one is a non-planar triangle with a massive loop [152], shown in fig. 3.8 (a). This sector has 2 MIs, f_{58} and f_{59}, which admit a representation in terms of *elliptic multiple polylogarithms* (*e*MPLs) [164]. The second sector whose analytic structure is characterised by the presence of elliptic functions is the top sector of the topology NPA, i.e. the non planar double-box integral, shown in fig. 3.8 (b), which contains the 4 MIs f_{60-63}. The subsystem of differential equations corresponding to the subset (I) has been put in canonical logarithmic form [19], for the planar topologies this result has been obtained for the first time in [51], while for the non-planar polylogarithmic subsectors this is an original result. The whole system of differential equations reads

$$\mathrm{d}\vec{f}(\vec{x}, \epsilon) = \mathrm{d}A(\vec{x}, \epsilon)\vec{f}(\vec{x}, \epsilon) \quad \mathrm{d}A(\vec{x}, \epsilon) = \epsilon\,\mathrm{d}A_{\mathrm{I}}(\vec{x}) + \mathrm{d}A_{\mathrm{II}}(\vec{x}, \epsilon), \tag{3.42}$$

where d is the total differential with respect to the kinematic invariants, and the matrices $\epsilon A_{\mathrm{I}}(\vec{x})$ and $A_{\mathrm{II}}(\vec{x}, \epsilon)$ are respectively the matrices of the subsystems (I) and (II). We stress that the subsystem (I) does not involve elliptic MIs of the subsystem (II), conversely the latter is coupled, as expected, to a subset of the MIs belonging to (I). The matrix $A_{\mathrm{I}}(\vec{x})$ does not depend on ϵ and it is a linear combination of logarithms:

$$A_{\mathrm{I}}(\vec{x}) = \sum_i c_i \log(w_i(\vec{x})). \tag{3.43}$$

[5]Note that s and t defined in eq. 3.41 are adimensional and so different from the ones defined in eq. 3.2

The c_i represent matrices of rational numbers, while $\{w_i(\vec{x})\}$ is the alphabet of the solution and it is made by algebraic functions of the kinematic invariants. The knowledge of the logarithmic canonical form for the subsystem (I) of the differential equations (3.42), would allow us, in principle, to obtain a fully analytic representation for the non elliptic MIs, i.e. $\{f_i\}$ with $i = 1, \cdots, 57$. However, the presence of the set of square roots, given in equations (A.72), makes the achievement of such analytic expression non trivial. Indeed, these square roots are not simultaneously rationalizable. As a consequence, in order to obtain a fully analytic representation of the solution one would have to exploit symbol level techniques [165,166]. For the purpose of this project, we found that the semi-analytic evaluation, which we achieved exploiting a generalised power series expansion method, was sufficient to perform phenomenological studies.

In the upcoming work [167] the full-analytic form of two-loop massive amplitudes for diphoton production in quark-antiquark and gluon fusion channels will be provided. The elliptic MIs will be given in $\epsilon-$factorised basis, found through the technique described in [49]. In this thesis we adopt the same canonical basis for polylogarithmic MIs defined in [167]. For the elliptic MIs we also use the precanonical form of [167]. A such definition of the integrals is slightly different with respect to the one previously provided in [4]. Nevertheless, we decided to rearrange the basis of MIs mainly for two reasons: a unique global system of differential equations for all the MIs contributing to the amplitude (included permutations) improves the efficiency of the numerical evaluation; we could easily provide intermediate analytical checks for the amplitude computed in [167].

The boundary conditions for the system are provided in the origin of the space of kinematic variables $s = t = 0$, where many simplifications occur, indeed the following canonical MIs vanish in this point:

$$f_i(0,0) = 0 \quad \text{if} \quad 5 \leq i \leq 22 \vee 25 \leq i \leq 57. \tag{3.44}$$

For the remaining MIs, except for the tadpole, the origin is a singular point, consequentially we have to provide at least an asymptotic behaviour. This can be easily achieved for the non elliptic MIs: f_1, f_2, f_3 and f_4, respectively the tadpole and the massless bubbles in s, t and u channel, have simple well-known analytical expressions:

$$f_1 = 1 \tag{3.45}$$

$$f_2 = -\left(-\frac{1}{s}\right)^{\epsilon} \frac{\Gamma(1-\epsilon)^2}{\Gamma(1-2\epsilon)} \tag{3.46}$$

$$f_3 = -\left(-\frac{1}{t}\right)^{\epsilon} \frac{\Gamma(1-\epsilon)^2}{\Gamma(1-2\epsilon)} \tag{3.47}$$

$$f_4 = -\left(-\frac{1}{u}\right)^{\epsilon} \frac{\Gamma(1-\epsilon)^2}{\Gamma(1-2\epsilon)}; \tag{3.48}$$

the canonical MI f_{23} (f_{24}) is the massless box in the u (t) channel, its analytical expression is

$$\begin{aligned} f_{23} = & \left(-\frac{1}{s}\right)^{\epsilon} \frac{\Gamma(1-\epsilon)^2}{\Gamma(1-2\epsilon)} \left\{ 4 \, - \, 2\,\epsilon\, H\left(0, \frac{u}{s}\right) \, - \, \pi^2\,\epsilon^2 + \epsilon^3 \left[-\pi^2 H\left(-1, \frac{u}{s}\right) + \right.\right. \\ & \pi^2 H\left(0, \frac{u}{s}\right) - 2H\left(-1, 0, 0, \frac{u}{s}\right) + 2H\left(0, 0, 0, \frac{u}{s}\right) - 2\zeta(3) \Big] + \\ & \epsilon^4 \left[-2\zeta(3) H\left(-1, \frac{u}{s}\right) + 2\zeta(3) H\left(0, \frac{u}{s}\right) - \pi^2 H\left(-1, -1, \frac{u}{s}\right) + \right. \\ & \pi^2 H\left(-1, 0, \frac{u}{s}\right) + \pi^2 H\left(0, -1, \frac{u}{s}\right) - \pi^2 H\left(0, 0, \frac{u}{s}\right) - \\ & 2H\left(-1, -1, 0, 0, \frac{u}{s}\right) + 4H\left(-1, 0, 0, 0, \frac{u}{s}\right) + 2H\left(0, -1, 0, 0, \frac{u}{s}\right) - \\ & \left.\left. 4H\left(0, 0, 0, 0, \frac{u}{s}\right) - \frac{\pi^4}{15} \right] \right\}, \end{aligned} \tag{3.49}$$

for f_{24} just swap $u \leftrightarrow t$. The last expression has been known for many years and it can be obtained, for example, integrating the corresponding differential equation and imposing the regularity of the solution along $t = 0$ (see [168] or chapter 2). The analytic continuation of 3.45–3.49 is given by the Feynman prescription: a Mandelstam invariant acquires a small positive imaginary part as long as it becomes positive,

$$s \to s + i\delta, \qquad t \to t + i\delta, \qquad u \to u + i\delta, \tag{3.50}$$

where δ is positive and small. The formula 3.49 was cross checked analytically with [168] and numerically with `AMFlow` [53]. For the elliptic MIs f_{58-63} we adopted the following strategy: *i*) introducing free parameters in the series solution around the origin; *ii*) evolving to a point (s_0, t_0) different from the origin; *iii*) matching the series solution with the `AMFlow` numerical solution, for the elliptic MIs, in the point (s_0, t_0), and so fixing the unknown parameters; *iv*) using (s_0, t_0) as the new boundary point to evolve the system to any other point.

Semi-Analytic solution with Generalised power series

We continue by describing the solution for the system of differential equations. As already mentioned, we choose to exploit the generalised power series method, as described in [32] and implemented in the software `DiffExp` [33], to obtain a semi-analytic solution for the set of MIs. This method has the advantage of not being limited by the functional space in which the MIs would be analytically represented. This feature allows us to avoid the issues connected with the presence of MIs which admit an analytic solution in terms of elliptic integrals, for which both the understanding of their analytic structure and the numerical evaluation can still represent a bottleneck for phenomenological applications.

We exploit the method to build a grid of points for the contribution of the corrections considered here to the hard function $\mathcal{H}^{\gamma\gamma}_{NNLO}$. After interpolation, the grid has been used in the fully massive NNLO phenomenological study for diphoton production in [5]. The grid has

been generated directly in the physical region of the phase-space for this process:

$$s > 0, \quad t = -\frac{s}{2}(1 - \cos\theta), \quad -s < t < 0, \tag{3.51}$$

where θ, $0 < \theta < \pi$, is the scattering angle in the partonic center of mass frame. Since the

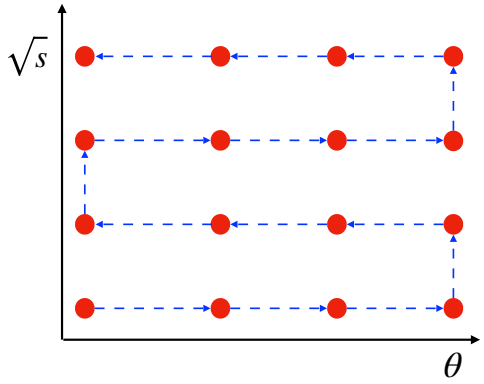

Figure 3.9. Schematic representation of the procedure exploited to optimise the grid construction within `DiffExp`. Red dots represents the points in which the MIs are evaluated and the blue dashed lines connect the sequential evaluations.

evaluation time, within `DiffExp`, for the MIs needed in this process is relatively low, we can build the grid of points as follows[6]. We consider a total number of 13752 points in the following range for the scattering angle θ and the energy of the center of mass $\sqrt{s}$:

$$-0.99 < \cos\theta < 0.99, \quad 8\,\text{GeV} < \sqrt{s} < 2.2\,\text{TeV}\,. \tag{3.52}$$

The points $p_{i,j} = (s_i, t_{i,j})$[7] of the grid are defined as follows:

$$p_{i,j} := \begin{cases} s_i = s_0 + (s_f - s_0)\frac{i}{572} \\ t_{i,j} = -\frac{s_i}{2}(1 - \cos\theta_j), \quad \cos\theta_j = \cos\theta_0 + (\cos\theta_f - \cos\theta_0)\frac{j}{23} \end{cases} \tag{3.53}$$

where $s_0 = 64\,\text{GeV}^2$, $s_f = 4.84 \cdot 10^6\,\text{GeV}^2$, $\cos\theta_0 = -0.99$, $\cos\theta_f = 0.99$ and the indices i, j take the values $i \in [0, 572]$, $j \in [0, 23]$. We constructed the grid by performing sequential numerical evaluations of the MIs in `DiffExp` as depicted schematically in figure 3.9. Starting from the origin of the phase-space, we perform a first evaluation in the physical point $p_{0,0}$. From this point, at fixed value of s, we move along the θ axis, from $\cos\theta = -0.99$ to $\cos\theta = 0.99$, up to the point $p_{0,23}$. Then, we increase the value of s and we move in the other direction along the θ axis up to the point $p_{1,0}$, and so on so forth. In order to optimise the grid generation, for each evaluation we use as boundary conditions the value of the MIs obtained at the previous point. This procedure effectively increases the efficiency of the evaluation for the MIs. In particular, we managed to evaluate the MIs in all the points of the grid, with a 16 digits accuracy, in about 13 hours, on a single core laptop.

[6] We notice that for more CPU demanding computations more refined approaches have to be used.

[7] For the purpose of this discussion we use the dimensional Mandelstam variables defined in Eq. 3.2

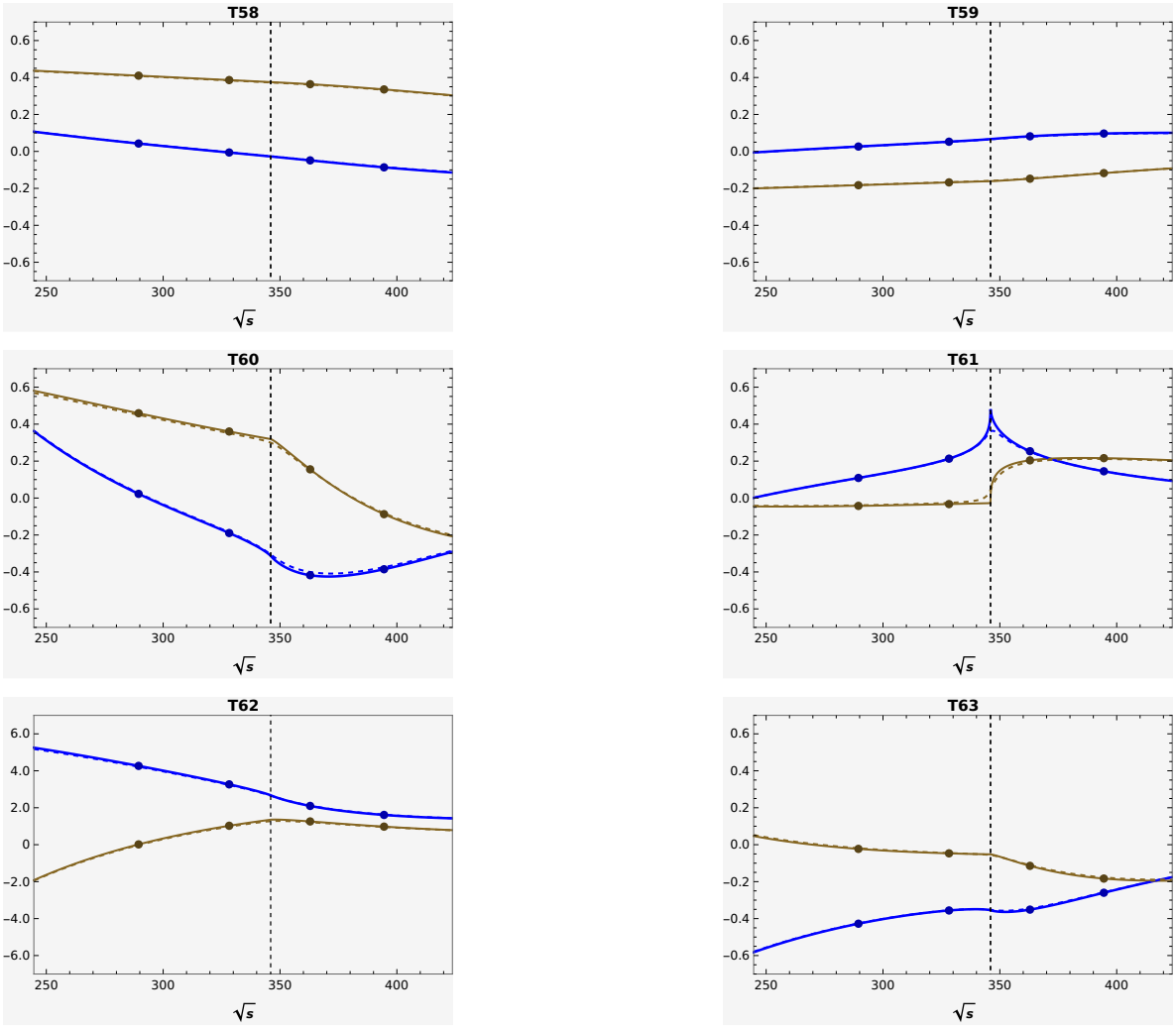

Figure 3.10. Numerical results for the dimensionless elliptic non-planar MIs $\mathcal{T}_{58}, \mathcal{T}_{59}, \mathcal{T}_{60}, \mathcal{T}_{61}, \mathcal{T}_{62}$ and $\mathcal{T}_{63}$. The plots show the order $\mathcal{O}(\epsilon^0)$. Continuous blue and yellow lines represent, respectively, the real and imaginary part of the MIs obtained with `DiffExp`, with a real top-quark mass $m_t = 173$ GeV. Dashed blue and yellow lines represent, respectively, the real and imaginary part of the MIs obtained with `SeaSyde`, with complex top-quark mass with a width $\Gamma_t = 1.76$ GeV. Dots represent numerical values obtained with `AMFlow`. The evaluations are performed for different values of $\sqrt{s}$ at fixed angle θ (in this case $\cos\theta = 0.5$). The vertical dashed black line represents the threshold at $2m_t$. We notice that the complex mass smoothens the singular behavior around threshold, especially for $\mathcal{T}_{61}$.

In order to validate our results, we performed numerical checks for the MIs against independent numerical evaluations done with the `AMFlow` package [53], which implements the auxiliary mass flow method [169, 170]. The MIs have been checked for several points in the physical phase-space region, finding an agreement between the two independent evaluations of at least 16 digits of accuracy in each point for every master. As a proof of concept of the numerical checks we show in figure 3.10 our results for the non-planar triangle and double-box MIs of the topology NPA.

In addition to the analytical continuation (3.50) of the Mandelstam variables, we need to know at which side of the branch-cut, $s > 4m_t^2$, we have to evaluate the solution after having

passed the top-quark threshold. To this aim, Feynman prescription once again comes to our assistance:

$$4 - s \to 4 - s - i\delta, \tag{3.54}$$

where we used the dimensionless variables (3.41).

In the Standard Model the top-quark is an unstable particle which decays through electroweak interactions and has a decay width Γ_t. Consequently dimensionless kinematic variables assume complex values in the physical region. They are given, in the approximation $\Gamma_t \ll m_t$, by the following substitution:

$$\frac{s}{m_t^2} \to \frac{s}{\mu^2}, \qquad \mu^2 = m_t^2 - i m_t \Gamma_t. \tag{3.55}$$

The task of finding the solution to the differential equation system as power series expansions around complex values of the kinematic variables has been automatized in the program `SeaSyde` [34]. The effect of the complex mass smoothens the behavior near the threshold of the master integrals. However, in our case the impact of the top-quark width turns out to be tiny and we have decided not to include it in phenomenological study.

The numerical grid for the master integrals has been used to construct a grid for each form factor. The last are the building blocks to set up the grid for the hard function, which is given by the following formula:

$$\mathcal{H}_{\gamma\gamma}^{(2;\mathtt{top})} = \frac{2 \sum_{jk} \mathcal{F}_j^{(0)} M_{jk} \overline{\mathcal{F}}_{k,\mathtt{top}}^{(2)}}{|\mathcal{A}_{q\bar{q},\gamma\gamma}^{(0)}|^2}, \tag{3.56}$$

where M is the projector matrix in $D = 4$ dimensions. A plot of the massive contribution to the hard function is shown in figure 3.11. The grid of the hard function has been interpolated with cubic splines, providing a `Fortran` routine for a fast numerical evaluation. The interpolation deviates from the true result within 0.3%.

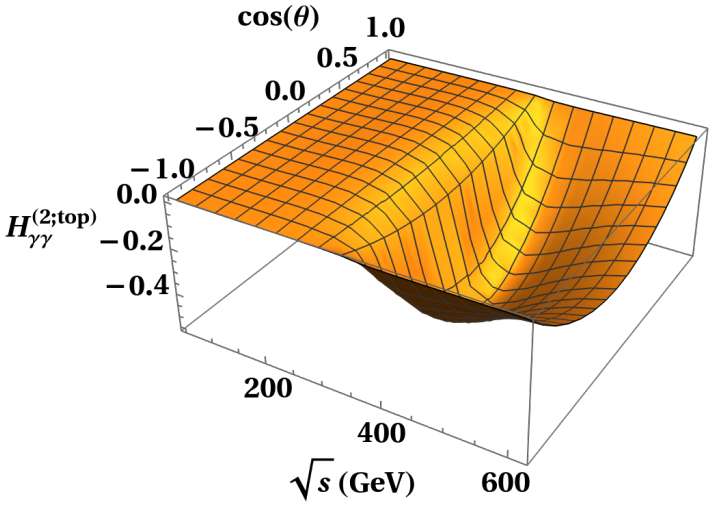

Figure 3.11. Contribution of the top-quark to the NNLO hard function is shown. We observe that the top-quark mass introduces a dependence on the energy $\sqrt{s}$ which is absent in the massless contribution. We notice also the negative bump around two times the top-quark mass.

Maximal cut of the elliptic sectors

We conclude this section analyzing the maximal cut of the elliptic sectors. The maximal cut of an integral can be obtained from it by replacing each propagator with a delta-function, then it is a solution of the homogeneous differential equation for the starting integral and contains information about the functional space of the full solution.

The non-polylogarithmic structure of the non-planar double-box is two-fold. First, the differential equations for the MIs f_{60}, f_{61}, f_{62} and f_{63} contain the triangle integrals f_{58} and f_{59} in the non-homogeneous part of the system. As a consequence the analytic solution of the differential equations requires the integration over kernels that contains eMPLs. Moreover, also the homogeneous part of the differential equation itself contains elliptic functions. This statement can be verified by studying the maximal cut of the double-box integral [20]:

$$I_{\text{NPA}}(1,1,1,1,0,1,1,1,0). \tag{3.57}$$

In order to perform such computation we adopted the loop-by-loop analysis [171, 172] of the Baikov [173] representation of the integral, we refer to refs. [171–174] for a description of the method. In order to emphasize the common features between the solution of the non-planar triangle and the double-box one, we also provide the maximal cut of the former. The results for the maximal cut of the two non-planar integrals read

$$\text{MCut}\left(I_{\text{NPA}}(1,1,1,0,0,1,1,1,0)\right) \propto \int \frac{\mathrm{d}z}{\sqrt{z(z+s)(z-z_+)(z-z_-)}}, \tag{3.58}$$

$$\text{MCut}\left(I_{\text{NPA}}(1,1,1,1,0,1,1,1,0)\right) \propto \int \frac{\mathrm{d}z}{(z-t)\sqrt{z(z+s)(z-z_+)(z-z_-)}}, \tag{3.59}$$

where $z_\pm = \frac{1}{2}\left(-s \pm \sqrt{s(s+16m_t^2)}\right)$, and we dropped overall terms which do not depend on z since they are immaterial for a qualitative study. As we can see from Eq. (3.59) the result of the maximal cut for the double box non planar integral in fig. 3.8 (b) is a one-fold integral. It is possible to show that Eq. (3.59) can be written in terms of complete elliptic integrals of first and third kind, where the elliptic curve is given by the polynomial of fourth-order in the integration variable z:

$$y^2 = z(z+s)(z-z_+)(z-z_-). \tag{3.60}$$

We observe that the elliptic curve (3.60) is the same curve of the non-planar triangle in fig. 3.8 (a) [141, 152, 164].

3.2 Top-quark mass dependence in diphoton production at NNLO in QCD

In this section, we consider diphoton production at NNLO, taking into account the full top quark mass dependence [116]. We include all NNLO massive contributions to the cross section: the box contribution in the gluon fusion channel [78], the two-loop corrections to $q\bar{q} \to \gamma\gamma$ [4] described in the previous section, and the real radiation contributions (double

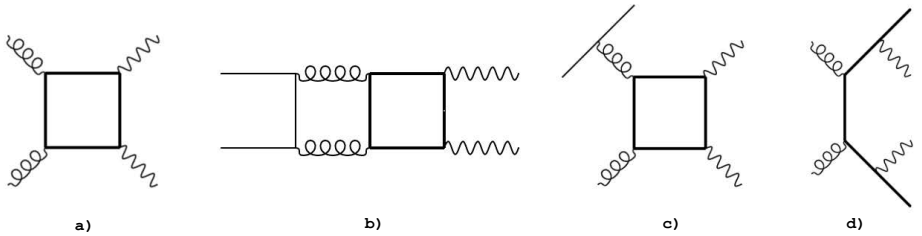

Figure 3.12. *Different types of contributions to the massive corrections at NNLO for diphoton production in perturbative QCD. The explanation of the different features is given in the text.*

real and real-virtual).

In 3.2.1 we explain the setup of our calculation and in 3.2.2 we present selected numerical results for the LHC phenomenology.

3.2.1 Organisation of the calculation

Since the massless (five light quark flavours) NNLO QCD corrections to diphoton production are known [77], our approach is to consider all the remaining massive scattering amplitudes and combine them in an appropriate way.

The first non-trivial massive corrections appear at NNLO. We classify the scattering amplitudes into four types of contributions. In first place, we consider the known massive one-loop box scattering amplitude $gg \to \gamma\gamma$ [78] as depicted in Fig. 3.12 `a)`. The two-loop (double-virtual) corrections to the Born sub-process $q\bar{q} \to \gamma\gamma$ [4] are shown with a representative Feynman diagram in Fig. 3.12 `b)`, where in the loop we consider a massive top quark. We also consider massive real-virtual contributions to diphoton production (see Fig. 3.12 `c)`), where the diphoton pair is produced in association with real radiation (quarks and gluons). This scattering amplitude is interfered with the corresponding tree-level matrix element ($q\bar{q} \to \gamma\gamma g$ or $qg \to \gamma\gamma q$ depending on the partonic channel). The partonic contributions to Fig. 3.12 `c)` are finite, not only in four dimensions, but also after integration over the transverse momentum of the diphoton pair ($p_T^{\gamma\gamma}$). This amplitude is presented in the appendix of ref. [78], but it is considered for its squared modulus (effective N^{3}LO contribution). In our case we calculated this contribution and we checked it numerically with `OpenLoops` [6, 175–179]. The last element that we considered (which completes the NNLO massive corrections) is shown in Fig. 3.12 `d)`; it is related to diphoton production in association to the emission of two on-shell top-quarks ($q\bar{q} \to \gamma\gamma t\bar{t}$ and $gg \to \gamma\gamma t\bar{t}$). We computed these double-real amplitudes and we checked them numerically with `OpenLoops`. Although this sub-process can be effectively detected experimentally and (therefore) then subtracted, we include it explicitly in our calculation. Indeed, LHC measurements of diphoton production take into account any kind of additional radiation accompanying the two isolated photons, and therefore this contribution must be taken into account in any comparison with LHC data [57–60] that claim full NNLO QCD massive corrections.

All our massive corrections are encoded in a new version of the 2γ`NNLO` code [77], which has been cross-checked with the `MATRIX` [180] numerical code (version 2.0.0) (which includes

the massless NNLO QCD corrections to diphoton production). The new version of the 2γNNLO code benefits from the fast integration routines of the DYTurbo framework [181, 182].

The double-real and real-virtual sub-processes (see Fig. 3.12 c) and d)) are not only finite in four dimensions, but they are also finite after integration over the transverse momentum of the diphoton pair. We have checked numerically that under q_T integration these contributions are finite and numerically stable in the whole q_T range.

3.2.2 NNLO results with full top-quark mass dependence

In this section, we present our results for the diphoton production at NNLO in perturbative QCD, taking into account the full top-quark mass dependence. We fix the pole mass m_t of the top quark to the value $m_t = 173$ GeV. Our computational setup that was explained in 3.2.1, has been encoded in a new version of the 2γNNLO code.

We consider isolated diphoton production in pp collisions at the centre–of–mass energy $\sqrt{s} = 13$ TeV. We apply the following kinematical cuts on photon transverse momenta and rapidities: $p_{T\gamma}^{\rm hard} \geq 40$ GeV, $p_{T\gamma}^{\rm soft} \geq 30$ GeV and the rapidity of both photons is limited in the range $|y_\gamma| < 2.37$, excluding the rapidity interval $1.37 < |y_\gamma| < 1.52$. The minimum angular separation between the two photons is $R_{\gamma\gamma}^{\rm min} = 0.4$. These are essentially the kinematical cuts used in the ATLAS Collaboration study of ref. [57].

In the perturbative calculation, the QED coupling constant α is fixed at $1/\alpha = 137.035999139$. We use the central set of the NNPDF3.1 PDFs [183] as implemented in the LHAPDF framework [184] and the associated strong coupling with $\alpha_s(M_Z) = 0.118$.

The central factorization and renormalization scale is chosen to be equal to the invariant mass of the diphoton pair $\mu \equiv \mu_R = \mu_F = M_{\gamma\gamma}$. The theoretical uncertainty is estimated by varying the default scale choice for μ_R and μ_F independently by factors of $\{1/2, 2\}$, while omitting combinations with $\mu_R/\mu_F = 4$ or $1/4$, resulting in the usual seven-point variation of scale combinations. Our standard choice of the central scale, can be replaced with other options, for instance the transverse mass of the diphoton pair, $M_{\gamma\gamma}^{\rm T} = \sqrt{(M_{\gamma\gamma})^2 + (p_T^{\gamma\gamma})^2}$. Since our aim is to show the impact of the new massive corrections, we refer the reader to more detailed studies on scale variation (and scale choices) to refs. [79, 80].

We use the smooth cone isolation criterion [185] (see also refs. [79, 186, 187]), which fixes the size R of the isolation cone (drawn around the direction of the photon) and requires that the hadronic activity E_T^{had} allowed inside the cone satisfies

$$E_T^{had}(r) \leq \epsilon\ p_{T\gamma}\ \chi(r;R)\ , \qquad \text{in } \textit{all} \text{ cones with } r \leq R\ , \tag{3.61}$$

where the function $\chi(r;R)$ is defined as

$$\chi(r;R) = \left(\frac{r}{R}\right)^{2n}\ . \tag{3.62}$$

The specific values of the isolation parameters in our case [57] are: $R = 0.4$, $\epsilon = 0.09$ and we take $n = 1$. The choice of the $\chi(r;R)$ function as well as the particular value of the exponent n is explained in ref. [79]. Since our aim is to present the effects of massive corrections, we suggest that the interested reader consult the isolation studies in refs. [79, 80]. The top quark

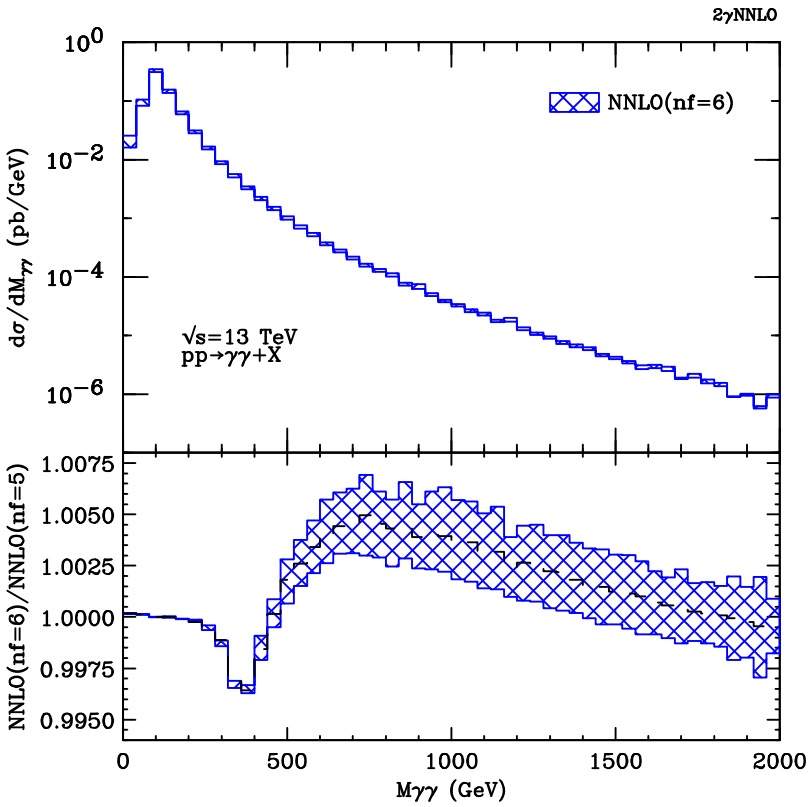

Figure 3.13. *NNLO invariant mass distribution with full top quark mass dependence. In the lower panel we plot the ratio of the NNLO invariant mass distribution between the massive result and that with only five light quark flavours. The bands are obtained (as explained in the text) using the customary 7-point scale variation. The central scale is shown with a black dashed line.*

threshold region (~ 346 GeV) is not particularly sensitive to the effects of the choice of isolation parameters [79].

Since we rely on the q_T subtraction method [154, 155] to perform our NNLO calculations, we use the technical parameter[8] (a cut on the transverse momentum of the diphoton pair) $r_{\rm cut} = 0.0005 < p_T^{\gamma\gamma}/M_{\gamma\gamma}$. The large diphoton invariant mass tail is not particularly sensitive to $r_{\rm cut}$ variations around our chosen value [180]. Studies on the impact of the fiducial power corrections and on the size of the $r_{\rm cut}$ parameter in colour singlet processes can be found in refs. [180, 188–190].

The rest of this section proceeds as follows: first, we anticipate our results for diphoton production at NNLO in perturbative QCD, taking into account the full top quark mass dependence. At the end of this section, we discuss the relative weight of the different massive contributions involved in the NNLO calculation.

In Fig. 3.13 we present our results regarding the invariant mass distribution of the photon pair at NNLO using the kinematical cuts described above. In the lower panel, we show the ratio between the fully massive NNLO result and the NNLO prediction for five light quark flavours (5lf). Around the region $M_{\gamma\gamma} \sim 2m_t$ (the top-quark pair threshold), the invariant

[8] We have also checked that in the extrapolation to $r_{\rm cut} = 0$ the associated results for the total cross sections and the differential distributions vary less than 1% when $r_{\rm cut} = 0.0005$ is used.

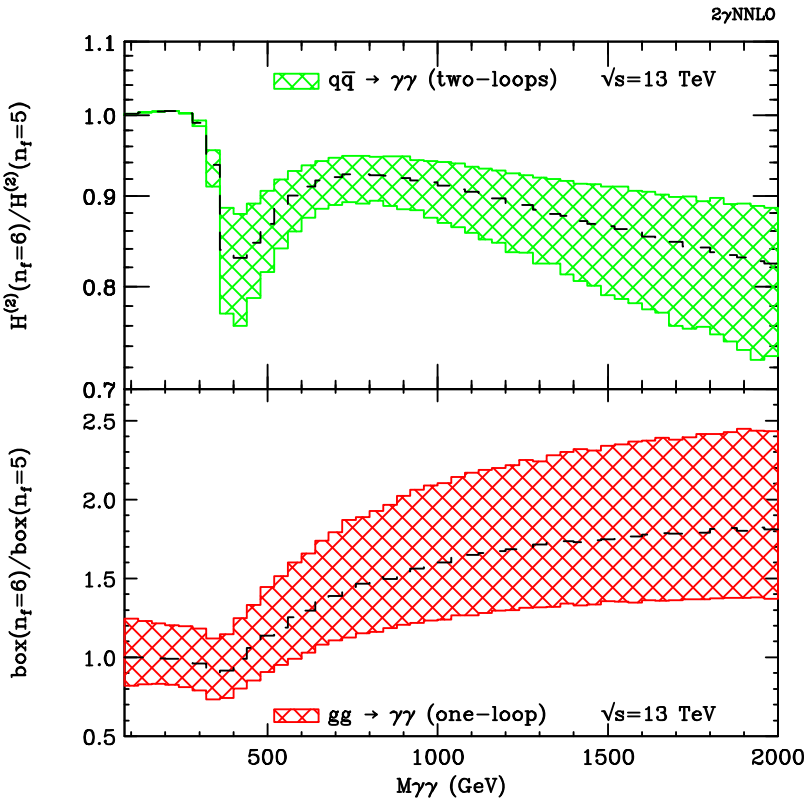

Figure 3.14. *Ratios of diverse massive corrections to the massless case. In the upper panel we show the ratio of the two-loop ($q\bar{q} \to \gamma\gamma$) massive contribution to the massless one. In the lower panel we show the corresponding ratio but for the 1-loop box ($gg \to \gamma\gamma$) contribution. The central scale is shown with a black dashed line.*

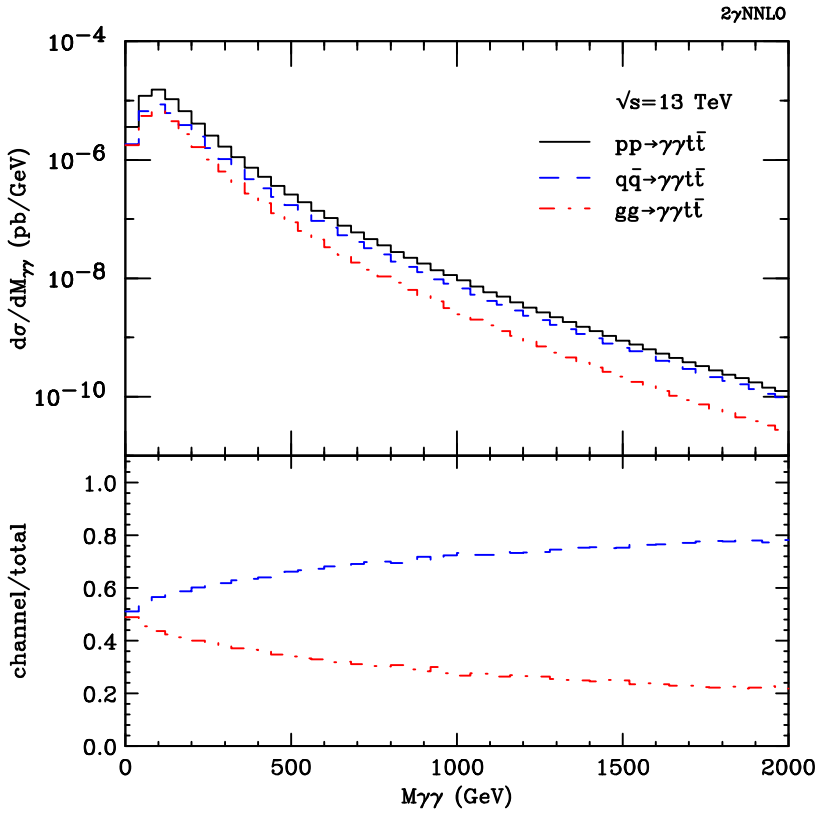

Figure 3.15. *Invariant mass distribution of the double-real ($pp \to \gamma\gamma t\bar{t}$) contribution to the NNLO fully massive result. In the lower panel we show the relative size of each one of the partonic channels that form the total double-real contribution. Only central scale results are shown.*

mass distribution exhibits its negative peak [9] due to a superposition of effects coming from the loop contributions. In the low-mass region ($M_{\gamma\gamma} < 2m_t$), the massive result is still slightly larger than the massless case since the real corrections can resolve the top quark loop because the total centre–of–mass energy can be larger than $2m_t$ [114]. Beyond the negative peak, the massive NNLO prediction presents its maximum (positive) deviation from the massless result at about 2.3 times of the value of the top quark pair threshold. The position (and shape) of this positive peak is the result of a competition between two opposite behaviours of (mainly) two contributions: the box scattering amplitude (gg-channel) and the two-loop form factor ($q\bar{q}$-channel) (see Fig. 3.14). We postpone the discussion of the decreasing tail in the ratio between the massive and massless result, to the end of this section. The effect of the massive corrections (within the fiducial cuts discussed above) in the invariant mass from 1 GeV to 2 TeV is a deviation from the massless result in the range [-0.4%, 0.8%]. The effect may be larger if we use different selection cuts and for values of $M_{\gamma\gamma} > 2$ TeV.

We now comment on the two-loop contribution to the NNLO invariant mass distribution[10], underlining the common features with the one-loop contribution in gluon-fusion channel. In Fig. 3.14 (upper panel) we show the ratio between the fully massive two-loop contribution and the massless case. The ratio is performed explicitly using the hard virtual factors $H^{(2)}$ defined in the *hard resummation scheme* as explained in ref. [155] and in our paper of the two-loop massive form factors [4], reported also in 3.1. The bands are computed implementing the usual 7-point scale variation as described above. As we can see from both of the panels in Fig. 3.14, in the region below the top-quark threshold ($M_{\gamma\gamma} < 2m_t$) the presence of a heavy-quark flavour inhibits the effect that would have a 6^{th} massless flavour. As in any massive loop contribution, the ratio exhibits the typical peak around the top quark threshold. In this region of the invariant mass the perturbative result mimics the production of a top-antitop pair on-shell which would tend to enhance the cross-section. This effect, combined with the common destructive interference between massive and massless amplitudes, results in a negative peak around the top-quark threshold. The size of both ratios, one-loop gg and two-loop, around the negative peak is quantitatively similar and amounts to roughly -15%. For invariant masses larger than $2m_t$ (and after a peak around $M_{\gamma\gamma} \sim 2.3 \times 2m_t$), the tail decreases. At this point we observed also, that the massless two-loop contribution obtained with six light quark flavours is smaller (in the whole invariant mass range) than the result with five light flavours and a massive one, confirming the mitigating effect of the top-mass. Moreover, at large invariant masses, the ratio between the massless results ($H^{(2)}(n_f = 6\text{lf})/H^{(2)}(n_f = 5)$) tends to get closer, as expected, to the corresponding massive result shown in Fig. 3.14 top panel. We postpone to future developments an exploration to larger values of the photon-pair invariant mass, which would allow us to determine the region where the massive and the six-flavour massless result overlap.

In the bottom panel of Fig. 3.14 we show the known behaviour of the ratio between the fully massive one-loop box contribution and the corresponding contribution with five light quark flavours. In the gluon-fusion channel there are two kinds of massive contributions:

[9] In the ratios, the corrections larger (smaller) than the unity are named *positive* (*negative*) since they are larger (smaller) than the five light flavour result.

[10] The representative Feynman diagram of this two-loop contribution is shown in Fig. 3.12 b).

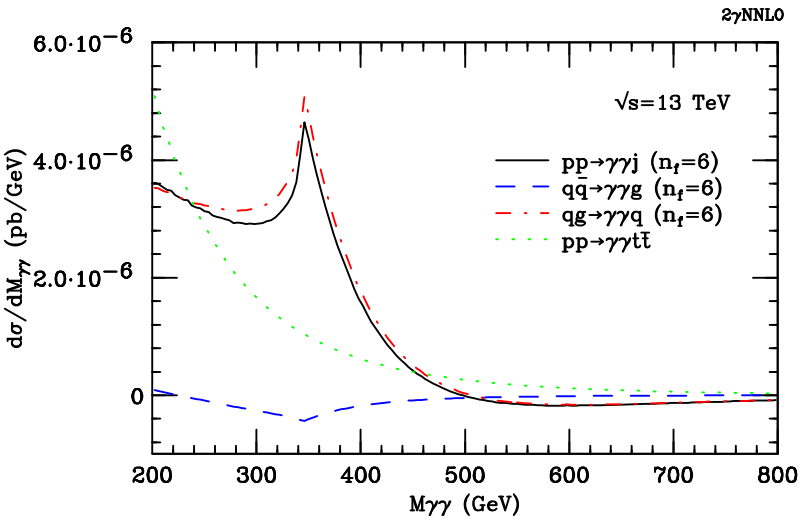

Figure 3.16. *Invariant mass distribution of the one-loop real emission massive contribution at NNLO. Only the massive top quark circulates in the loop. The light quark flavours are already considered in the massless part of the calculation. We show the different partonic channels and a comparison with the size of the double real correction shown in Fig. 3.15.*

the interference between the massless one-loop box and the massive one, and the squared modulus of the massive one-loop box. In this case, for large values of $M_{\gamma\gamma} \gg m_t$, the ratio asymptotically[11] approaches the value

$$\frac{\left(\sum_{n_f=6} Q_q^2\right)^2}{\left(\sum_{n_f=5} Q_q^2\right)^2} = \frac{225}{121}, \tag{3.63}$$

implying that the massive contribution behaves as if it were composed of 6 light quark flavours [78]. The one-loop in gluon-fusion and two-loop in quark channel are the two most sizable massive contributions at NNLO accuracy. The distinctive and opposite behaviour of these two contributions at large values of $M_{\gamma\gamma}$ (taking into account also the vanishing luminosity of the gluon) determines the position of the positive peak in the ratio of Fig. 3.13.

We now consider the massive double real corrections ($pp \to \gamma\gamma t\bar{t} + X$). In Fig. 3.15 we show the invariant mass distribution obtained from the partonic sub-processes $gg \to \gamma\gamma t\bar{t}$ and $q\bar{q} \to \gamma\gamma t\bar{t}$. Since we produce two on-shell top quarks, and since we are dealing with tree-level scattering amplitudes, there is no top quark threshold in the distribution (it has a continuously decreasing (logarithmic) tail as in the massless case). The only peak in this invariant mass distribution is due to kinematic effects (it peaks at about $2 \times p_{T\gamma}^{\text{hard cut}} = 80$ GeV, as in the massless case). This kinematic effect is explained in detail in ref. [79] for the massless result. In the bottom panel of Fig. 3.15 we show the relative size of the different channels (the $q\bar{q}$ and gg channels) with respect to the total. For large values of $M_{\gamma\gamma}$ the luminosity of the gluon decreases and the total contribution is (mainly) due to the $q\bar{q}$ channel. The vanishing

[11] For the kinematical cuts considered here, the asymptotic regime is reached at (roughly) 3 TeV, which is not shown in these plots.

luminosity (at large invariant masses) of the gluon explains why the $q\bar{q}$ channel dominates at large values of $M_{\gamma\gamma}$ in the total NNLO invariant mass distribution. The prevalence of the $q\bar{q}$ channel in the tail, explains why the ratio in Fig. 3.13 decreases at large values of $M_{\gamma\gamma}$, even though the fully massive box contribution (gg channel) is almost twice the massless box in the tail (see Fig. 3.14 bottom panel). At large invariant masses the partonic channels containing at least one gluon vanish and the massive real corrections are almost negligible. Conversely, the negative corrections coming from the $q\bar{q}$ channel (massive two-loop contribution) are still present, and in the full result the ratio turns out to be negative in this kinematic region (see the ratio in Fig. 3.13 around $M_{\gamma\gamma} \sim 2$ TeV).

In the following, we discuss the real-virtual contribution of the one-loop NNLO massive corrections to diphoton production ($pp \to \gamma\gamma j + X$). In Fig. 3.16 we compare the invariant mass distribution of the different channels with respect to the total correction. The $q\bar{q}$ and qg channels show very different behaviour (being the qg initiated sub process the channel that dominates the contribution around the top quark threshold). The positive peak behaviour around the top quark threshold is also found in the box contribution when only a massive top quark is circulating in the loop [114]. As the remaining five light flavours are also included in the loop, the destructive interference between these two types of terms dominates the box contribution, producing the typical negative peak (as it is shown in Fig. 3.14 bottom panel).

Here (in the real-virtual case), since the one-loop scattering amplitudes (see Fig. 3.12 c)) are interfered with the corresponding tree-level matrix elements, there is no such mixing between massive and massless quarks circulating through the loop. For large values of the invariant mass ($M_{\gamma\gamma} > 500$ GeV) the contribution of the real-virtual term is negative, slightly enhancing the decreasing behaviour in the tail of the ratio in Fig. 3.13.

In Fig. 3.16 we also show the contribution of the whole $pp \to \gamma\gamma t\bar{t} + X$ sub-process. The size of the real-virtual and the double-real contributions are roughly of the same order, and they are subdominant with respect to the one-loop box and two-loop form factors.

Finally, in Fig. 3.17 we show the ratios of each of the massive contributions (schematically drawn in Fig. 3.12) with respect to the massless NNLO differential prediction. As expected from the previous paragraphs, the two-loop $q\bar{q}$ (dot-dashed black line) and the one-loop box corrections (solid red line) dominate throughout the invariant mass range. The effect of the real-virtual contribution (dashed green line) is subdominant and reduces the size of the negative peak at the top quark threshold. The effect of the massive double real corrections (emission of two on-shell top quarks) is tiny and not relevant for the phenomenology (dotted blue line). The correction introduced by the two-loop massive contribution at large values of the invariant mass is negative and reduces the cross section. For $M_{\gamma\gamma} > 2$ TeV it is the dominant massive effect.

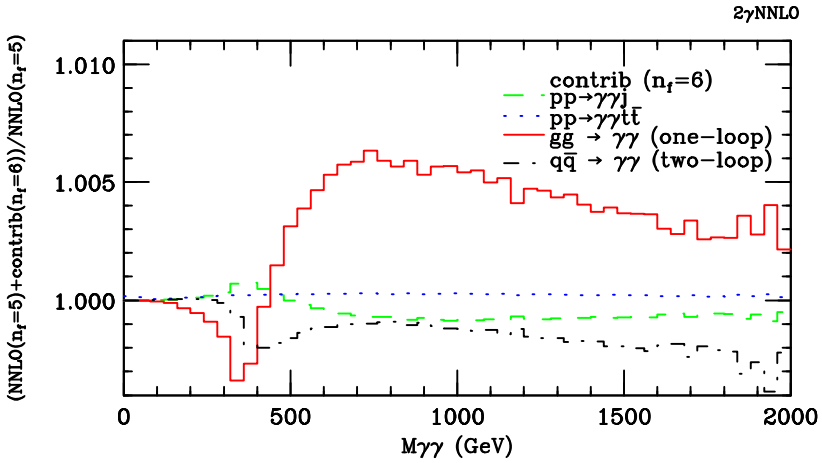

Figure 3.17. *Ratios of each one of the massive contributions with respect to the NNLO massless cross section as a function of the invariant mass.*

Chapter 4

Two-loop mixed QCD-EW corrections to quark-induced Higgs production at hadron colliders

After the discovery of the Higgs boson with the Large Hadron Collider (LHC) at CERN in 2012 [1, 191], the work of the LHC community has focused on the study of the Higgs sector, which provides a stringent test of the Standard Model of particles (SM) and a fertile environment for the search of New Physics (NP) signals [192–204].

Two of the most relevant observables in Higgs studies are the Higgs total cross section and the Higgs transverse momentum (p_T) distribution. The dominant Higgs production mode at the LHC is the gluon fusion channel. In the production via gluon fusion, the coupling of the Higgs boson to gluons is mediated by a heavy-quark loop. This gives the opportunity to test the Standard Model of particles and to look for possible deviations from it, if the NP particles couple to the Higgs boson. Since Higgs coupling with the gluons is proportional to the Yukawa coupling y_Q, and thus to the mass m_Q, of the heavy quark circulating in the loop, in the Standard Model the largest contribution comes from the top-quark loop, making the Higgs production cross section roughly proportional to y_t^2.

The Higgs production cross section was computed at leading order in the '70s [205], and at next-to-leading-order (NLO) in strong coupling constant α_s in the '90s [206, 207], where the exact dependence on the heavy-quark mass has been retained. NLO QCD corrections are sizable ($\sim 100\%$) and considering higher-orders is thus indispensable. The next-to-next-to-leading-order (NNLO) [208–210] and the next-next-to-next-to-leading-order (N^{3}LO) [211, 212] corrections in α_s have been computed in the Higgs Effective Field Theory (HEFT) approach, i.e. in the limit of a top quark much heavier than the Higgs boson, $m_t \gg m_h$, assuming all other quarks are massless. HEFT replaces the loop-mediated coupling by an effective tree-level coupling, reducing by one both the number of loops and the number of scales in the computation of the relevant amplitudes. NNLO and N^{3}LO corrections are found to be respectively of the order of $\sim 20\%$ and $\sim 3\%$ of the cross section.

The NNLO and N^{3}LO corrections in α_s to the Higgs total cross section are respectively $\mathcal{O}\left(\alpha\alpha_s^4\right)$ and $\mathcal{O}\left(\alpha\alpha_s^5\right)$. Since $\alpha \sim \alpha_s^2$, the last two corrections call the mixed QCD-Electroweak

(QCD-EW) contribution, which starts at $\mathcal{O}\left(\alpha^2\alpha_s^2\right)$, and the corresponding NLO corrections in α_s ($\mathcal{O}\left(\alpha^2\alpha_s^3\right)$). In the light-quark mixed QCD-EW contribution the Higgs is produced through its gauge coupling to the EW bosons $V = W, Z$. Introducing a heavy quark, we open other two channels for Higgs production: the Yukawa coupling to the heavy quark and the trilinear self-coupling. Mixed QCD-EW contribution with full heavy-quark mass dependence [213–216] increases the N^{3}LO cross section by about 2% [217]. As for QCD corrections also for the QCD-EW contribution the dominant mode for the Higgs production is the gluon fusion channel because of the high gluon luminosity at LHC. Since the largest part ($\sim 98\%$) of the increase at $\mathcal{O}\left(\alpha^2\alpha_s^2\right)$ is due to the light-quark part of the mixed QCD-EW contribution, the evaluation of the NLO corrections has been aimed at the light-quark part. These have been computed in [218] for $gg \to H$, and, as it is usual for QCD NLO corrections in gluon channel, turned out to be sizeable, in this case of the same magnitude of the $\mathcal{O}\left(\alpha^2\alpha_s^2\right)$ contribution. Briefly, mixed QCD-EW corrections (LO+NLO) increase of $\sim 5\%$ the total Higgs cross section.

In [217] all the main effects mentioned so far have been combined, where approximated results have been used for those that had not yet been determined. As result the following prediction for the gluon-fusion cross-section at the LHC, with a center-of-mass energy of 13 TeV, for a Higgs boson with a mass $m_h = 125$ GeV, was presented:

$$\sigma = 48.58\,\text{pb}^{+2.22\,\text{pb}\,(+4.56\%)}_{-3.27\,\text{pb}\,(-6.72\%)}\ (\text{theory}) \pm 1.56\,\text{pb}\,(3.20\%)\ (\text{PDF}+\alpha_s)\,. \tag{4.1}$$

The breakdown of the different effects is:

$$\begin{aligned}
48.58\,\text{pb} = \quad & 16.00\,\text{pb} && (+32.9\%) && (\text{LO, rHEFT}) \\
+\,& 20.84\,\text{pb} && (+42.9\%) && (\text{NLO, rHEFT}) \\
-\,& 2.05\,\text{pb} && (-4.2\%) && ((t,b,c), \text{exact NLO}) \\
+\,& 9.56\,\text{pb} && (+19.7\%) && (\text{NNLO, rHEFT}) \\
+\,& 0.34\,\text{pb} && (+0.2\%) && (\text{NNLO, } 1/m_t) \\
+\,& 2.40\,\text{pb} && (+4.9\%) && (\text{EW, QCD-EW}) \\
+\,& 1.49\,\text{pb} && (+3.1\%) && (\text{N}^3\text{LO, rHEFT}),
\end{aligned} \tag{4.2}$$

where rHEFT is the contribution in the large-m_t limit, rescaled by the ratio R_{LO} of the exact LO cross-section by the cross-section in the HEFT:

$$R_{LO} = \frac{\sigma^{LO}_{ex;t}}{\sigma^{LO}_{EFT}} = 1.063. \tag{4.3}$$

Specifically, the first line, (LO, rHEFT), is the cross-section at LO taking into account only the top quark. The second line, (NLO, rHEFT), are the NLO corrections in the rescaled HEFT, and the third line, ((t, b, c), exact NLO), is the correction that needs to be added to the first two lines in order to obtain the exact QCD cross-section through NLO, including the full dependence on top, bottom and charm quark masses. The fourth and fifth lines contain the NNLO QCD corrections in the rescaled HEFT: (NNLO, rHEFT) denotes the

NNLO corrections in the HEFT rescaled by R_{LO}, and (NNLO, $1/m_t$) contains subleading corrections in the top mass at NNLO computed as an expansion in $1/m_t$. The sixth line, (EW, QCD-EW), contains the two-loop electroweak corrections, computed exactly, and three-loop mixed QCD-electroweak corrections, computed in an effective theory approach. The last line, ($\mathrm{N^3LO}$, rHEFT), contains the $\mathrm{N^3LO}$ corrections rescaled by R_{LO}. Resummation effects contribute at the per mille level and are therefore negligible.

Physical effects of the exact dependence on the quark masses beyond NLO ($\mathcal{O}\left(\alpha_s^3\right)$) have been considered for a few years. The one-loop Higgs + 4 partons amplitudes with exact dependence on the heavy-quark mass have been computed in [219] and [220]. The three-loop $gg \to H$ amplitudes have been computed in [221] with only one top loop, and in [222] with one and two top loops, while in [223] two scales amplitudes, with a loop of top-quark and a loop of bottom-quark, have been considered. However the main obstacle when calculating the total cross section with full heavy-quark mass dependence are the two-loop Higgs + 3 partons amplitudes. These have been calculated numerically in [224] and [225], and semi-analytically in the form of one-dimensional generalised power series in [226]. In [225] the phenomenological impact of the full top-quark mass dependence on the total cross section has been studied, and in [227] also the top-bottom interference has been included. The NNLO ($\mathcal{O}\left(\alpha_s^4\right)$) top correction is found to raise the central value of $\sim 0.3\%$, while top-bottom interference at the same perturbative order increases the cross section of $\sim 1\%$. It has also been noticed that top-bottom interference is as large at ($\mathcal{O}\left(\alpha_s^4\right)$) as it is at ($\mathcal{O}\left(\alpha_s^3\right)$), but with opposite sign. On the other hand, the NNLO top correction is smaller than the NLO one, with still an opposite sign.

If, from the QCD frontier, one aims to better understand the quark masses effects, also the electroweak corrections are being studied, in particular the efforts are focused on the reduction of the theoretical uncertainty coming from the NLO mixed QCD-EW corrections. To this task, the attempts of the community go towards the computation of the relevant two-loop one real emission amplitudes in all the partonic channels with an exact dependence on the electroweak boson masses. The $\mathcal{O}\left(\alpha^2\alpha_s^3\right)$ corrections consist of three parts: the one-loop $2 \to 3$, the three-loop $2 \to 1$, and the two-loop $2 \to 2$. In [228], the one-loop $2 \to 3$ processes were computed and found to yield a negligible contribution. The three-loop contribution was evaluated analytically and expressed in terms of multiple polylogarithms (MPLs) [229]. In [230], the two-loop $2 \to 2$ process in the soft emission approximation was added and in [231] the total cross section was evaluated in the small EW-boson mass limit $m_V \ll m_h$. The complete helicity amplitudes, with the exact EW-boson mass, for $gg \to Hg$ were presented in [232], where the calculation was done analytically, expressing the results in terms of MPLs. In [233] an independent computation of the same amplitudes, based on the series solution method of [32], was done.

Including the two-loop real-emission $gg \to Hg$ with exact EW-boson mass dependence, the EW contribution to the Higgs cross section in gluon fusion channel at LHC13 is [233]:

$$\sigma_{gg\to H+X}^{(\alpha_s^2\alpha^2+\alpha_s^3\alpha^2)} = 1.467(2)\,{}^{+18.7\%}_{-14.6\%}\ (\mu_R \text{ var.})\ \pm 2\%\ (\text{PDF})\ \text{pb}\,,$$

which represents 5.1% of the NLO QCD cross section, result very close to the 5.2% obtained in

the infinite weak boson mass limit [231]. This result therefore allowed to reduce the uncertainty of $\pm 1\%$ assigned previously to the EW gluon-induced contribution in order to reflect the absence of an exact weak boson mass treatment at NLO. Furthermore, the rescaling of the cross section with higher-order QCD corrections, computed in HEFT, and the evaluation of other partially unknown effects yields the best estimate of $6.91 \pm 0.93\%$ (relative to the gluon-induced NLO QCD) for all the corrections of EW origin to Higgs production at LHC [233].

At this stage an important source of uncertainty comes from the NLO quark-induced EW contribution. The relevant two-loop amplitudes, $qg \to Hq$, $\bar{q}g \to H\bar{q}$ and $q\bar{q} \to Hg$, with exact EW-boson mass dependence, have been computed analytically and expressed in terms of multiple polylogarithms (MPLs) in [234]. However the complexity of the amplitudes results in a large evaluation time: for a single point in the phase space and requiring 20 digits accuracy the evaluation with `Ginac` [27] takes about 30 minutes. Then, in order to reduce the evaluation time and facilitate a phenomenological study of the NLO quark-induced EW corrections, we performed an independent calculation of $qg \to Hq$, and crossed channels, where the relevant MIs have been computed exploiting the differential equations method and one-dimension generalised power series expansions.

In 4.1 we describe the structure of the light-quark two-loop amplitude $qg \to Hq$. We discuss the form factors computation along with their UV and IR singularity structure. In 4.2 we report on the MIs calculation, describing the basis and the system of differential equations.

4.1 Amplitude structure

We consider the light-quark part of the NLO quark-induced EW corrections to Higgs production with one real emission, retaining the exact electroweak-boson mass dependence. At the partonic level, the relevant two-loop scattering amplitudes are $gq \to Hq$, $g\bar{q} \to H\bar{q}$ and $q\bar{q} \to Hg$. We computed the first of them and obtained the others by crossing. We assigned the momenta as follows,

$$g(p_1) + q(p_2) \to q(p_3) + H(p_4). \tag{4.4}$$

The kinematics for this process is described by the Mandelstam variables

$$s = (p_1 + p_2)^2, \quad t = (p_1 - p_3)^2, \quad u = (p_2 - p_3)^2, \text{ with } s + t + u = m_h^2, \tag{4.5}$$

where the external particles are on-shell, i.e. $p_1^2 = p_2^2 = p_3^2 = 0$ and $p_4^2 = m_h^2$, and we indicate with m_h and m_W (m_Z) respectively the Higgs and W (Z) mass. The bare scattering amplitude can be written as

$$\mathcal{M}_{gq,Hq} = (2\pi)^4 \left(\frac{i\,\alpha^{3/2} m_W}{2\sin^3\theta_W} \right) i\,T^a_{ij}\,\epsilon^{\mu}_{\lambda_1}(p_1)\,\overline{u}_{s_3}(p_3)\mathcal{A}_{\mu} u_{s_2}(p_2), \tag{4.6}$$

where T^a_{ij} is the generator of the fundamental representation of $SU(N_c)$ (being N_c the number of colors), with a and $i(j)$ the color indices of the gluon and the outgoing (incoming) quark respectively, α is the QED coupling and θ_W the Weinberg angle, $\epsilon^{\mu}_{\lambda_1}(p_1)$ is the gluon polarisation

and $\overline{u}_{s_3}(p_3)$, $u_{s_2}(p_2)$ the quark spinors.

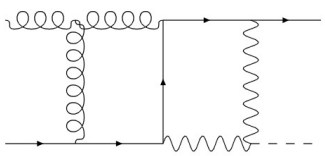

Figure 4.1. (a)

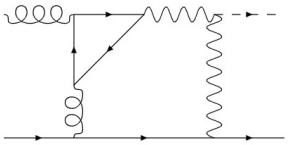

Figure 4.2. (b)

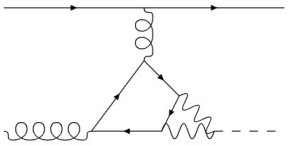

Figure 4.3. (c)

Figure 4.4. Representative diagrams contributing to the amplitude $gq \to Hq$.

The Feynman diagrams which contribute to the amplitude are of two classes: the diagrams which contain a fermion loop, and the diagrams which have only an open fermion current. We will refer to the latter as "open" diagrams, and to the former as "closed" diagrams. A representative open diagram is shown in fig. 4.1, while fig. 4.2 and 4.3 show two closed diagrams. The amplitude will be the sum of the two contributions,

$$\mathcal{A}_\mu = \mathcal{A}_\mu^{\text{open}} + \mathcal{A}_\mu^{\text{closed}}. \tag{4.7}$$

The contribution to the amplitude coming from the open diagrams, $\mathcal{A}_\mu^{\text{open}}$, can be decomposed in a left-handed and a right-handed part

$$\mathcal{A}_\mu^{\text{open}} = \mathcal{A}_{L,\mu}^{\text{open}} + \mathcal{A}_{R,\mu}^{\text{open}}. \tag{4.8}$$

The left-handed (L) and the right-handed (R) projectors are defined as

$$\mathbb{P}_L = \frac{\mathbb{I} - \gamma_5}{2}, \qquad \mathbb{P}_R = \frac{\mathbb{I} + \gamma_5}{2}. \tag{4.9}$$

The left-handed open fermion current reads

$$\overline{u}_{s_3}(p_3)\Gamma_1\gamma^\alpha(g_V^v + \gamma_5 g_V^a)\gamma^\delta\Gamma_2\gamma^\beta(g_V^v + \gamma_5 g_V^a)\Gamma_3\mathbb{P}_L u_{s_2}(p_2), \tag{4.10}$$

where Γ_1, Γ_2 and Γ_3 are chains of an even number of γ matrices and $\gamma^\mu(g_V^v + \gamma_5 g_V^a)$ is the coupling of the electroweak boson V with the quark. As always, in our computation we use dimensional regularization with $d = 4 - 2\epsilon$. Furthermore, we adopted the naive dimensional regularization scheme (NDR) [235] which assumes that the usual anticommutation relations valid in four dimensions hold also in d dimensions

$$\{\gamma_\mu, \gamma_\nu\} = 2g_{\mu\nu}, \qquad \{\gamma_\mu, \gamma_5\} = 0, \qquad \gamma_5^2 = \mathbb{I}. \tag{4.11}$$

Anticommuting γ_5 in (4.10) until it gets contracted with a chiral projector, and using $\gamma_5\mathbb{P}_L = -\mathbb{P}_L$, the open fermion current can be written as

$$(g_V^v - g_V^a)^2\,\overline{u}_{s_3}(p_3)\Gamma_1\gamma^\alpha\gamma^\delta\Gamma_2\gamma^\beta\Gamma_3\mathbb{P}_L u_{s_2}(p_2). \tag{4.12}$$

Similarly, the right-handed open fermion current,

$$\overline{u}_{s_3}(p_3)\Gamma_1\gamma^\alpha(g_V^v + \gamma_5 g_V^a)\gamma^\delta\Gamma_2\gamma^\beta(g_V^v + \gamma_5 g_V^a)\Gamma_3\mathbb{P}_R u_{s_2}(p_2), \tag{4.13}$$

can be written as

$$(g_V^v + g_V^a)^2\, \overline{u}_{s_3}(p_3)\Gamma_1\gamma^\alpha\gamma^\delta\Gamma_2\gamma^\beta\Gamma_3\mathbb{P}_R u_{s_2}(p_2). \tag{4.14}$$

From (4.12) and (4.14) we observe that we can replace the electroweak boson coupling with an effective vector coupling: $(g_V^v - g_V^a)\gamma^\mu$ for the left-handed open amplitude and $(g_V^v + g_V^a)\gamma^\mu$ for the right-handed one. Then the computation proceeds through the usual techniques that we would adopt in the pure QCD case: determine the tensor structures, construct and apply projectors to extract the form factors. We adopt the 't Hooft Veltman scheme with four-dimensional external states. So we have two independent four-dimensional tensors

$$\mathcal{T}_1 = \epsilon^\mu_{\lambda_1}(p_1)\, \overline{u}(p_3)\, \tau_{1,\mu}\, u(p_2), \tag{4.15}$$

$$\mathcal{T}_2 = \epsilon^\mu_{\lambda_1}(p_1)\, \overline{u}(p_3)\, \tau_{2,\mu}\, u(p_2), \tag{4.16}$$

where

$$\tau_{1,\mu} = \not{p}_1 p_{2\mu} - p_2 \cdot p_1 \gamma_\mu\,, \qquad \tau_{2,\mu} = \not{p}_1 p_{3\mu} - p_1 \cdot p_3 \gamma_\mu\,. \tag{4.17}$$

With these definitions of the tensors the projectors are

$$\mathcal{P}_1 = \frac{2-d}{2(d-3)s^2u}\mathcal{T}_1^\dagger + \frac{4-d}{2(d-3)stu}\mathcal{T}_2^\dagger, \tag{4.18}$$

$$\mathcal{P}_2 = \frac{4-d}{2(d-3)stu}\mathcal{T}_1^\dagger + \frac{2-d}{2(d-3)t^2u}\mathcal{T}_2^\dagger. \tag{4.19}$$

Choosing p_2 as the reference vector for $\epsilon^\mu(p_1)$, the sum over the polarisations of the gluon is

$$\sum_{pol} \epsilon_\mu(p_1)\epsilon^*_\nu(p_1) = -g_{\mu\nu} + \frac{p_{1\mu}p_{2\nu} + p_{1\nu}p_{2\mu}}{p_1 \cdot p_2}. \tag{4.20}$$

According to the normalization (4.6), the electroweak boson couplings g_V^v and g_V^a are

$$g_W^v = \frac{1}{2} \qquad\qquad g_W^a = \frac{1}{2} \tag{4.21}$$

$$g_Z^v = \frac{\sqrt{2}}{\cos^2\theta_W}\left(\frac{T_q}{2} - \sin^2\theta_W Q_q\right) \qquad\qquad g_Z^a = \frac{\sqrt{2}}{\cos^2\theta_W}\frac{T_q}{2}, \tag{4.22}$$

where Q_q and T_q are respectively the electric charge and the third generator of the quark q. Finally, using (4.21) and (4.22), we arrive to the following structure for the left-handed and right-handed open amplitudes:

$$\mathcal{A}^{\text{open}}_{L,\mu} = \left(\frac{2}{\cos^4\theta_W}Q_q^2\sin^4\theta_W\right)\left[\tau_{1,\mu}F^{\text{open}}_{1,m_Z} + \tau_{2,\mu}F^{\text{open}}_{2,m_Z}\right]\mathbb{P}_L, \tag{4.23}$$

$$\begin{aligned}\mathcal{A}^{\text{open}}_{R,\mu} = &\left[\tau_{1,\mu}F^{\text{open}}_{1,m_W} + \tau_{2,\mu}F^{\text{open}}_{2,m_W}\right]\mathbb{P}_R \\ &+ \frac{2}{\cos^4\theta_W}\left(T_q - Q_q\sin^2\theta_W\right)^2\left[\tau_{1,\mu}F^{\text{open}}_{1,m_Z} + \tau_{2,\mu}F^{\text{open}}_{2,m_Z}\right]\mathbb{P}_R.\end{aligned} \tag{4.24}$$

We notice that the left-handed amplitude receives contribution only from the Z boson. We stress that we extracted the form factors F^{open}_{1,m_V} and F^{open}_{2,m_V} applying the projectors (4.18) and

(4.19) to the amplitude after having replaced the electroweak boson coupling with the effective vector coupling. The dependence on the quark polarization is embedded into a rescaling of the coupling constant.

An exact evaluation of the entire contribution coming from the closed diagrams is challenging, essentially due to the top-quark circulating in the loop, which, with a mass of the order of the electroweak scale, is much heavier than all the other quarks. Considering an exact analytic dependence on the top-quark mass is a highly non-trivial task, first of all for the reduction to the master integrals, and it is beyond the scope of this thesis. However, as already mentioned, the heavy-quark contribution has been found to be a few percent of the light-quark correction for Higgs production via gluon-fusion, and it is believed to be small also in quark initiated channels. Still, we postpone to future developments an approximated estimation of the heavy-quark contribution, for example exploiting the infinite top-quark mass limit of the HEFT. For now, in order to capture the most sizeable contribution to the next-to-leading mixed QCD-EW corrections to quark-induced Higgs production, we ignored the top-quark and considered contribution coming from five massless quark flavours u, d, s, c and b.

The closed diagrams are, in turn, of two types, depending on how many vector bosons are attached to the quark-loop. The vector part of the diagrams with only one electroweak boson attached to the quark-loop (see Fig. 4.2) vanishes for Furry's theorem, the corresponding axial vector part vanishes summing over complete degenerate isospin doublets. The third generation, which is incomplete, gives rise to an axial vector anomalous contribution, that, in the calculation presented in this thesis, has not been included. Consequentially, closed diagrams with one-boson insertion, shown in Fig. 4.2, do not contribute to our form factors.

The closed non-anomalous contribution comes entirely from diagrams with two electroweak bosons attached to the quark-loop, as the one shown in Fig. 4.3. Anticommuting γ_5 inside the Dirac trace, we can find a vector contribution proportional to $(g_V^v)^2 + (g_V^a)^2$, and an axial vector contribution proportional to $g_V^v g_V^a \gamma_5$, which vanishes summing over complete degenerate isospin-doublets. As in the case of one-boson insertion, the b-quark contribution gives rise to an anomalous term, which, for the computation described in this thesis, has not been considered. We notice that, as far as we neglect any kind of top-quark contribution, the anomaly arises only from diagrams with a Z boson. We plan to include this anomalous contribution, both for one- and two-boson insertion, in further developments of this work, exploiting the prescription given in [236, 237] to treat γ_5.

We computed the (non-anomalous) contribution to the amplitude coming from closed diagrams replacing (as for the open diagrams) the electroweak boson coupling with an effective vector coupling. We took into account different light-quark flavours: the first two generations ((u, d) and (c, s)) for diagrams with a W boson, the first two generations and the single b-quark for diagrams with a Z boson. Using the coupling constants (4.21) and (4.22) we find the

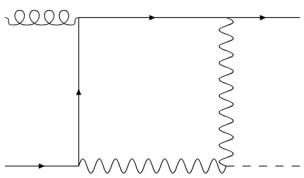

Figure 4.5. Representative diagram contributing to the leading order amplitude $gq \to Hq$.

following structure for the closed amplitude,

$$\begin{aligned}\mathcal{A}_\mu^{\text{closed}} = N_{\text{iso}} &\left[\tau_{1,\mu} F_{1,m_W}^{\text{closed}} + \tau_{2,\mu} F_{2,m_W}^{\text{closed}}\right] \\ &+ \frac{2}{\cos^4\theta_W}\left[N_d\left(Q_d^2 \sin^4\theta_W - Q_d \sin^2\theta_W T_d + \frac{T_d^2}{2}\right)\right. \\ &\left.+ N_u\left(Q_u^2 \sin^4\theta_W - Q_u \sin^2\theta_W T_u + \frac{T_u^2}{2}\right)\right]\left[\tau_{1,\mu} F_{1,m_Z}^{\text{closed}} + \tau_{2,\mu} F_{2,m_Z}^{\text{closed}}\right],\end{aligned} \tag{4.25}$$

where N_{iso} is the number of generations circulating in the loop for the W boson contribution, and N_u (N_d) is the number of up-like (down-like) quarks circulating in the loop for the Z boson contribution. In accordance with what was stated above, we have set for phenomenological applications $N_{\text{iso}} = 2$, $N_u = 2$ and $N_d = 3$. The form factors $F_{1,m_V}^{\text{closed}}$ and $F_{2,m_V}^{\text{closed}}$ have been obtained applying the projectors (4.18) and (4.19) to closed diagrams with two bosons attached to the quark-loop (Fig. 4.3).

The form factors F_{j,m_V}^{open} and $F_{j,m_V}^{\text{closed}}$ admit an expansion in the strong coupling constant

$$\begin{aligned}F_{j,m_V}^{\text{open}} &= \sqrt{\alpha_s}\left[F_{j,m_V}^{\text{open},(1)} + \left(\frac{\alpha_s}{2\pi}\right) F_{j,m_V}^{\text{open},(2)} + \mathcal{O}\left(\alpha_s^2\right)\right], \\ F_{j,m_V}^{\text{closed}} &= \sqrt{\alpha_s}\left[\left(\frac{\alpha_s}{2\pi}\right) F_{j,m_V}^{\text{closed},(2)} + \mathcal{O}\left(\alpha_s^2\right)\right],\end{aligned} \tag{4.26}$$

where $F_{j,m_V}^{\text{class},(l)}$ is the l-loop contribution of the corresponding class of diagrams and m_V can be either m_Z or m_W. The open contribution starts at leading order (see Fig. 4.5), while the closed contribution is a next-to leading order effect. While $F_{j,m_V}^{\text{open},(1)}$ and $F_{j,m_V}^{\text{closed},(2)}$ have a trivial color structure, $F_{j,m_V}^{\text{open},(2)}$ can be decomposed in a leading and a subleading color contribution,

$$F_{j,m_V}^{\text{open},(2)} = \frac{1}{m_V^4}\left[N_c\, C_{j,m_V}\left(\frac{s}{m_V^2}, \frac{t}{m_V^2}, \frac{u}{m_V^2}, \epsilon\right) + \frac{1}{N_c} D_{j,m_V}\left(\frac{s}{m_V^2}, \frac{t}{m_V^2}, \frac{u}{m_V^2}, \epsilon\right)\right], \tag{4.27}$$

where C_{j,m_V} and D_{j,m_V} are dimensionless functions of the kinematic invariants and the dimension regulator ϵ.

In order to obtain the scattering amplitude, we generated the relevant Feynman diagrams using `qgraf` [238]. The Feynman diagrams contributing to this process belong to 6 different scalar integral families: PL, PLx13, PLx123, NA, NB and NBx132, reported in appendix C.1. We used `FORM` [158, 159] to apply the projectors to the amplitude and perform the Dirac algebra. We have used a `Mathematica` script to map each diagram to one of the families

defined in appendix C.1, the same script converts the `qgraf` output into `FORM` expressions. The scalar integrals appearing in the expressions of the form factors are written in terms of a basis of 180 master integrals. The decomposition in terms of MIs is performed using Integration-by-Parts identities [10, 11], via the Laporta Algorithm [12], implemented in the computer code `KIRA` [35, 36]. After the reduction, we end up with 10 seven-denominator top-sectors including permutations of external legs (all of them are shown in fig. 4.16).

In the calculation we employed two bases of master integrals: the precanonical basis, $\{\mathcal{J}_i\}$, and a partially canonical basis, $\{\mathcal{G}_i\}$, both defined in appendix C. Form factors are expressed in terms of the $\epsilon-$expanded $\mathcal{J}_i$, while the basis $\{\mathcal{G}_i\}$ has been used to solve the system of differential equations, described in section 4.2. In the rest of this section we report on the construction of the finite remainders.

4.1.1 UV renormalization and infrared structure

We need only the renormalization of α_s which, in $\overline{\text{MS}}$ scheme, is

$$\alpha_s = \overline{\alpha}_s S_\epsilon^{-1} \mu^{2\epsilon} \left[1 - \left(\frac{\overline{\alpha}_s}{2\pi}\right) \frac{\beta_0}{\epsilon}\right] + \mathcal{O}\left(\overline{\alpha}_s^3\right), \tag{4.28}$$

where $\overline{\alpha}_s$ is the renormalized coupling, $S_\epsilon = (4\pi)^\epsilon e^{-\epsilon\gamma}$ and

$$\beta_0 = \frac{11 C_A - 4 N_f T_R}{6}, \tag{4.29}$$

where $C_A = N_c$ is the casimir of the adjoint representation, N_f is the number of active flavours, in our case 5, and $T_R = \frac{1}{2}$.

The renormalized form factors are then:

$$\overline{F}^{\text{open}}_{j,m_V} = \sqrt{\overline{\alpha}_s} \left[\overline{F}^{\text{open},(1)}_{j,m_V} + \left(\frac{\overline{\alpha}_s}{2\pi}\right) \overline{F}^{\text{open},(2)}_{j,m_V} + \mathcal{O}\left(\overline{\alpha}_s^2\right)\right], \tag{4.30}$$

$$\overline{F}^{\text{closed}}_{j,m_V} = \sqrt{\overline{\alpha}_s} \left[\left(\frac{\overline{\alpha}_s}{2\pi}\right) \overline{F}^{\text{closed},(2)}_{j,m_V} + \mathcal{O}\left(\overline{\alpha}_s^2\right)\right], \tag{4.31}$$

where

$$\overline{F}^{\text{open},(1)}_{j,m_V} = F^{\text{open},(1)}_{j,m_V} \tag{4.32}$$

$$\overline{F}^{\text{closed},(2)}_{j,m_V} = F^{\text{closed},(2)}_{j,m_V} \tag{4.33}$$

$$\overline{F}^{\text{open},(2)}_{j,m_V} = F^{\text{open},(2)}_{j,m_V} - \frac{1}{2}\frac{\beta_0}{\epsilon}\left(\frac{m_V^2}{\mu^2}\right)^\epsilon F^{\text{open},(1)}_{j,m_V}. \tag{4.34}$$

After renormalization, $\overline{F}^{\text{open},(2)}_{j,m_V}$ still contains IR poles. The structure of such singularities for QCD virtual NLO corrections is well-known and is fully captured by Catani's operator $\mathbf{I}^{(1)}$ [239]. After subtraction of the infrared singularities, the finite reminder is

$$\mathcal{F}^{\text{open},(2)}_{j,m_V} = \overline{F}^{\text{open},(2)}_{j,m_V} - \mathbf{I}^{(1)}\left(\frac{m_V^2}{\mu^2}\right)^\epsilon F^{\text{open},(1)}_{j,m_V}, \tag{4.35}$$

where Catani's operator $\mathbf{I}^{(1)}$ reads

$$\mathbf{I}^{(1)} = -\frac{1}{2}\frac{\mathrm{e}^{\epsilon\gamma}}{\Gamma(1-\epsilon)}\left\{\mathcal{V}_q^{\mathrm{sing}}(\epsilon)\frac{2C_F - C_A}{C_F}\left(-\frac{\mu^2}{u}\right)^{\epsilon} + \right. \\ \left. + \frac{1}{2}\left(\mathcal{V}_g^{\mathrm{sing}}(\epsilon) + \frac{C_A}{C_F}\mathcal{V}_q^{\mathrm{sing}}(\epsilon)\right)\left[\left(-\frac{\mu^2}{t}\right)^{\epsilon} + \left(-\frac{\mu^2}{s}\right)^{\epsilon}\right]\right\}, \tag{4.36}$$

where $C_F = (N_c^2 - 1)/(2N_c)$ is the casimir of the fundamental representation and the $\mathcal{V}^{\mathrm{sing}}$ are given by the following,

$$\mathcal{V}_q^{\mathrm{sing}}(\epsilon) = \frac{C_F}{\epsilon^2} + \frac{3C_F}{2\epsilon}, \tag{4.37}$$

$$\mathcal{V}_g^{\mathrm{sing}}(\epsilon) = \frac{C_A}{\epsilon^2} + \frac{11C_A - 2N_f}{6\epsilon}. \tag{4.38}$$

According to Feynman prescription Mandelstam invariants carry an implicit small positive imaginary part. Finally, the finite remainders have the following structures,

$$\mathcal{F}^{\mathrm{open},(1)}_{j,m_V} = \frac{1}{m_V^4}\mathcal{A}_{j,m_V}\left(\frac{s}{m_V^2}, \frac{t}{m_V^2}, \frac{u}{m_V^2}\right) \tag{4.39}$$

$$\mathcal{F}^{\mathrm{open},(2)}_{j,m_V} = \frac{1}{m_V^4}\left[N_f\,\mathcal{B}_{j,m_V}\left(\frac{s}{m_V^2}, \frac{t}{m_V^2}, \frac{u}{m_V^2}, \frac{\mu^2}{m_V^2}\right)\right. \tag{4.40}$$

$$+ N_c\,\mathcal{C}_{j,m_V}\left(\frac{s}{m_V^2}, \frac{t}{m_V^2}, \frac{u}{m_V^2}, \frac{\mu^2}{m_V^2}\right) \tag{4.41}$$

$$\left. + \frac{1}{N_c}\,\mathcal{D}_{j,m_V}\left(\frac{s}{m_V^2}, \frac{t}{m_V^2}, \frac{u}{m_V^2}, \frac{\mu^2}{m_V^2}\right)\right] \tag{4.42}$$

$$\mathcal{F}^{\mathrm{closed},(2)}_{j,m_V} = \frac{1}{m_V^4}\mathcal{E}_{j,m_V}\left(\frac{s}{m_V^2}, \frac{t}{m_V^2}, \frac{u}{m_V^2}\right), \tag{4.43}$$

where the functions $\mathcal{A}_{j,m_V}$, $\mathcal{B}_{j,m_V}$, $\mathcal{C}_{j,m_V}$, $\mathcal{D}_{j,m_V}$ and $\mathcal{E}_{j,m_V}$ depend only on the kinematics.

4.2 Master Integrals Computation

In this section we discuss the details of the MIs computation. The scalar integrals appearing in the amplitude can be reduced to a basis of 180 master integrals. All the seven-denominator top-sectors, including those obtained with a permutation of the external particles, are shown in fig. 4.16.

The MIs of the planar seven-denominator topology of fig. 4.6 (and permuted configurations) have been solved analytically in [240] in terms of Multiple Polylogarithms, integrating the canonical form of the differential equation system. For the non-planar topology NA, shown in fig. 4.13, the analytical solution, in terms of MPLs, has been found in [232], and a semi-analytical solution of the canonical MIs, as one-dimension generalised power series, is also available [233]. All the other master integrals, not mentioned so far, which contribute to the process studied in this chapter, have been computed analytically, in terms of MPLs, in [234], where a direct integration over Feynman parameters has been adopted.

In [234] the authors provide analytical expressions for the different parts of the two-loop finite remainder. In particular, the different components of the form factors are expressed, after non-trivial simplifications, as sum of independent algebraic prefactors multiplied by (non-zero) transcendental functions with maximum weight 4. Despite the efforts made to simplify and reduce the size of the NLO form factors, the expressions provided in [234] still contain several thousands of different MPLs. The numerical evaluation, performed with `Ginac`, is time consuming (30 minutes for a single phase-space point requiring an accuracy of 20 digits), preventing the possibility of a direct implementation of the analytic expression of the amplitude inside a Montecarlo integrator. The objective of our work is to overcome this time issue, facilitating a phenomenological study of the corrections computed. To this purpose, we performed an independent calculation of all the MIs by means of the differential equations method [13–20]. In particular we solved the system of differential equations semi-analytically exploiting the generalised power series expansion technique, as described in [32] and implemented in the software `DiffExp` [33]. In our approach, the number of expansions needed for a numerical evaluation of the amplitude is lower since the number of non-zero entries of the differential equation matrix is typically smaller than the number of different MPLs[1]. Furthermore, in the differential equation approach, each evaluation point can be related to the previous one, with an effective decreasing of the evaluation time (up to a minimum given by the time needed for a single expansion). In the following we describe the construction and the solution of the differential equation system.

We have built the system of differential equations including all the MIs coming from the amplitude, considering permutations of the external legs. The six integral families to which the MIs belong are defined as follows:

$$I_{\texttt{topo}}(n_1,...,n_9) = \int \frac{\mathcal{D}k_1\mathcal{D}k_2}{D_1^{n_1}D_2^{n_2}D_3^{n_3}D_4^{n_4}D_5^{n_5}D_6^{n_6}D_7^{n_7}D_8^{n_8}D_9^{n_9}}, \tag{4.44}$$

where $\texttt{topo} \in \{\text{PL}, \text{PLx13}, \text{PLx123}, \text{NA}, \text{NB}, \text{NBx132}\}$ labels the families and the corresponding propagators $D_1, ..., D_9$ are given in appendix C.1. The computation is done in dimensional regularization with $d = 4 - 2\epsilon$ dimensions, and our convention for the integration measure is

$$\mathcal{D}k_i = \frac{\mathrm{d}^d k_i}{i\pi^{2-\epsilon}}\, \mathrm{e}^{\epsilon\gamma}\, m_V^{2\epsilon}. \tag{4.45}$$

We derived the differential equations with respect to the kinematic variables:

$$S = \frac{s}{m_V^2}, \quad T = \frac{t}{m_V^2}, \quad \omega = \frac{m_h^2}{m_V^2}. \tag{4.46}$$

Master integrals of the precanonical basis, $\{\mathcal{J}_i\}$, defined in appendix C.2, solve the system of differential equations,

$$\mathrm{d}\vec{\mathcal{J}}(\vec{x},\epsilon) = \mathrm{d}A(\vec{x},\epsilon)\vec{\mathcal{J}}(\vec{x},\epsilon), \qquad \vec{x} = (S,T,\omega)\,, \tag{4.47}$$

[1]The redundancy in the numerical evaluation of the analytical expression can be eliminated expanding once for all the independent kernels of the MPLs.

where d is the total differential with respect to the kinematic invariants S, T and ω. After rescaling each integral $\mathcal{J}_i$ with a suitable power of ϵ, the matrix $\mathrm{d}A(\vec{x},\epsilon)$ admits a Taylor expansion in ϵ,

$$\mathrm{d}A(\vec{x},\epsilon) = \mathrm{d}A_0(\vec{x}) + \sum_{j=1}^{4} \epsilon^j \, \mathrm{d}A_j(\vec{x}) + \mathcal{O}(\epsilon^5). \tag{4.48}$$

We observed that integrating out $\mathrm{d}A_0(\vec{x})$ leads to a speedup, by a factor of four, of the series expansion algorithm. Indeed, for a null $A_0(\vec{x})$, the solution can be directly expressed as iterated integrals[2]. Then we define a new basis, $\{\mathcal{G}_i\}$, reported in C.2, which satisfies the following differential equation system,

$$\mathrm{d}\vec{\mathcal{G}}(\vec{x},\epsilon) = \mathrm{d}B(\vec{x},\epsilon)\vec{\mathcal{G}}(\vec{x},\epsilon), \qquad \mathrm{d}B(\vec{x},\epsilon) = \epsilon\,\mathrm{d}B_1(\vec{x}) + \epsilon^2\,\mathrm{d}B_2(\vec{x}), \tag{4.49}$$

$$\vec{\mathcal{G}}(\vec{x},\epsilon) = \Omega(\vec{x},\epsilon)\vec{\mathcal{J}}(\vec{x},\epsilon), \tag{4.50}$$

where $\Omega(\vec{x},\epsilon)$ is algebraic in the kinematics variables and the $\mathcal{G}_i$ admit a Taylor expansion in ϵ. The basis $\{\mathcal{G}_i\}$ is an ϵ-factorised basis up to the non-planar top-sector of fig. 4.14 (and the permuted 4.15), which contains three MIs. Indeed $(\mathrm{d}B_2)_{ij}$ is non-zero only for $(173 \leq i \leq 175, 1 \leq j \leq 172)$ and $(178 \leq i \leq 180, 1 \leq j \leq 177)$, i.e. the non-homogeneous part of the differential equation system for the non-planar top-sectors of the topologies NB and NBx132.

In general, in the polylogarithmic case, for a given sector, there exists a basis of MIs, which, rescaled by suitable powers of ϵ, decouple as soon as $\epsilon = 0$, this is usually referred to as the precanonical basis. This happens also in our case, up to a non-planar six-denominator sub-sector of the topology NA, shown in fig. 4.17, whose two out of the three MIs remain fully coupled even at $\epsilon = 0$ (the same occurs for the permuted sector shown in fig. 4.18). The same sector appears also in the electroweak corrections to $gg \to Hg$. To find an ϵ-factorised basis for this sector, we adopted the same non-standard change of basis used in [54], in which the interested precanonical MIs are multiplied by polynomials in ϵ where the coefficients are functions of the kinematics invariants.

We exploit crossing symmetry to evaluate the different amplitudes, $gq \to Hq$, $g\bar{q} \to H\bar{q}$ and $q\bar{q} \to Hg$, needed for the cross-section. Each amplitude corresponds to a specific physical region in the plane (s,t):

$$\{s < 0, t < 0\} \qquad \text{for} \qquad q\bar{q} \to Hg \tag{4.51}$$

$$\{s < 0, t > -s + m_h^2\} \qquad \text{for} \qquad g\bar{q} \to H\bar{q} \tag{4.52}$$

$$\{t < 0, s > -t + m_h^2\} \qquad \text{for} \qquad gq \to Hq \tag{4.53}$$

A graphical representation of the scattering regions is given in fig. 4.20.

We computed numerical boundary conditions, exploiting the auxilary mass flow method, using the package `Amflow`. A boundary condition has been computed in each physical region.

[2]We note that such a solution has not necessary a uniform transcendentality according to the definition given in [46].

From the boundary point we evolve the solution expanding in one-dimension power series in the plane (S,T) using `Diffexp`. No physical thresholds have to be crossed since the center-of-mass energy is greater than the Higgs mass which is greater than W and Z boson masses. Nevertheless, we had to provide, for the evaluation in `Diffexp`, the following prescription:

$$\sqrt{4-S-T} \to \sqrt{4-S-T-i\delta}. \tag{4.54}$$

To numerically evaluate $\mathcal{J}_i$ we need to evaluate square roots C.92–C.103 on their branch-cut using Feynman prescription. The square roots that have a small positive imaginary part in the physical regions are automatically processed by `Diffexp`, which attributes to them a $+i\delta$ by default. While we have to manually provide the analytic continuation of square roots which have both a branch-cut in the physical regions and a small negative imaginary part, in our case only (4.54). However we observe that changing prescription consistently in the series solution for the $\mathcal{G}_i$ and in the numerical evaluation of the $\mathcal{J}_i$ would not affect the final result since no physical thresholds are crossed.

The time needed to evolve the solution in `Diffexp` between two points which in the (s,t) plane are $3\cdot 10^4$ GeV^2 distant, with 16 digits accuracy and making a single expansion, is 30 seconds on avarage on a single core laptop. In the following table benchmark values for the different components of the LO and NLO form factors and for the different physical regions are reported.

	qg	$\bar{q}g$	$\bar{q}q$
$\mathcal{A}_{1,W}$	$-0.002079+0.000537i$	$-0.001350+0.001737i$	0.010919
$\mathcal{B}_{1,W}$	$-0.001551+0.000981i$	$-0.000644+0.001767i$	0.005944
$\mathcal{C}_{1,W}$	$0.010654-0.007064i$	$0.006335-0.010879i$	$-0.004454-0.000206i$
$\mathcal{D}_{1,W}$	$0.001225-0.021369i$	$-0.004808-0.011242i$	$0.011864+0.039780i$
$\mathcal{E}_{1,W}$	$0.142207+0.012437i$	$0.142207+0.012437i$	$0.000561-0.001206i$

In the table we used the following values of the kinematics variables:

$$qg: \qquad \{s=10^6 \text{ GeV}^2, t=-944915.8824 \text{ GeV}^2\} \tag{4.55}$$

$$\bar{q}g: \qquad \{s=-944915.8824 \text{ GeV}^2, t=10^6 \text{ GeV}^2\} \tag{4.56}$$

$$\bar{q}q: \qquad \{s=-944915.8824 \text{ GeV}^2, t=-39371.4951 \text{ GeV}^2\}. \tag{4.57}$$

We used the following values for the W mass and the renormalization scale:

$$m_W = 80.3850 \text{ GeV} \qquad \mu = 85.7863 \text{ GeV}\,. \tag{4.58}$$

Finally, we compared numerically our results with [234] and found complete agreement in all the phase space regions.

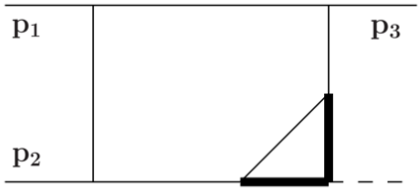

Figure 4.6. PL$(1,1,1,1,1,1,1,0,0)$

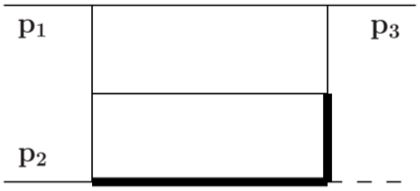

Figure 4.7. PL$(0,1,1,1,1,1,1,1,0)$

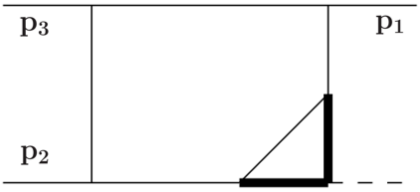

Figure 4.8. PLx13$(1,1,1,1,1,1,1,0,0)$

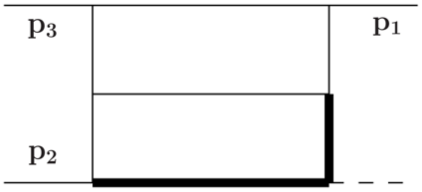

Figure 4.9. PLx13$(0,1,1,1,1,1,1,1,0)$

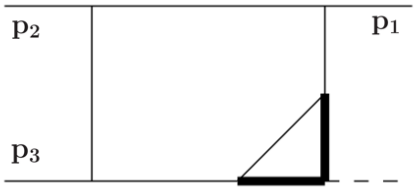

Figure 4.10. PLx123$(1,1,1,1,1,1,1,0,0)$

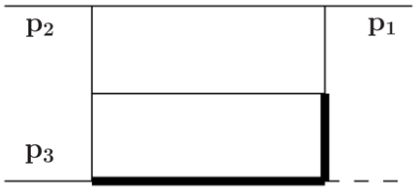

Figure 4.11. PLx123$(0,1,1,1,1,1,1,1,0)$

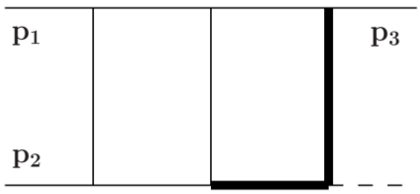

Figure 4.12. PL$(1,1,1,1,1,0,1,0,1)$

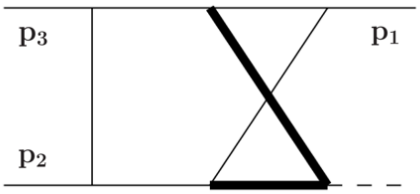

Figure 4.13. NA$(1,1,1,1,1,1,1,0,0)$

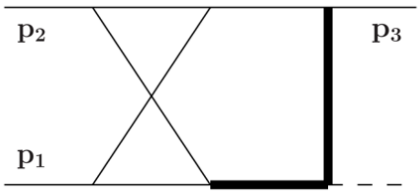

Figure 4.14. NB$(1,1,1,1,0,1,1,1,0)$

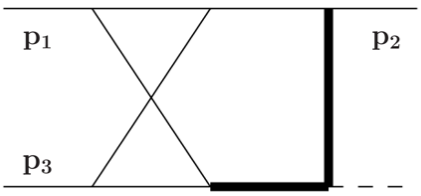

Figure 4.15. NBx132$(1,1,1,1,0,1,1,1,0)$

Figure 4.16. The figure shows the seven-denominator top-sectors for the master integrals. All the possible permutations of external legs arising from the amplitude are shown. Subfigures 4.6 to 4.12 are planar topologies, while subfigures 4.13 to 4.15 are non-planar topologies. Thin black lines represents massless particles, thick black lines heavy particles and dashed line the Higgs.

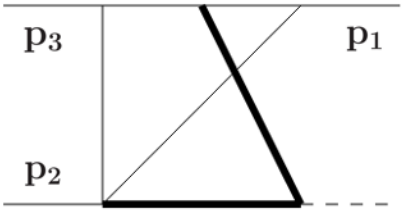

Figure 4.17. NA$(1,1,1,1,0,1,1,0,0)$

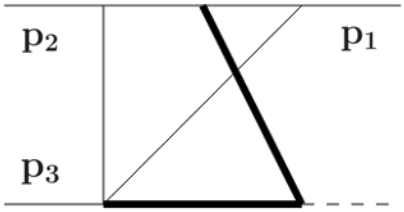

Figure 4.18. NA$(0,1,1,1,1,1,1,0,0)$

Figure 4.19. The figure shows the sectors whose precanonical MIs remain coupled at $\epsilon = 0$ (see the text for more details). Thin black lines represents massless particles, thick black lines heavy particles and dashed line the Higgs.

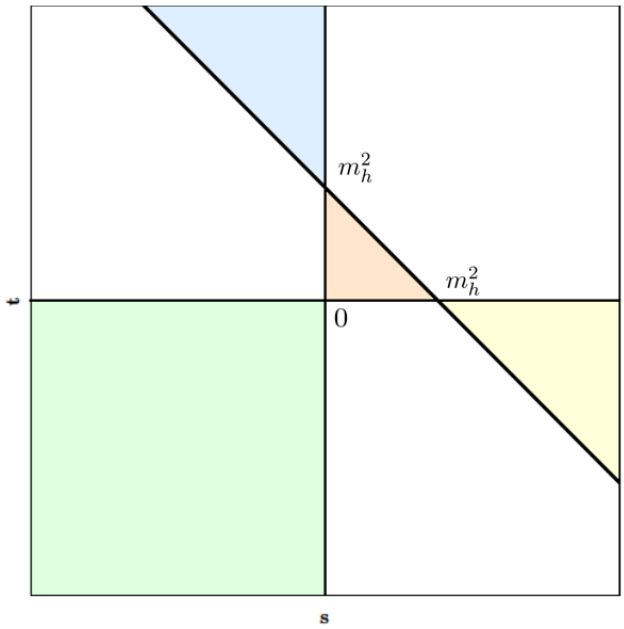

Figure 4.20. The figure shows the physical regions for the different partonic subprocesses contributing to the cross-section. The green region corresponds to $q\bar{q} \to Hg$, the blue region corresponds to $g\bar{q} \to H\bar{q}$ and the yellow region corresponds to $gq \to Hq$. The orange region corresponds to the decay $H \to q\bar{q}g$.

Conclusions

In this thesis we presented two-loop corrections, with exact dependence on internal masses, to two relevant processes at hadron colliders.

In chapter 3 we presented the diphoton production at NNLO with top quark mass dependence. In particular, in section 3.1 we described the computation of the two-loop form factors for diphoton production in the $q\bar{q}$ channel, where Feynman diagrams with a loop of top quark have been considered [4].

The non-planar topology which contributes to this process contains two sectors of MIs whose analytic representation cannot be given in terms of MPLs. In order to be able to exploit our results for phenomenological applications, we computed the MIs by means of differential equations, exploiting the generalised power series technique. This method proves to be of great use for phenomenological applications, especially in cases where the functional space for the MIs contains not only polylogarithmic functions.

In section 3.2 we presented a phenomenological study for diphoton production at NNLO which fully takes into account the dependence on the top quark mass in all the relevant channels [5]. We presented a detailed study of the impact of the massive corrections in the invariant mass distribution around the top quark threshold. We have shown the different components of the total NNLO QCD massive result. The two most significant contributions are the one-loop ($gg \to \gamma\gamma$) box term [78] and the two-loop ($q\bar{q} \to \gamma\gamma$) massive amplitude [4]. The negative peak around the top quark threshold is, therefore, the result of (mainly) these two contributions showing the same (negative peak) behaviour. The moderated size of the positive peak introduced by the real-virtual contribution (see Fig. 3.16) only slightly modifies the size of the negative peak. The position of the positive peak in the ratio of Fig. 3.13 is the result of the two competing opposite behaviours of the two dominant contributions (see Fig. 3.14).

The precedent discussion suggests that the massive corrections presented are relevant not only for the invariant mass region around the top mass threshold but also for larger values ($m_{\gamma\gamma} > 2m_t$). This kinematic region ($m_{\gamma\gamma} \geq 500$ GeV) is of interest for BSM searches.

We leave the inclusion of partial N^{3}LO massless and massive effects to further studies.

In chapter 4 we presented the two-loop mixed QCD-Electroweak corrections to $qg \to Hq$ and its crossed channels, $\bar{q}g \to H\bar{q}$ and $q\bar{q} \to Hg$, considering the light-quark contribution and the exact dependence on the electroweak boson mass. The relevant master integrals have been computed by means of the differential equations method and exploiting the semi-analytical approach based on generalised power series expansion. Compared to the analytical result in

terms of Multiple Polylogarithms [234], our `Diffexp` implementation allows to considerably reduce the evaluation time of the relevant scattering amplitudes. On the other hand our expressions do not see all the cancellations that happen in the analytical formulae.

We are going to include these corrections, in the near future, in a phenomenological study of Higgs production, investigating their impact on the Higgs total cross section and p_T distribution.

Appendix A

Integral families and master integrals for diphoton

A.1 Integral families

The two-loop Feynman diagrams with a loop of heavy-quark, contributing to the process $q(p_1)+\overline{q}(p_2)+\gamma(p_3)+\gamma(p_4)\to 0$, can be mapped into 5 different scalar integral families, NPA, PLA, PLAx12, PLAx124 and PLAx1234. We define the scalar integrals as

$$I_{\texttt{topo}}(n_1,...,n_9)=\int\frac{\mathcal{D}k_1\mathcal{D}k_2}{D_1^{n_1}D_2^{n_2}D_3^{n_3}D_4^{n_4}D_5^{n_5}D_6^{n_6}D_7^{n_7}D_8^{n_8}D_9^{n_9}}, \tag{A.1}$$

where depending on the topology the set of the propagators $\{D_i\}$ can be one of the following:

- **family NPA**

$$\begin{aligned}
D_1 &= k_1^2\\
D_2 &= k_2^2-m_t^2\\
D_3 &= (-k_2+k_1)^2-m_t^2\\
D_4 &= (-p_1+k_1)^2\\
D_5 &= (-p_1+k_2)^2\\
D_6 &= (-p_2-p_1+k_1)^2\\
D_7 &= (p_3-k_2+k_1)^2-m_t^2\\
D_8 &= (-p_3-p_2-p_1+k_2)^2-m_t^2\\
D_9 &= (-p_2-p_1-k_2+k_1)^2
\end{aligned}$$

- **family PLA**

$$\begin{aligned}
D_1 &= k_1^2\\
D_2 &= k_2^2-m_t^2\\
D_3 &= (-k_2+k_1)^2-m_t^2
\end{aligned}$$

$$
\begin{aligned}
D_4 &= (-p_1 + k_1)^2 \\
D_5 &= (-p_1 + k_2)^2 \\
D_6 &= (-p_2 - p_1 + k_1)^2 \\
D_7 &= (-p_2 - p_1 + k_2)^2 - m_t^2 \\
D_8 &= (-p_3 - p_2 - p_1 + k_1)^2 \\
D_9 &= (-p_3 - p_2 - p_1 + k_2)^2 - m_t^2
\end{aligned}
$$

- **family PLAx12**

$$
\begin{aligned}
D_1 &= k_1^2 \\
D_2 &= k_2^2 - m_t^2 \\
D_3 &= (-k_2 + k_1)^2 - m_t^2 \\
D_4 &= (-p_2 + k_1)^2 \\
D_5 &= (-p_2 + k_2)^2 \\
D_6 &= (-p_2 - p_1 + k_1)^2 \\
D_7 &= (-p_2 - p_1 + k_2)^2 - m_t^2 \\
D_8 &= (-p_3 - p_2 - p_1 + k_1)^2 \\
D_9 &= (-p_3 - p_2 - p_1 + k_2)^2 - m_t^2
\end{aligned}
$$

- **family PLAx124**

$$
\begin{aligned}
D_1 &= k_1^2 \\
D_2 &= k_2^2 - m_t^2 \\
D_3 &= (-k_2 + k_1)^2 - m_t^2 \\
D_4 &= (-p_2 + k_1)^2 \\
D_5 &= (-p_2 + k_2)^2 \\
D_6 &= (p_3 + p_1 + k_1)^2 \\
D_7 &= (p_3 + p_1 + k_2)^2 - m_t^2 \\
D_8 &= (p_1 + k_1)^2 \\
D_9 &= (p_1 + k_2)^2 - m_t^2
\end{aligned}
$$

- **family PLAx1234**

$$
\begin{aligned}
D_1 &= k_1^2 \\
D_2 &= k_2^2 - m_t^2 \\
D_3 &= (-k_2 + k_1)^2 - m_t^2 \\
D_4 &= (-p_2 + k_1)^2 \\
D_5 &= (-p_2 + k_2)^2
\end{aligned}
$$

$$
\begin{aligned}
D_6 &= (-p_3 - p_2 + k_1)^2 \\
D_7 &= (-p_3 - p_2 + k_2)^2 - m_t^2 \\
D_8 &= (p_1 + k_1)^2 \\
D_9 &= (p_1 + k_2)^2 - m_t^2
\end{aligned}
$$

A.2 Precanonical basis

After IBPs reduction all the scalar integrals coming from the amplitude can be reduced to a basis of 63 master integrals, that we chose as following:

$$
\begin{aligned}
\mathcal{T}_1 &= I_{\mathrm{PLA}}(0,2,2,0,0,0,0,0,0) \\
\mathcal{T}_2 &= I_{\mathrm{PLA}}(2,2,0,0,0,1,0,0,0) \\
\mathcal{T}_3 &= I_{\mathrm{PLA}}(0,2,2,0,0,1,0,0,0) \\
\mathcal{T}_4 &= I_{\mathrm{PLA}}(0,2,1,0,0,2,0,0,0) \\
\mathcal{T}_5 &= I_{\mathrm{PLA}}(0,2,2,0,0,0,1,0,0) \\
\mathcal{T}_6 &= I_{\mathrm{PLA}}(0,2,0,2,0,0,0,1,0) \\
\mathcal{T}_7 &= I_{\mathrm{PLAx12}}(0,2,0,2,0,0,0,1,0) \\
\mathcal{T}_8 &= I_{\mathrm{PLA}}(0,0,2,2,0,0,0,0,1) \\
\mathcal{T}_9 &= I_{\mathrm{PLA}}(0,0,2,1,0,0,0,0,2) \\
\mathcal{T}_{10} &= I_{\mathrm{PLAx12}}(0,0,2,2,0,0,0,0,1) \\
\mathcal{T}_{11} &= I_{\mathrm{PLAx12}}(0,0,2,1,0,0,0,0,2) \\
\mathcal{T}_{12} &= I_{\mathrm{PLA}}(0,1,2,1,0,0,1,0,0) \\
\mathcal{T}_{13} &= I_{\mathrm{PLA}}(0,1,1,2,0,0,1,0,0) \\
\mathcal{T}_{14} &= I_{\mathrm{PLA}}(0,2,2,1,0,0,1,0,0) \\
\mathcal{T}_{15} &= I_{\mathrm{PLA}}(2,2,0,0,0,1,1,0,0) \\
\mathcal{T}_{16} &= I_{\mathrm{PLA}}(0,1,3,1,0,0,0,0,1) \\
\mathcal{T}_{17} &= I_{\mathrm{PLAx12}}(0,1,3,1,0,0,0,0,1) \\
\mathcal{T}_{18} &= I_{\mathrm{PLA}}(1,0,2,0,0,1,0,0,1) \\
\mathcal{T}_{19} &= I_{\mathrm{PLA}}(2,0,2,0,0,1,0,0,1) \\
\mathcal{T}_{20} &= I_{\mathrm{PLA}}(0,1,3,0,0,1,0,0,1) \\
\mathcal{T}_{21} &= I_{\mathrm{PLA}}(0,1,2,0,0,0,1,0,1) \\
\mathcal{T}_{22} &= I_{\mathrm{PLA}}(1,1,1,0,0,1,1,0,0) \\
\mathcal{T}_{23} &= I_{\mathrm{PLA}}(1,2,0,1,0,1,0,1,0) \\
\mathcal{T}_{24} &= I_{\mathrm{PLAx12}}(1,2,0,1,0,1,0,1,0) \\
\mathcal{T}_{25} &= I_{\mathrm{PLA}}(1,1,1,0,0,1,0,0,1) \\
\mathcal{T}_{26} &= I_{\mathrm{PLA}}(1,0,2,1,0,1,0,0,1) \\
\mathcal{T}_{27} &= I_{\mathrm{PLA}}(1,0,2,1,0,1,0,-1,1)
\end{aligned}
$$

$$
\begin{aligned}
\mathcal{T}_{28} &= I_{\mathrm{PLAx12}}(1,0,2,1,0,1,0,0,1)\\
\mathcal{T}_{29} &= I_{\mathrm{PLAx12}}(1,0,2,1,0,1,0,-1,1)\\
\mathcal{T}_{30} &= I_{\mathrm{PLA}}(0,1,1,1,0,1,0,0,1)\\
\mathcal{T}_{31} &= I_{\mathrm{PLA}}(0,1,2,1,0,1,0,0,1)\\
\mathcal{T}_{32} &= I_{\mathrm{PLAx12}}(0,1,1,1,0,1,0,0,1)\\
\mathcal{T}_{33} &= I_{\mathrm{PLAx12}}(0,1,2,1,0,1,0,0,1)\\
\mathcal{T}_{34} &= I_{\mathrm{PLA}}(0,1,2,1,0,0,1,0,1)\\
\mathcal{T}_{35} &= I_{\mathrm{PLA}}(0,1,3,1,0,0,1,0,1)\\
\mathcal{T}_{36} &= I_{\mathrm{PLA}}(0,1,2,1,-1,0,1,0,1)\\
\mathcal{T}_{37} &= I_{\mathrm{PLAx12}}(0,1,2,1,0,0,1,0,1)\\
\mathcal{T}_{38} &= I_{\mathrm{PLAx12}}(0,1,3,1,0,0,1,0,1)\\
\mathcal{T}_{39} &= I_{\mathrm{PLAx12}}(0,1,2,1,-1,0,1,0,1)\\
\mathcal{T}_{40} &= I_{\mathrm{PLA}}(2,1,0,0,0,1,1,0,1)\\
\mathcal{T}_{41} &= I_{\mathrm{NPA}}(1,1,1,0,0,0,1,1,0)\\
\mathcal{T}_{42} &= I_{\mathrm{NPA}}(0,1,1,1,0,0,1,1,0)\\
\mathcal{T}_{43} &= I_{\mathrm{NPA}}(0,1,1,1,0,0,1,2,0)\\
\mathcal{T}_{44} &= I_{\mathrm{NPA}}(0,1,1,2,0,0,1,1,0)\\
\mathcal{T}_{45} &= I_{\mathrm{PLA}}(1,1,1,1,0,1,0,0,1)\\
\mathcal{T}_{46} &= I_{\mathrm{PLAx12}}(1,1,1,1,0,1,0,0,1)\\
\mathcal{T}_{47} &= I_{\mathrm{PLA}}(1,1,1,0,0,1,1,0,1)\\
\mathcal{T}_{48} &= I_{\mathrm{NPA}}(1,1,1,1,0,0,1,1,0)\\
\mathcal{T}_{49} &= I_{\mathrm{NPA}}(1,2,1,1,0,0,1,1,0)\\
\mathcal{T}_{50} &= I_{\mathrm{PLA}}(1,1,1,1,0,1,1,0,1)\\
\mathcal{T}_{51} &= I_{\mathrm{PLA}}(1,1,1,1,-1,1,1,0,1)\\
\mathcal{T}_{52} &= I_{\mathrm{PLA}}(1,1,1,1,0,1,1,-1,1)\\
\mathcal{T}_{53} &= I_{\mathrm{PLA}}(1,1,1,1,-1,1,1,-1,1)\\
\mathcal{T}_{54} &= I_{\mathrm{PLAx12}}(1,1,1,1,0,1,1,0,1)\\
\mathcal{T}_{55} &= I_{\mathrm{PLAx12}}(1,1,1,1,-1,1,1,0,1)\\
\mathcal{T}_{56} &= I_{\mathrm{PLAx12}}(1,1,1,1,0,1,1,-1,1)\\
\mathcal{T}_{57} &= I_{\mathrm{PLAx12}}(1,1,1,1,-1,1,1,-1,1)\\
\mathcal{T}_{58} &= I_{\mathrm{NPA}}(1,1,1,0,0,1,1,1,0)\\
\mathcal{T}_{59} &= I_{\mathrm{NPA}}(1,2,1,0,0,1,1,1,0)\\
\mathcal{T}_{60} &= I_{\mathrm{NPA}}(1,1,1,1,0,1,1,1,-1)\\
\mathcal{T}_{61} &= I_{\mathrm{NPA}}(1,2,1,1,0,1,1,1,-1)\\
\mathcal{T}_{62} &= I_{\mathrm{NPA}}(1,1,1,1,0,1,1,1,-2)\\
\mathcal{T}_{63} &= I_{\mathrm{NPA}}(1,1,1,1,0,1,1,1,0).
\end{aligned}
$$

A.3 Semi-Canonical basis

The basis f_i, canonical only for the non-elliptic MIs f_{1-57} which are the same of [167], has the following definition in terms of the $\mathcal{T}_i$:

$$f_1 = \epsilon^2\,\mathcal{T}_1 \tag{A.2}$$
$$f_2 = s\,\epsilon^2\,\mathcal{T}_2 \tag{A.3}$$
$$f_3 = t\,\epsilon^2\,\mathcal{T}_7 \tag{A.4}$$
$$f_4 = -(s+t)\,\epsilon^2\,\mathcal{T}_6 \tag{A.5}$$
$$f_5 = r_1\,\epsilon^2\,\mathcal{T}_5 \tag{A.6}$$
$$f_6 = s\,\epsilon^2\,\mathcal{T}_3 \tag{A.7}$$
$$f_7 = \frac{1}{2}\,r_1\,\epsilon^2\,\mathcal{T}_3 + r_1\,\epsilon^2\,\mathcal{T}_4 \tag{A.8}$$
$$f_8 = t\,\epsilon^2\,\mathcal{T}_{11} \tag{A.9}$$
$$f_9 = r_2\,\epsilon^2\,\mathcal{T}_{10} + \frac{1}{2}\,r_2\,\epsilon^2\,\mathcal{T}_{11} \tag{A.10}$$
$$f_{10} = -(s+t)\,\epsilon^2\,\mathcal{T}_9 \tag{A.11}$$
$$f_{11} = r_3\,\epsilon^2\,\mathcal{T}_8 + \frac{1}{2}\,r_3\,\epsilon^2\,\mathcal{T}_9 \tag{A.12}$$
$$f_{12} = s\,\epsilon^3\,\mathcal{T}_{12} \tag{A.13}$$
$$f_{13} = s\,\epsilon^3\,\mathcal{T}_{13} \tag{A.14}$$
$$f_{14} = r_1\,\epsilon^3\,\mathcal{T}_{12} + \frac{1}{2}\,r_1\,\epsilon^3\,\mathcal{T}_{13} + r_1\,\epsilon^2\,\mathcal{T}_{14} \tag{A.15}$$
$$f_{15} = r_1\,s\,\epsilon^2\,\mathcal{T}_{15} \tag{A.16}$$
$$f_{16} = s\,\epsilon^3\,\mathcal{T}_{18} \tag{A.17}$$
$$f_{17} = r_4\,s\,\epsilon^2\,\mathcal{T}_{19} - \frac{r_4\,\epsilon^3\,\mathcal{T}_1}{4\epsilon+2} \tag{A.18}$$
$$f_{18} = s\,\epsilon^2\,\mathcal{T}_{20} \tag{A.19}$$
$$f_{19} = t\,\epsilon^2\,\mathcal{T}_{17} \tag{A.20}$$
$$f_{20} = -(s+t)\,\epsilon^2\,\mathcal{T}_{16} \tag{A.21}$$
$$f_{21} = s\,\epsilon^3\,\mathcal{T}_{21} \tag{A.22}$$
$$f_{22} = -s\,\epsilon^3(2\epsilon-1)\,\mathcal{T}_{22} \tag{A.23}$$
$$f_{23} = -s(s+t)\,\epsilon^3\,\mathcal{T}_{23} \tag{A.24}$$
$$f_{24} = s\,t\,\epsilon^3\,\mathcal{T}_{24} \tag{A.25}$$
$$f_{25} = r_3\,s\,\epsilon^3\,\mathcal{T}_{26} \tag{A.26}$$
$$f_{26} = s(s+t)\,\epsilon^3\,\mathcal{T}_{26} + s\,\epsilon^3\,\mathcal{T}_{27} \tag{A.27}$$
$$f_{27} = r_2\,s\,\epsilon^3\,\mathcal{T}_{28} \tag{A.28}$$
$$f_{28} = s\,\epsilon^3\,\mathcal{T}_{29} - s\,t\,\epsilon^3\,\mathcal{T}_{28} \tag{A.29}$$
$$f_{29} = s\,\epsilon^4\,\mathcal{T}_{25} \tag{A.30}$$

$$f_{30} = t\,\epsilon^4\,\mathcal{T}_{30} \tag{A.31}$$
$$f_{31} = r_8\,\epsilon^3\,\mathcal{T}_{31} \tag{A.32}$$
$$f_{32} = -(s+t)\,\epsilon^4\,\mathcal{T}_{32} \tag{A.33}$$
$$f_{33} = r_7\,\epsilon^3\,\mathcal{T}_{33} \tag{A.34}$$
$$f_{34} = r_{10}\,\epsilon^3\,\mathcal{T}_{34} \tag{A.35}$$
$$f_{35} = r_8\,\epsilon^3\,\mathcal{T}_{34} + r_8\,\epsilon^2\,\mathcal{T}_{35} \tag{A.36}$$
$$f_{36} = s\,\epsilon^3\,\mathcal{T}_{36} \tag{A.37}$$
$$f_{37} = r_{11}\,\epsilon^3\,\mathcal{T}_{37} \tag{A.38}$$
$$f_{38} = r_7\,\epsilon^3\,\mathcal{T}_{37} + r_7\,\epsilon^2\,\mathcal{T}_{38} \tag{A.39}$$
$$f_{39} = s\,\epsilon^3\,\mathcal{T}_{39} \tag{A.40}$$
$$f_{40} = s^2\,\epsilon^3\,\mathcal{T}_{40} \tag{A.41}$$
$$f_{41} = s\,\epsilon^4\,\mathcal{T}_{41} \tag{A.42}$$
$$f_{42} = s\,\epsilon^4\,\mathcal{T}_{42} \tag{A.43}$$
$$f_{43} = \frac{s(4-t)\,\epsilon^4\,\mathcal{T}_{10}}{t(\epsilon-1)} - \frac{s(s+t+4)\,\epsilon^4\,\mathcal{T}_8}{t(\epsilon-1)} + \frac{s^2\,\epsilon^3\,\mathcal{T}_{43}}{t} + \tag{A.44}$$
$$\frac{2\,s\,\epsilon^3\,\mathcal{T}_{16}(-(s+t)(\epsilon-1)+2\epsilon-1)}{t(\epsilon-1)} + \frac{s\,\epsilon^3\,\mathcal{T}_{11}(2t\epsilon-2\epsilon+3)}{2t(\epsilon-1)} + \tag{A.45}$$
$$\frac{s\,\epsilon^3\,\mathcal{T}_9(2(s+t)\epsilon+2\epsilon-3)}{2t(\epsilon-1)} - \frac{2\,s\,\epsilon^3\,\mathcal{T}_{17}(t(\epsilon-1)+2\epsilon-1)}{t(\epsilon-1)} \tag{A.46}$$
$$f_{44} = r_9\,\epsilon^3\,\mathcal{T}_{44} \tag{A.47}$$
$$f_{45} = r_1\,s\,\epsilon^4\,\mathcal{T}_{47} \tag{A.48}$$
$$f_{46} = -s(s+t)\,\epsilon^4\,\mathcal{T}_{45} \tag{A.49}$$
$$f_{47} = s\,t\,\epsilon^4\,\mathcal{T}_{46} \tag{A.50}$$
$$f_{48} = r_{16}\,\epsilon^4\,\mathcal{T}_{48} \tag{A.51}$$
$$f_{49} = -\frac{1}{4}\,s^2\,\epsilon^3\,\mathcal{T}_{33} - \frac{1}{4}\,(s+t)^2\,\epsilon^3\,\mathcal{T}_{44} - s(s+t)\,\epsilon^3\,\mathcal{T}_{49} - \frac{1}{4}\,s(s+t)\,(4\epsilon+1)\epsilon^3\,\mathcal{T}_{48} \tag{A.52}$$
$$f_{50} = r_8\,s\,\epsilon^4\,\mathcal{T}_{50} \tag{A.53}$$
$$f_{51} = s^2\,\epsilon^4\,\mathcal{T}_{51} - s^2\,\epsilon^4\,\mathcal{T}_{50} \tag{A.54}$$
$$f_{52} = r_1\,s(s+t)\,\epsilon^4\,\mathcal{T}_{50} + r_1\,s\,\epsilon^4\,\mathcal{T}_{52} - r_1\,(s+t)\,\epsilon^3\,\mathcal{T}_{31} + 2\,r_1\,(s+t)\,\epsilon^3\,\mathcal{T}_{34} + \tag{A.55}$$
$$2\,r_1\,(s+t)\,\epsilon^2\,\mathcal{T}_{35} \tag{A.56}$$
$$f_{53} = -2\,s\,\epsilon^4\,\mathcal{T}_{30} - \frac{1}{2}\,s^2\,\epsilon^4\,\mathcal{T}_{47} + \frac{1}{2}\,s^2(s+t)\,\epsilon^4\,\mathcal{T}_{50} + \frac{1}{2}\,(s-2)s\,\epsilon^4\,\mathcal{T}_{52} + \tag{A.57}$$
$$s\,\epsilon^4\,\mathcal{T}_{53} - \frac{1}{2}\,s\,\epsilon^3\,\mathcal{T}_{22} - \frac{1}{2}\,s(s+t)\,\epsilon^3\,\mathcal{T}_{31} + s(s+t)\,\epsilon^3\,\mathcal{T}_{34} - \tag{A.58}$$
$$s\,t\,\epsilon^3\,\mathcal{T}_{40} + s(s+t)\,\epsilon^2\,\mathcal{T}_{35} \tag{A.59}$$
$$f_{54} = r_7\,s\,\epsilon^4\,\mathcal{T}_{54} \tag{A.60}$$
$$f_{55} = s^2\,\epsilon^4\,\mathcal{T}_{55} - s^2\,\epsilon^4\,\mathcal{T}_{54} \tag{A.61}$$
$$f_{56} = -r_1\,s\,t\,\epsilon^4\,\mathcal{T}_{54} + r_1\,s\,\epsilon^4\,\mathcal{T}_{56} + r_1\,t\,\epsilon^3\,\mathcal{T}_{33} - 2\,r_1\,t\,\epsilon^3\,\mathcal{T}_{37} - 2\,r_1\,t\,\epsilon^2\,\mathcal{T}_{38} \tag{A.62}$$

$$f_{57} = -2\,s\,\epsilon^4\,\mathcal{T}_{32} - \frac{1}{2}\,s^2\,\epsilon^4\,\mathcal{T}_{47} - \frac{1}{2}\,s^2\,t\,\epsilon^4\,\mathcal{T}_{54} + \frac{1}{2}\,(s-2)s\,\epsilon^4\,\mathcal{T}_{56} + \tag{A.63}$$

$$s\,\epsilon^4\,\mathcal{T}_{57} - \frac{1}{2}\,s\,\epsilon^3\,\mathcal{T}_{22} + \frac{1}{2}\,s\,t\,\epsilon^3\,\mathcal{T}_{33} - s\,t\,\epsilon^3\,\mathcal{T}_{37} + \tag{A.64}$$

$$s(s+t)\,\epsilon^3\,\mathcal{T}_{40} - s\,t\,\epsilon^2\,\mathcal{T}_{38} \tag{A.65}$$

$$f_{58} = s\,\epsilon^4\,\mathcal{T}_{58} \tag{A.66}$$

$$f_{59} = s^2(s+16)\,\epsilon^4\,\mathcal{T}_{59} \tag{A.67}$$

$$f_{60} = \epsilon^4\,\mathcal{T}_{60} \tag{A.68}$$

$$f_{61} = \epsilon^4\,\mathcal{T}_{61} \tag{A.69}$$

$$f_{62} = \epsilon^4\,\mathcal{T}_{62} \tag{A.70}$$

$$f_{63} = \epsilon^4\,\mathcal{T}_{63}, \tag{A.71}$$

where $r_1, \cdots, r_{16}$ are square roots of the kinematic invariants:

$$r_1 = \sqrt{s-4}\sqrt{s} \tag{A.72}$$

$$r_2 = \sqrt{t-4}\sqrt{t} \tag{A.73}$$

$$r_3 = \sqrt{s+t}\sqrt{s+t+4} \tag{A.74}$$

$$r_4 = \sqrt{s}\sqrt{s+4} \tag{A.75}$$

$$r_7 = \sqrt{s}\sqrt{t}\sqrt{st-4(s+t)} \tag{A.76}$$

$$r_8 = \sqrt{s}\sqrt{s+t}\sqrt{s(s+t)-4t} \tag{A.77}$$

$$r_9 = \sqrt{t}\sqrt{s+t}\sqrt{t(s+t)-4s} \tag{A.78}$$

$$r_{10} = \sqrt{s}\sqrt{s(s+t+1)^2-4(s+t)^2} \tag{A.79}$$

$$r_{11} = \sqrt{s}\sqrt{s(t-1)^2-4t^2} \tag{A.80}$$

$$r_{16} = \sqrt{s}\sqrt{t}\sqrt{-(s+t)}. \tag{A.81}$$

Appendix B

Counter terms for the heavy-quark contribution to $q\overline{q} \to \gamma\gamma$

$$
\begin{aligned}
\delta\overline{\mathcal{F}}^{(2)}_{1,\mathtt{top};0} =& \pi^{-2\epsilon}\Gamma^2(1+\epsilon)\left(\frac{\mu^2}{m_t^2}\right)^{2\epsilon} 4\pi\alpha_{em}\delta_{ij}\,Q_q^2\,C_F N_h \\
& \left\{ \frac{1}{\epsilon^3}\left[-\frac{1}{12(s+u)}\right] + \right. \\
& \frac{1}{\epsilon^2}\left[\frac{2\log\left(-\frac{s}{m_t^2}\right)-3}{24(s+u)}\right] + \\
& \frac{1}{\epsilon}\left[-\frac{1}{24(s+u)}\log^2\left(-\frac{s}{m_t^2}\right) + \frac{1}{8(s+u)}\log\left(-\frac{s}{m_t^2}\right) - \right. \\
& \frac{-s^2+su+u^2}{24s(s+u)^2}\log^2\left(\frac{u}{s}\right) + \\
& \frac{1}{288}\left(\frac{-84u(s+u)-4\pi^2(s-2u)(3s+2u)}{u(s+u)^2} - \frac{9}{t}\right) + \\
& \frac{1}{24}\left(\frac{1}{s+u}+\frac{1}{s}-\frac{1}{u}\right)\log^2\left(\frac{t}{s}\right) + \frac{1}{24}\left(\frac{3}{s+u}-\frac{1}{s}\right)\log\left(\frac{t}{s}\right) + \\
& \left.\frac{1}{24}\left(\frac{2}{s+u}+\frac{1}{s}\right)\log\left(\frac{u}{s}\right)\right] + \\
& \left[\left(\frac{\pi^2}{24(s+u)}+\frac{\pi^2}{24s}-\frac{\pi^2}{24u}\right)H\left(-1,\frac{t}{s}\right) + \right. \\
& \left(\frac{1}{12(s+u)}+\frac{1}{12s}-\frac{1}{12u}\right)H\left(-1,0,0,\frac{t}{s}\right) + \\
& \left(-\frac{\pi^2 u}{24(s+u)^2}+\frac{\pi^2}{12(s+u)}-\frac{\pi^2}{24s}\right)H\left(-1,\frac{u}{s}\right) + \\
& \left(-\frac{u}{12(s+u)^2}+\frac{1}{6(s+u)}-\frac{1}{12s}\right)H\left(-1,0,0,\frac{u}{s}\right) + \\
& \log\left(-\frac{s}{m_t^2}\right)\left(\left(-\frac{1}{24(s+u)}-\frac{1}{24s}+\frac{1}{24u}\right)\log^2\left(\frac{t}{s}\right) + \right.
\end{aligned}
$$

$$\left(\frac{1}{24s}-\frac{1}{8(s+u)}\right)\log\left(\frac{t}{s}\right)+\frac{21-10\pi^2}{72(s+u)}+$$
$$\frac{\pi^2 u}{24(s+u)^2}+\left(\frac{u}{24(s+u)^2}-\frac{1}{12(s+u)}+\frac{1}{24s}\right)\log^2\left(\frac{u}{s}\right)+$$
$$\left(-\frac{1}{12(s+u)}-\frac{1}{24s}\right)\log\left(\frac{u}{s}\right)+\frac{\pi^2}{24u}\Bigg)+$$
$$\frac{\log^3\left(-\frac{s}{m_t^2}\right)}{72(s+u)}-\frac{\log^2\left(-\frac{s}{m_t^2}\right)}{16(s+u)}+\left(-\frac{1}{36(s+u)}-\frac{1}{36s}+\frac{1}{36u}\right)\log^3\left(\frac{t}{s}\right)+$$
$$\left(-\frac{1}{16(s+u)}+\frac{7}{48s}-\frac{1}{24u}\right)\log^2\left(\frac{t}{s}\right)+$$
$$\left(\frac{7-\pi^2}{24(s+u)}+\frac{-3-\pi^2}{24s}+\frac{\pi^2}{24u}\right)\log\left(\frac{t}{s}\right)+$$
$$\frac{20\zeta(3)+7\pi^2-28}{48(s+u)}+\frac{-2u\zeta(3)-\pi^2 u}{24(s+u)^2}+$$
$$\left(\frac{u}{36(s+u)^2}-\frac{1}{18(s+u)}+\frac{1}{36s}\right)\log^3\left(\frac{u}{s}\right)+$$
$$\left(-\frac{u}{24(s+u)^2}+\frac{1}{12(s+u)}-\frac{7}{48s}\right)\log^2\left(\frac{u}{s}\right)+$$
$$\left(\frac{2-\pi^2}{12(s+u)}+\frac{\pi^2 u}{24(s+u)^2}+\frac{3+\pi^2}{24s}\right)\log\left(\frac{u}{s}\right)-\frac{16t\zeta(3)+8\pi^2 t-5u}{192tu}\Bigg]\Bigg\},$$

$$\delta\overline{\mathcal{F}}^{(2)}_{2,\mathtt{top};0}=-\,\delta\overline{\mathcal{F}}^{(2)}_{1,\mathtt{top};0},$$

$$\delta\overline{\mathcal{F}}^{(2)}_{3,\mathtt{top};0}=\pi^{-2\epsilon}\Gamma^2(1+\epsilon)\left(\frac{\mu^2}{m_t^2}\right)^{2\epsilon}4\pi\alpha_{em}\delta_{ij}\,Q_q^2\,C_F N_h$$
$$\Bigg\{\frac{1}{\epsilon^3}\left[\frac{1}{6u(s+u)}\right]+$$
$$\frac{1}{\epsilon^2}\left[\frac{3-2\log\left(-\frac{s}{m_t^2}\right)}{12u(s+u)}\right]+$$
$$\frac{1}{\epsilon}\Bigg[\frac{\log^2\left(-\frac{s}{m_t^2}\right)}{12u(s+u)}-\frac{\log\left(-\frac{s}{m_t^2}\right)}{4u(s+u)}-\frac{(s^3+2su^2+u^3)\log^2\left(\frac{u}{s}\right)}{12su(s+u)^3}+$$
$$\frac{1}{12}\left(\frac{1}{s^2+su}-\frac{1}{u^2}\right)\log^2\left(\frac{t}{s}\right)+$$
$$\frac{3u(s+u)^2(33s+16u)-4\pi^2 s\left(3s^3+13s^2u+8su^2+4u^3\right)}{144su^2(s+u)^3}-$$
$$\frac{(u-2s)\log\left(\frac{t}{s}\right)}{12su(s+u)}-\frac{(s-u)(3s+u)\log\left(\frac{u}{s}\right)}{12su(s+u)^2}\Bigg]+$$

$$
\left[
-\frac{\log^3\left(-\frac{s}{m_t^2}\right)}{36u(s+u)}+\frac{\log^2\left(-\frac{s}{m_t^2}\right)}{8u(s+u)}+
\right.
$$
$$
\left(\left(\frac{1}{12u^2}+\frac{1}{12u(s+u)}-\frac{1}{12su}\right)\log^2\left(\frac{t}{s}\right)+\right.
$$
$$
\left(\frac{1}{12su}-\frac{1}{4u(s+u)}\right)\log\left(\frac{t}{s}\right)+
$$
$$
\left(\frac{u}{6(s+u)^3}+\frac{1}{12su}-\frac{1}{4(s+u)^2}\right)\log^2\left(\frac{u}{s}\right)+
$$
$$
\left(\frac{1}{3u(s+u)}-\frac{1}{3(s+u)^2}-\frac{1}{12su}\right)\log\left(\frac{u}{s}\right)-
$$
$$
\left.\frac{1}{3su}+\frac{\pi^2}{12u^2}+\frac{-15+4\pi^2}{36u(s+u)}-\frac{\pi^2}{4(s+u)^2}+\frac{\pi^2 u}{6(s+u)^3}\right)\log\left(-\frac{s}{m_t^2}\right)+
$$
$$
\left(\frac{1}{18u^2}+\frac{1}{18u(s+u)}-\frac{1}{18su}\right)\log^3\left(\frac{t}{s}\right)+
$$
$$
\left(\frac{u}{9(s+u)^3}+\frac{1}{18su}-\frac{1}{6(s+u)^2}\right)\log^3\left(\frac{u}{s}\right)+
$$
$$
\left(-\frac{1}{12u^2}-\frac{3}{8u(s+u)}+\frac{7}{24su}\right)\log^2\left(\frac{t}{s}\right)+
$$
$$
\left(-\frac{u}{12(s+u)^3}-\frac{7}{24su}+\frac{5}{12u(s+u)}+\frac{1}{4(s+u)^2}\right)\log^2\left(\frac{u}{s}\right)+
$$
$$
\left(-\frac{\pi^2}{12u^2}-\frac{\pi^2}{12u(s+u)}+\frac{\pi^2}{12su}\right)H\left(-1,\frac{t}{s}\right)+
$$
$$
\left(-\frac{\pi^2 u}{6(s+u)^3}-\frac{\pi^2}{12su}+\frac{\pi^2}{4(s+u)^2}\right)H\left(-1,\frac{u}{s}\right)+
$$
$$
\left(-\frac{1}{6u^2}-\frac{1}{6u(s+u)}+\frac{1}{6su}\right)H\left(-1,0,0,\frac{t}{s}\right)+
$$
$$
\left(-\frac{u}{3(s+u)^3}-\frac{1}{6su}+\frac{1}{2(s+u)^2}\right)H\left(-1,0,0,\frac{u}{s}\right)+
$$
$$
\left(\frac{-3-\pi^2}{12su}+\frac{\pi^2}{12u^2}+\frac{7+\pi^2}{12u(s+u)}\right)\log\left(\frac{t}{s}\right)+
$$
$$
\left(\frac{2-\pi^2}{4(s+u)^2}+\frac{3+\pi^2}{12su}-\frac{1}{u(s+u)}+\frac{\pi^2 u}{6(s+u)^3}\right)\log\left(\frac{u}{s}\right)+
$$
$$
\left.\left.\frac{6\zeta(3)+5\pi^2}{12(s+u)^2}+\frac{-48\zeta(3)-4\pi^2+85}{96u(s+u)}+\frac{-\pi^2 u-4\zeta(3)u}{12(s+u)^3}+\frac{2}{3su}-\frac{2\zeta(3)+\pi^2}{12u^2}\right]\right\},
$$

$$
\delta\overline{\mathcal{F}}^{(2)}_{4,\mathtt{top};0} = \pi^{-2\epsilon}\Gamma^2(1+\epsilon)\left(\frac{\mu^2}{m_t^2}\right)^{2\epsilon} 4\pi\alpha_{em}\delta_{ij}\,Q_q^2\,C_F N_h
$$
$$
\left\{\frac{1}{\epsilon^3}\left[-\frac{s+2u}{12u(s+u)}\right]+\right.
$$

$$\frac{1}{\epsilon^2}\left[\frac{(s+2u)\left(2\log\left(-\frac{s}{m_t^2}\right)-3\right)}{24u(s+u)}\right]+$$
$$\frac{1}{\epsilon}\left[-\frac{(s+2u)\log^2\left(-\frac{s}{m_t^2}\right)}{24u(s+u)}+\frac{1}{8}\left(\frac{1}{s+u}+\frac{1}{u}\right)\log\left(-\frac{s}{m_t^2}\right)+\right.$$
$$\frac{(s+2u)\left(4\pi^2\left(3s^2+4su+4u^2\right)-99u(s+u)\right)}{288u^2(s+u)^2}+$$
$$\frac{1}{24}\left(\frac{s}{u^2}+\frac{1}{s+u}\right)\log^2\left(\frac{t}{s}\right)+$$
$$\frac{(u-2s)\log\left(\frac{t}{s}\right)}{24u(s+u)}+\frac{1}{24}\left(\frac{1}{u}-\frac{s}{(s+u)^2}\right)\log^2\left(\frac{u}{s}\right)+$$
$$\left.\frac{(3s+u)\log\left(\frac{u}{s}\right)}{24u(s+u)}\right]+$$
$$\left[\left(\frac{\pi^2 s}{24u^2}+\frac{\pi^2}{24(s+u)}\right)H\left(-1,\frac{t}{s}\right)+\right.$$
$$\left(\frac{s}{12u^2}+\frac{1}{12(s+u)}\right)H\left(-1,0,0,\frac{t}{s}\right)+$$
$$\left(\frac{\pi^2 u}{24(s+u)^2}-\frac{\pi^2}{24(s+u)}+\frac{\pi^2}{24u}\right)H\left(-1,\frac{u}{s}\right)+$$
$$\left(\frac{u}{12(s+u)^2}-\frac{1}{12(s+u)}+\frac{1}{12u}\right)H\left(-1,0,0,\frac{u}{s}\right)+$$
$$\log\left(-\frac{s}{m_t^2}\right)\left(\left(-\frac{s}{24u^2}-\frac{1}{24(s+u)}\right)\log^2\left(\frac{t}{s}\right)+\right.$$
$$\left(\frac{1}{12u}-\frac{1}{8(s+u)}\right)\log\left(\frac{t}{s}\right)-\frac{\pi^2 s}{24u^2}+\frac{27-\pi^2}{72(s+u)}-$$
$$\frac{\pi^2 u}{24(s+u)^2}+\left(-\frac{u}{24(s+u)^2}+\frac{1}{24(s+u)}-\frac{1}{24u}\right)\log^2\left(\frac{u}{s}\right)+$$
$$\left.\left(\frac{1}{12(s+u)}-\frac{1}{8u}\right)\log\left(\frac{u}{s}\right)-\frac{4\pi^2-27}{72u}\right)+$$
$$\left(\frac{1}{72(s+u)}+\frac{1}{72u}\right)\log^3\left(-\frac{s}{m_t^2}\right)+$$
$$\left(-\frac{1}{16(s+u)}-\frac{1}{16u}\right)\log^2\left(-\frac{s}{m_t^2}\right)+$$
$$\left(-\frac{s}{36u^2}-\frac{1}{36(s+u)}\right)\log^3\left(\frac{t}{s}\right)+$$
$$\left(\frac{s}{24u^2}-\frac{1}{16(s+u)}\right)\log^2\left(\frac{t}{s}\right)+$$
$$\left(-\frac{\pi^2 s}{24u^2}-\frac{(\pi-3)(3+\pi)}{24(s+u)}-\frac{1}{6u}\right)\log\left(\frac{t}{s}\right)+$$
$$\frac{s\left(2\zeta(3)+\pi^2\right)}{24u^2}+\frac{32\zeta(3)-12\pi^2-149}{192(s+u)}+\frac{2u\zeta(3)+\pi^2 u}{24(s+u)^2}+$$

$$\left(-\frac{u}{36(s+u)^2}+\frac{1}{36(s+u)}-\frac{1}{36u}\right)\log^3\left(\frac{u}{s}\right)+$$
$$\left(\frac{u}{24(s+u)^2}-\frac{1}{24(s+u)}-\frac{1}{16u}\right)\log^2\left(\frac{u}{s}\right)+$$
$$\left(\frac{(\pi-2)(2+\pi)}{24(s+u)}-\frac{\pi^2 u}{24(s+u)^2}-\frac{(\pi-3)(3+\pi)}{24u}\right)\log\left(\frac{u}{s}\right)-$$
$$\left.\frac{-48\zeta(3)+4\pi^2+149}{192u}\right]\Bigg\}.$$

Appendix C

Integral families and master integrals for Higgs production

C.1 Integral families

The two-loop Feynman diagrams, contributing to the process $g(p_1)+q(p_2) \to q(p_3)+H(p_4)$ and described in sec. 4.1, can be mapped into 6 different scalar integral families, PL, PLx13, PLx123, NA, NB and NBx132. We define the scalar integrals as

$$I_{\texttt{topo}}(n_1,...,n_9) = \int \frac{\mathcal{D}k_1 \mathcal{D}k_2}{D_1^{n_1} D_2^{n_2} D_3^{n_3} D_4^{n_4} D_5^{n_5} D_6^{n_6} D_7^{n_7} D_8^{n_8} D_9^{n_9}}, \tag{C.1}$$

where depending on the topology the set of the propagators $\{D_i\}$ can be one of the following:

- **family PL**

$$\begin{aligned}
D_1 &= k_1^2 \\
D_2 &= k_2^2 - m_V^2 \\
D_3 &= (k_1 - k_2)^2 \\
D_4 &= (k_1 - p_2)^2 \\
D_5 &= (k_1 - p_2 - p_1)^2 \\
D_6 &= (k_1 - p_1 - p_2 + p_3)^2 \\
D_7 &= (k_2 - p_1 - p_2 + p_3)^2 - m_V^2 \\
D_8 &= (k_2 - p_2)^2 \\
D_9 &= (k_2 - p_2 - p_1)^2
\end{aligned}$$

- **family PLx13**

$$\begin{aligned}
D_1 &= k_1^2 \\
D_2 &= k_2^2 - m_V^2 \\
D_3 &= (k_1 - k_2)^2
\end{aligned}$$

$$
\begin{aligned}
D_4 &= (k_1 - p_2)^2 \\
D_5 &= (k_1 - p_2 + p_3)^2 \\
D_6 &= (k_1 - p_1 - p_2 + p_3)^2 \\
D_7 &= (k_2 - p_1 - p_2 + p_3)^2 - m_V^2 \\
D_8 &= (k_2 - p_2)^2 \\
D_9 &= (k_2 - p_2 + p_3)^2
\end{aligned}
$$

- **family PLx123**

$$
\begin{aligned}
D_1 &= k_1^2 \\
D_2 &= k_2^2 - m_V^2 \\
D_3 &= (k_1 - k_2)^2 \\
D_4 &= (k_1 + p_3)^2 \\
D_5 &= (k_1 - p_2 + p_3)^2 \\
D_6 &= (k_1 - p_1 - p_2 + p_3)^2 \\
D_7 &= (k_2 - p_1 - p_2 + p_3)^2 - m_V^2 \\
D_8 &= (k_2 + p_3)^2 \\
D_9 &= (k_2 - p_2 + p_3)^2
\end{aligned}
$$

- **family NA**

$$
\begin{aligned}
D_1 &= k_1^2 \\
D_2 &= (k_1 - k_2 + p_1)^2 \\
D_3 &= (k_1 - p_2)^2 \\
D_4 &= k_2^2 - m_V^2 \\
D_5 &= (k_1 - p_2 + p_3)^2 \\
D_6 &= (k_2 - p_1 - p_2 + p_3)^2 - m_V^2 \\
D_7 &= (k_1 - k_2)^2 \\
D_8 &= (k_2 - p_1 - p_2)^2 - m_V^2 \\
D_9 &= (k_1 - p_1 - p_2)^2
\end{aligned}
$$

- **family NB**

$$
\begin{aligned}
D_1 &= k_1^2 \\
D_2 &= (k_1 - k_2 + p_1)^2 \\
D_3 &= (k_1 - p_2)^2 \\
D_4 &= k_2^2 - m_V^2 \\
D_5 &= (k_1 - p_2 + p_3)^2
\end{aligned}
$$

$$D_6 = (k_2 - p_1 - p_2 + p_3)^2 - m_V^2$$
$$D_7 = (k_1 - k_2)^2$$
$$D_8 = (k_2 - p_1 - p_2)^2$$
$$D_9 = (k_1 - p_1 - p_2)^2$$

- **family NBx132**

$$D_1 = k_1^2$$
$$D_2 = (k_1 - k_2 - p_3)^2$$
$$D_3 = (k_1 - p_1)^2$$
$$D_4 = (k_2)^2 - m_V^2$$
$$D_5 = (k_1 - p_1 - p_2)^2$$
$$D_6 = (k_2 - p_1 - p_2 + p_3)^2 - m_V^2$$
$$D_7 = (k_1 - k_2)^2$$
$$D_8 = (k_2 - p_1 + p_3)^2$$
$$D_9 = (k1 - p_1 + p_3)^2$$

C.2 Bases of MIs

After IBPs reduction all the scalar integrals appearing in the amplitude can be reduced to a basis of 180 master integrals, that we chose as following:

$$\mathcal{J}_1 = I_{\rm PL}(2,1,1,0,0,0,0,0,0) \qquad \mathcal{J}_2 = I_{\rm PL}(2,2,0,0,1,0,0,0,0) \tag{C.2}$$
$$\mathcal{J}_3 = I_{\rm PL}(0,1,2,0,2,0,0,0,0) \qquad \mathcal{J}_4 = I_{\rm PL}(0,2,2,0,1,0,0,0,0) \tag{C.3}$$
$$\mathcal{J}_5 = I_{\rm PL}(2,2,0,0,0,1,0,0,0) \qquad \mathcal{J}_6 = I_{\rm PL}(0,1,2,0,0,2,0,0,0) \tag{C.4}$$
$$\mathcal{J}_7 = I_{\rm PL}(0,2,2,0,0,1,0,0,0) \qquad \mathcal{J}_8 = I_{\rm PL}(0,2,0,2,0,1,0,0,0) \tag{C.5}$$
$$\mathcal{J}_9 = I_{\rm PL}(0,1,2,1,0,1,0,0,0) \qquad \mathcal{J}_{10} = I_{\rm PL}(0,2,2,1,0,1,0,0,0) \tag{C.6}$$
$$\mathcal{J}_{11} = I_{\rm PL}(1,2,0,1,1,1,0,0,0) \qquad \mathcal{J}_{12} = I_{\rm PL}(0,1,2,1,1,1,0,0,0) \tag{C.7}$$
$$\mathcal{J}_{13} = I_{\rm PL}(0,2,1,1,1,1,0,0,0) \qquad \mathcal{J}_{14} = I_{\rm PL}(2,1,1,0,0,0,2,0,0) \tag{C.8}$$
$$\mathcal{J}_{15} = I_{\rm PL}(0,0,2,2,0,0,1,0,0) \qquad \mathcal{J}_{16} = I_{\rm PL}(0,0,1,2,0,0,2,0,0) \tag{C.9}$$
$$\mathcal{J}_{17} = I_{\rm PL}(0,1,2,1,0,0,1,0,0) \qquad \mathcal{J}_{18} = I_{\rm PL}(0,1,2,1,0,0,2,0,0) \tag{C.10}$$
$$\mathcal{J}_{19} = I_{\rm PL}(1,1,1,1,0,0,1,0,0) \qquad \mathcal{J}_{20} = I_{\rm PL}(2,2,0,0,1,0,1,0,0) \tag{C.11}$$
$$\mathcal{J}_{21} = I_{\rm PL}(1,0,2,0,1,0,1,0,0) \qquad \mathcal{J}_{22} = I_{\rm PL}(1,0,2,0,1,0,2,0,0) \tag{C.12}$$
$$\mathcal{J}_{23} = I_{\rm PL}(0,1,2,0,1,0,1,0,0) \qquad \mathcal{J}_{24} = I_{\rm PL}(0,2,2,0,1,0,1,0,0) \tag{C.13}$$
$$\mathcal{J}_{25} = I_{\rm PL}(1,1,1,0,1,0,1,0,0) \qquad \mathcal{J}_{26} = I_{\rm PL}(1,1,2,0,1,0,1,0,0) \tag{C.14}$$
$$\mathcal{J}_{27} = I_{\rm PL}(2,1,1,0,1,0,2,0,0) \qquad \mathcal{J}_{28} = I_{\rm PL}(1,1,1,0,1,0,2,0,0) \tag{C.15}$$
$$\mathcal{J}_{29} = I_{\rm PL}(1,0,2,1,1,0,1,0,0) \qquad \mathcal{J}_{30} = I_{\rm PL}(1,0,1,1,1,0,2,0,0) \tag{C.16}$$
$$\mathcal{J}_{31} = I_{\rm PL}(0,1,1,1,1,0,1,0,0) \qquad \mathcal{J}_{32} = I_{\rm PL}(0,1,2,1,1,0,1,0,0) \tag{C.17}$$

$$\mathcal{J}_{33} = I_{\text{PL}}(1,1,1,1,1,0,1,0,0) \qquad \mathcal{J}_{34} = I_{\text{PL}}(1,1,1,1,1,-1,1,0,0) \tag{C.18}$$

$$\mathcal{J}_{35} = I_{\text{PL}}(1,1,1,1,1,0,2,0,0) \qquad \mathcal{J}_{36} = I_{\text{PL}}(2,2,0,0,0,1,1,0,0) \tag{C.19}$$

$$\mathcal{J}_{37} = I_{\text{PL}}(1,2,1,0,0,1,1,0,0) \qquad \mathcal{J}_{38} = I_{\text{PL}}(0,2,0,2,0,1,1,0,0) \tag{C.20}$$

$$\mathcal{J}_{39} = I_{\text{PL}}(0,1,1,1,0,1,1,0,0) \qquad \mathcal{J}_{40} = I_{\text{PL}}(0,1,2,1,0,1,1,0,0) \tag{C.21}$$

$$\mathcal{J}_{41} = I_{\text{PL}}(0,2,1,1,0,2,1,0,0) \qquad \mathcal{J}_{42} = I_{\text{PL}}(0,2,1,1,0,1,1,0,0) \tag{C.22}$$

$$\mathcal{J}_{43} = I_{\text{PL}}(0,1,1,0,1,1,1,0,0) \qquad \mathcal{J}_{44} = I_{\text{PL}}(1,1,0,1,1,1,1,0,0) \tag{C.23}$$

$$\mathcal{J}_{45} = I_{\text{PL}}(0,1,1,1,1,1,1,0,0) \qquad \mathcal{J}_{46} = I_{\text{PL}}(-1,1,1,1,1,1,1,0,0) \tag{C.24}$$

$$\mathcal{J}_{47} = I_{\text{PL}}(0,2,1,1,1,1,1,0,0) \qquad \mathcal{J}_{48} = I_{\text{PL}}(1,1,1,1,1,1,1,0,0) \tag{C.25}$$

$$\mathcal{J}_{49} = I_{\text{PL}}(0,0,2,0,0,2,0,1,0) \qquad \mathcal{J}_{50} = I_{\text{PL}}(1,0,2,0,0,1,0,1,0) \tag{C.26}$$

$$\mathcal{J}_{51} = I_{\text{PL}}(0,1,2,0,0,1,0,1,0) \qquad \mathcal{J}_{52} = I_{\text{PL}}(1,1,2,0,0,1,0,1,0) \tag{C.27}$$

$$\mathcal{J}_{53} = I_{\text{PL}}(1,2,1,0,0,1,0,1,0) \qquad \mathcal{J}_{54} = I_{\text{PL}}(1,2,1,0,0,2,0,1,0) \tag{C.28}$$

$$\mathcal{J}_{55} = I_{\text{PL}}(0,1,1,0,1,1,0,1,0) \qquad \mathcal{J}_{56} = I_{\text{PL}}(0,1,2,0,1,1,0,1,0) \tag{C.29}$$

$$\mathcal{J}_{57} = I_{\text{PL}}(1,0,2,0,0,0,1,1,0) \qquad \mathcal{J}_{58} = I_{\text{PL}}(1,1,2,0,0,0,1,1,0) \tag{C.30}$$

$$\mathcal{J}_{59} = I_{\text{PL}}(0,0,2,0,1,0,1,1,0) \qquad \mathcal{J}_{60} = I_{\text{PL}}(0,1,1,0,1,0,2,1,0) \tag{C.31}$$

$$\mathcal{J}_{61} = I_{\text{PL}}(0,1,2,0,1,0,1,1,0) \qquad \mathcal{J}_{62} = I_{\text{PL}}(0,0,2,0,0,1,1,2,0) \tag{C.32}$$

$$\mathcal{J}_{63} = I_{\text{PL}}(0,1,2,0,0,1,1,1,0) \qquad \mathcal{J}_{64} = I_{\text{PL}}(0,0,0,1,0,2,1,2,0) \tag{C.33}$$

$$\mathcal{J}_{65} = I_{\text{PL}}(0,1,0,2,0,1,1,1,0) \qquad \mathcal{J}_{66} = I_{\text{PL}}(0,0,1,0,1,1,1,1,0) \tag{C.34}$$

$$\mathcal{J}_{67} = I_{\text{PL}}(0,1,2,0,1,1,1,1,0) \qquad \mathcal{J}_{68} = I_{\text{PL}}(-1,1,1,1,1,1,1,1,0) \tag{C.35}$$

$$\mathcal{J}_{69} = I_{\text{PL}}(0,1,1,1,1,1,1,1,0) \qquad \mathcal{J}_{70} = I_{\text{PL}}(0,1,1,1,1,1,1,1,-1) \tag{C.36}$$

$$\mathcal{J}_{71} = I_{\text{PL}}(2,0,2,0,0,0,0,0,1) \qquad \mathcal{J}_{72} = I_{\text{PL}}(2,1,1,0,0,0,0,0,2) \tag{C.37}$$

$$\mathcal{J}_{73} = I_{\text{PL}}(0,1,2,1,0,0,0,0,1) \qquad \mathcal{J}_{74} = I_{\text{PL}}(1,1,1,1,0,0,0,0,1) \tag{C.38}$$

$$\mathcal{J}_{75} = I_{\text{PL}}(1,1,0,0,2,0,0,0,2) \qquad \mathcal{J}_{76} = I_{\text{PL}}(1,0,2,0,0,0,1,0,1) \tag{C.39}$$

$$\mathcal{J}_{77} = I_{\text{PL}}(1,1,2,0,0,0,1,0,1) \qquad \mathcal{J}_{78} = I_{\text{PL}}(1,0,1,1,0,0,1,0,1) \tag{C.40}$$

$$\mathcal{J}_{79} = I_{\text{PL}}(1,0,2,1,0,0,1,0,1) \qquad \mathcal{J}_{80} = I_{\text{PL}}(0,1,1,1,0,0,2,0,1) \tag{C.41}$$

$$\mathcal{J}_{81} = I_{\text{PL}}(0,1,2,1,0,0,1,0,1) \qquad \mathcal{J}_{82} = I_{\text{PL}}(1,1,2,1,0,0,1,0,1) \tag{C.42}$$

$$\mathcal{J}_{83} = I_{\text{PL}}(2,1,0,0,1,0,1,0,1],) \qquad \mathcal{J}_{84} = I_{\text{PL}}(1,0,1,0,1,0,1,0,1) \tag{C.43}$$

$$\mathcal{J}_{85} = I_{\text{PL}}(1,1,1,1,1,-1,1,0,1) \qquad \mathcal{J}_{86} = I_{\text{PL}}(1,1,1,1,1,0,1,0,1) \tag{C.44}$$

$$\mathcal{J}_{87} = I_{\text{PL}}(1,1,1,1,1,0,1,-1,1) \qquad \mathcal{J}_{88} = I_{\text{PL}}(0,1,2,0,0,1,0,0,1) \tag{C.45}$$

$$\mathcal{J}_{89} = I_{\text{PL}}(0,1,2,0,0,1,1,0,1) \qquad \mathcal{J}_{90} = I_{\text{PL}}(0,1,2,0,0,1,0,1,1) \tag{C.46}$$

$$\mathcal{J}_{91} = I_{\text{PL}}(0,1,2,0,0,1,1,1,1) \qquad \mathcal{J}_{92} = I_{\text{PL}}(1,0,2,0,0,0,1,1,1) \tag{C.47}$$

$$\mathcal{J}_{93} = I_{\text{PL}}(1,1,2,0,0,0,1,1,1) \qquad \mathcal{J}_{94} = I_{\text{PLx13}}(2,2,0,0,1,0,0,0,0) \tag{C.48}$$

$$\mathcal{J}_{95} = I_{\text{PLx13}}(0,1,2,0,2,0,0,0,0) \qquad \mathcal{J}_{96} = I_{\text{PLx13}}(0,2,2,0,1,0,0,0,0) \tag{C.49}$$

$$\mathcal{J}_{97} = I_{\text{PLx13}}(1,2,0,1,1,1,0,0,0) \qquad \mathcal{J}_{98} = I_{\text{PLx13}}(0,1,2,1,1,1,0,0,0) \tag{C.50}$$

$$\mathcal{J}_{99} = I_{\text{PLx13}}(0,2,1,1,1,1,0,0,0) \qquad \mathcal{J}_{100} = I_{\text{PLx13}}(2,2,0,0,1,0,1,0,0) \tag{C.51}$$

$$\mathcal{J}_{101} = I_{\text{PLx13}}(1,0,2,0,1,0,1,0,0) \qquad \mathcal{J}_{102} = I_{\text{PLx13}}(1,0,2,0,1,0,2,0,0) \tag{C.52}$$

$$\mathcal{J}_{103} = I_{\text{PLx13}}(0,1,2,0,1,0,1,0,0) \qquad \mathcal{J}_{104} = I_{\text{PLx13}}(0,2,2,0,1,0,1,0,0) \tag{C.53}$$

$$\mathcal{J}_{105} = I_{\text{PLx13}}(1,1,1,0,1,0,1,0,0) \qquad \mathcal{J}_{106} = I_{\text{PLx13}}(1,1,2,0,1,0,1,0,0) \tag{C.54}$$
$$\mathcal{J}_{107} = I_{\text{PLx13}}(2,1,1,0,1,0,2,0,0) \qquad \mathcal{J}_{108} = I_{\text{PLx13}}(1,1,1,0,1,0,2,0,0) \tag{C.55}$$
$$\mathcal{J}_{109} = I_{\text{PLx13}}(1,0,2,1,1,0,1,0,0) \qquad \mathcal{J}_{110} = I_{\text{PLx13}}(1,0,1,1,1,0,2,0,0) \tag{C.56}$$
$$\mathcal{J}_{111} = I_{\text{PLx13}}(0,1,1,1,1,0,1,0,0) \qquad \mathcal{J}_{112} = I_{\text{PLx13}}(0,1,2,1,1,0,1,0,0) \tag{C.57}$$
$$\mathcal{J}_{113} = I_{\text{PLx13}}(1,1,1,1,1,0,1,0,0) \qquad \mathcal{J}_{114} = I_{\text{PLx13}}(1,1,1,1,1,-1,1,0,0) \tag{C.58}$$
$$\mathcal{J}_{115} = I_{\text{PLx13}}(1,1,1,1,1,0,2,0,0) \qquad \mathcal{J}_{116} = I_{\text{PLx13}}(0,1,1,0,1,1,1,0,0) \tag{C.59}$$
$$\mathcal{J}_{117} = I_{\text{PLx13}}(1,1,0,1,1,1,1,0,0) \qquad \mathcal{J}_{118} = I_{\text{PLx13}}(0,1,1,1,1,1,1,0,0) \tag{C.60}$$
$$\mathcal{J}_{119} = I_{\text{PLx13}}(-1,1,1,1,1,1,1,0,0) \qquad \mathcal{J}_{120} = I_{\text{PLx13}}(0,2,1,1,1,1,1,0,0) \tag{C.61}$$
$$\mathcal{J}_{121} = I_{\text{PLx13}}(1,1,1,1,1,1,1,0,0) \qquad \mathcal{J}_{122} = I_{\text{PLx13}}(0,1,1,0,1,1,0,1,0) \tag{C.62}$$
$$\mathcal{J}_{123} = I_{\text{PLx13}}(0,1,2,0,1,1,0,1,0) \qquad \mathcal{J}_{124} = I_{\text{PLx13}}(0,1,1,0,1,0,2,1,0) \tag{C.63}$$
$$\mathcal{J}_{125} = I_{\text{PLx13}}(0,1,2,0,1,0,1,1,0) \qquad \mathcal{J}_{126} = I_{\text{PLx13}}(0,1,2,0,1,1,1,1,0) \tag{C.64}$$
$$\mathcal{J}_{127} = I_{\text{PLx13}}(-1,1,1,1,1,1,1,1,0) \qquad \mathcal{J}_{128} = I_{\text{PLx13}}(0,1,1,1,1,1,1,1,0) \tag{C.65}$$
$$\mathcal{J}_{129} = I_{\text{PLx13}}(0,1,1,1,1,1,1,1,-1) \qquad \mathcal{J}_{130} = I_{\text{PLx123}}(1,2,0,1,1,1,0,0,0) \tag{C.66}$$
$$\mathcal{J}_{131} = I_{\text{PLx123}}(0,1,2,1,1,1,0,0,0) \qquad \mathcal{J}_{132} = I_{\text{PLx123}}(0,2,1,1,1,1,0,0,0) \tag{C.67}$$
$$\mathcal{J}_{133} = I_{\text{PLx123}}(1,0,2,1,1,0,1,0,0) \qquad \mathcal{J}_{134} = I_{\text{PLx123}}(1,0,1,1,1,0,2,0,0) \tag{C.68}$$
$$\mathcal{J}_{135} = I_{\text{PLx123}}(0,1,1,1,1,0,1,0,0) \qquad \mathcal{J}_{136} = I_{\text{PLx123}}(0,1,2,1,1,0,1,0,0) \tag{C.69}$$
$$\mathcal{J}_{137} = I_{\text{PLx123}}(1,1,1,1,1,0,1,0,0) \qquad \mathcal{J}_{138} = I_{\text{PLx123}}(1,1,1,1,1,-1,1,0,0) \tag{C.70}$$
$$\mathcal{J}_{139} = I_{\text{PLx123}}(1,1,1,1,1,0,2,0,0) \qquad \mathcal{J}_{140} = I_{\text{PLx123}}(1,1,0,1,1,1,1,0,0) \tag{C.71}$$
$$\mathcal{J}_{141} = I_{\text{PLx123}}(0,1,1,1,1,1,1,0,0) \qquad \mathcal{J}_{142} = I_{\text{PLx123}}(-1,1,1,1,1,1,1,0,0) \tag{C.72}$$
$$\mathcal{J}_{143} = I_{\text{PLx123}}(0,2,1,1,1,1,1,0,0) \qquad \mathcal{J}_{144} = I_{\text{PLx123}}(1,1,1,1,1,1,1,0,0) \tag{C.73}$$
$$\mathcal{J}_{145} = I_{\text{PLx123}}(0,1,1,0,1,1,0,1,0) \qquad \mathcal{J}_{146} = I_{\text{PLx123}}(0,1,2,0,1,1,0,1,0) \tag{C.74}$$
$$\mathcal{J}_{147} = I_{\text{PLx123}}(0,1,1,0,1,0,1,1,0) \qquad \mathcal{J}_{148} = I_{\text{PLx123}}(0,1,2,0,1,0,1,1,0) \tag{C.75}$$
$$\mathcal{J}_{149} = I_{\text{PLx123}}(0,1,2,0,1,1,1,1,0) \qquad \mathcal{J}_{150} = I_{\text{PLx123}}(-1,1,1,1,1,1,1,1,0) \tag{C.76}$$
$$\mathcal{J}_{151} = I_{\text{PLx123}}(0,1,1,1,1,1,1,1,0) \qquad \mathcal{J}_{152} = I_{\text{PLx123}}(0,1,1,1,1,1,1,1,-1) \tag{C.77}$$
$$\mathcal{J}_{153} = I_{\text{NA}}(1,1,1,1,0,0,1,0,0) \qquad \mathcal{J}_{154} = I_{\text{NA}}(1,1,0,1,1,0,1,0,0) \tag{C.78}$$
$$\mathcal{J}_{155} = I_{\text{NA}}(0,1,1,1,1,0,1,0,0) \qquad \mathcal{J}_{156} = I_{\text{NA}}(0,1,1,2,1,0,1,0,0) \tag{C.79}$$
$$\mathcal{J}_{157} = I_{\text{NA}}(1,1,1,0,0,1,1,0,0) \qquad \mathcal{J}_{158} = I_{\text{NA}}(1,1,1,0,0,2,1,0,0) \tag{C.80}$$
$$\mathcal{J}_{159} = I_{\text{NA}}(1,1,1,1,0,1,1,0,0) \qquad \mathcal{J}_{160} = I_{\text{NA}}(1,1,1,1,-1,1,1,0,0) \tag{C.81}$$
$$\mathcal{J}_{161} = I_{\text{NA}}(1,1,1,2,0,1,1,0,0) \qquad \mathcal{J}_{162} = I_{\text{NA}}(0,1,1,0,1,1,1,0,0) \tag{C.82}$$
$$\mathcal{J}_{163} = I_{\text{NA}}(1,1,0,1,1,1,1,0,0) \qquad \mathcal{J}_{164} = I_{\text{NA}}(0,1,1,1,1,1,1,0,0) \tag{C.83}$$
$$\mathcal{J}_{165} = I_{\text{NA}}(-1,1,1,1,1,1,1,0,0) \qquad \mathcal{J}_{166} = I_{\text{NA}}(0,1,1,1,1,2,1,0,0) \tag{C.84}$$
$$\mathcal{J}_{167} = I_{\text{NA}}(1,1,1,1,1,1,1,0,0) \qquad \mathcal{J}_{168} = I_{\text{NA}}(1,1,1,1,1,1,1,0,-1) \tag{C.85}$$
$$\mathcal{J}_{169} = I_{\text{NA}}(1,1,1,1,1,1,1,0,-2) \qquad \mathcal{J}_{170} = I_{\text{NA}}(1,1,1,1,1,1,1,-1,-1) \tag{C.86}$$
$$\mathcal{J}_{171} = I_{\text{NB}}(1,1,1,1,0,0,1,1,0) \qquad \mathcal{J}_{172} = I_{\text{NB}}(1,1,1,0,0,1,1,1,0) \tag{C.87}$$
$$\mathcal{J}_{173} = I_{\text{NB}}(1,1,1,1,0,1,1,1,0) \qquad \mathcal{J}_{174} = I_{\text{NB}}(1,1,1,1,0,1,1,1,-1) \tag{C.88}$$
$$\mathcal{J}_{175} = I_{\text{NB}}(1,1,1,1,-1,1,1,1,-1) \qquad \mathcal{J}_{176} = I_{\text{NBx132}}(1,1,1,1,0,0,1,1,0) \tag{C.89}$$

$$\mathcal{J}_{177} = I_{\text{NBx132}}(1,1,1,0,0,1,1,1,0) \qquad \mathcal{J}_{178} = I_{\text{NBx132}}(1,1,1,1,0,1,1,1,0) \tag{C.90}$$

$$\mathcal{J}_{179} = I_{\text{NBx132}}(1,1,1,1,0,1,1,1,-1) \qquad \mathcal{J}_{180} = I_{\text{NBx132}}(1,1,1,1,-1,1,1,1,-1). \tag{C.91}$$

The basis $\{\mathcal{G}_i\}$, which makes simpler the differential equation system, has the following definition in terms of the $\mathcal{J}_i$:

$$\mathcal{G}_1 = \mathcal{J}_1(\epsilon-1)\epsilon^2$$

$$\mathcal{G}_2 = \mathcal{J}_2 S\epsilon^2$$

$$\mathcal{G}_3 = \mathcal{J}_3(S-1)\epsilon^2 - 2\mathcal{J}_4\epsilon^2$$

$$\mathcal{G}_4 = \mathcal{J}_4 S\epsilon^2$$

$$\mathcal{G}_5 = \mathcal{J}_5\omega\epsilon^2$$

$$\mathcal{G}_6 = \mathcal{J}_6\left(\omega-1\right)\epsilon^2 - 2\mathcal{J}_7\epsilon^2$$

$$\mathcal{G}_7 = \mathcal{J}_7\omega\epsilon^2$$

$$\mathcal{G}_8 = \mathcal{J}_8 T\epsilon^2$$

$$\mathcal{G}_9 = \frac{6\mathcal{J}_9\left(T-\omega\right)\epsilon^3}{\omega-T+2} - \frac{2\mathcal{J}_6\left(\omega-1\right)\epsilon^2}{\omega-T+2} + \frac{2\mathcal{J}_7\left(\omega+2\right)\epsilon^2}{\omega-T+2} - \frac{\mathcal{J}_{10}\left(\omega-T-1\right)\left(\omega-T\right)\epsilon^2}{\omega-T+2} - \frac{2\mathcal{J}_8 T\epsilon^2}{\omega-T+2}$$

$$\mathcal{G}_{10} = \mathcal{J}_9\left(T-\omega\right)\epsilon^3$$

$$\mathcal{G}_{11} = \mathcal{J}_{11} ST\epsilon^3$$

$$\mathcal{G}_{12} = \mathcal{J}_{12}(S-1)T\epsilon^3 - \mathcal{J}_{13}T\epsilon^3$$

$$\mathcal{G}_{13} = \mathcal{J}_{13} ST\epsilon^3$$

$$\mathcal{G}_{14} = \mathcal{J}_{14} q_1 q_2\epsilon^2 - \frac{\mathcal{J}_7\left(\omega-1\right)q_1\epsilon^2}{2q_2} - \frac{\mathcal{J}_1 q_1(\epsilon-1)\epsilon^2}{2q_2} - \frac{\mathcal{J}_6\left(\omega-1\right)q_1\epsilon^2}{4q_2}$$

$$\mathcal{G}_{15} = \mathcal{J}_{15}(T-1)\epsilon^2 - 2\mathcal{J}_{16}\epsilon^2$$

$$\mathcal{G}_{16} = \mathcal{J}_{16} T\epsilon^2$$

$$\mathcal{G}_{17} = \frac{3\mathcal{J}_{17} q_1 q_2\left(\omega-T\right)\epsilon^3}{2\left(\omega-2T\right)} + \frac{\mathcal{J}_{18} q_1 q_2\left(\omega(T-1)-T^2\right)\epsilon^2}{\omega-2T} + \frac{\mathcal{J}_1 q_1 q_2(\epsilon-1)\epsilon^2}{2\left(\omega-2T\right)} + \frac{\mathcal{J}_{16} q_1 q_2(T-1)\epsilon^2}{2\left(\omega-2T\right)} + \frac{\mathcal{J}_{15} q_1 q_2(T-1)\epsilon^2}{4\left(\omega-2T\right)}$$

$$\mathcal{G}_{18} = \mathcal{J}_{17}\left(T-\omega\right)\epsilon^3$$

$$\mathcal{G}_{19} = \mathcal{J}_{19}\left(T-\omega\right)\epsilon^4$$

$$\mathcal{G}_{20} = \mathcal{J}_{20} q_1 q_2 S\epsilon^2$$

$$\mathcal{G}_{21} = \frac{6\mathcal{J}_{21}\left(S-\omega\right)\epsilon^3}{\omega-S+2} - \frac{2\mathcal{J}_6\left(\omega-1\right)\epsilon^2}{\omega-S+2} + \frac{2\mathcal{J}_7\left(\omega+2\right)\epsilon^2}{\omega-S+2} - \frac{\mathcal{J}_{22}\left(\omega-S-1\right)\left(\omega-S\right)\epsilon^2}{\omega-S+2} - \frac{2\mathcal{J}_2 S\epsilon^2}{\omega-S+2}$$

$$\mathcal{G}_{22} = \mathcal{J}_{21}\left(S-\omega\right)\epsilon^3$$

$$\mathcal{G}_{23} = \frac{3\mathcal{J}_{23} q_1 q_2\left(\omega-S\right)\epsilon^3}{2\left(\omega-2S\right)} + \frac{\mathcal{J}_{24} q_1 q_2\left(\omega(S-1)-S^2\right)\epsilon^2}{\omega-2S} +$$

$$\frac{\mathcal{J}_1 q_1 q_2(\epsilon-1)\epsilon^2}{2\,(\omega-2S)}+\frac{\mathcal{J}_4 q_1 q_2(S-1)\epsilon^2}{2\,(\omega-2S)}+\frac{\mathcal{J}_3 q_1 q_2(S-1)\epsilon^2}{4\,(\omega-2S)}$$

$$\mathcal{G}_{24}=\mathcal{J}_{23}\,(S-\omega)\,\epsilon^3$$

$$\mathcal{G}_{25}=2\mathcal{J}_{25}\omega\epsilon^4+\frac{1}{2}\mathcal{J}_{28}\omega\,(\omega+S)\,\epsilon^3+\frac{2\mathcal{J}_{21}\omega\,(\omega-S-1)\,\epsilon^3}{\omega-S+2}+\frac{\mathcal{J}_{23}\omega\,(7S-5\omega)\,\epsilon^3}{2\,(\omega-2S)}+$$
$$\mathcal{J}_{14}\omega\epsilon^2+\mathcal{J}_{20}\omega S\epsilon^2+\mathcal{J}_{27}\omega S\epsilon^2+\frac{\mathcal{J}_2\omega S\epsilon^2}{\omega-S+2}+\frac{\mathcal{J}_{22}\omega\,(-\omega+S+1)\,\epsilon^2}{\omega-S+2}+$$
$$\frac{\mathcal{J}_6\,(\omega-1)\,(3\omega+S-2)\,\epsilon^2}{4\,(\omega-S+2)}+\frac{\mathcal{J}_{24}\omega\,(-S\omega+\omega+S^2)\,\epsilon^2}{\omega-2S}-$$
$$\frac{\mathcal{J}_7\,((3\omega-S+5)\,\omega+S-2)\,\epsilon^2}{2\,(\omega-S+2)}-\frac{\mathcal{J}_1\,(\omega-S)\,(\epsilon-1)\epsilon^2}{\omega-2S}-$$
$$\frac{\mathcal{J}_4\omega(S-1)\epsilon^2}{2\,(\omega-2S)}-\frac{\mathcal{J}_3\omega(S-1)\epsilon^2}{4\,(\omega-2S)}$$

$$\mathcal{G}_{26}=\mathcal{J}_{28}q_1q_2\,(S-\omega)\,\epsilon^3$$

$$\mathcal{G}_{27}=\mathcal{J}_{25}\,(S-\omega)\,\epsilon^4$$

$$\mathcal{G}_{28}=\mathcal{J}_{26}\,(S-\omega)\,\epsilon^3$$

$$\mathcal{G}_{29}=\mathcal{J}_{29}S(T-1)\epsilon^3-\mathcal{J}_{30}S\epsilon^3$$

$$\mathcal{G}_{30}=\mathcal{J}_{30}ST\epsilon^3$$

$$\mathcal{G}_{31}=\mathcal{J}_{31}(S+T)\epsilon^4$$

$$\mathcal{G}_{32}=\mathcal{J}_{32}(-TS+S+T)\epsilon^3$$

$$\mathcal{G}_{33}=\mathcal{J}_{33}S\,(T-\omega)\,\epsilon^4$$

$$\mathcal{G}_{34}=\mathcal{J}_{33}\omega S\epsilon^4+\mathcal{J}_{34}S\epsilon^4+\mathcal{J}_{31}T\epsilon^4$$

$$\mathcal{G}_{35}=\frac{\mathcal{J}_{24}q_1\left(\omega(S-1)-S^2\right)\epsilon^2\,(\omega)^{3/2}}{(\omega-2S)\,(\omega-2T)}-\frac{\mathcal{J}_{14}q_1\epsilon^2\,(\omega)^{3/2}}{\omega-2T}-\frac{\mathcal{J}_{20}q_1S\epsilon^2\,(\omega)^{3/2}}{\omega-2T}-$$
$$\frac{\mathcal{J}_{27}q_1S\epsilon^2\,(\omega)^{3/2}}{\omega-2T}-\frac{\mathcal{J}_{28}q_1\,(\omega+S)\,\epsilon^3\,(\omega)^{3/2}}{2\,(\omega-2T)}+\frac{\mathcal{J}_{34}q_1q_2S\epsilon^4}{\omega-2T}+\frac{\mathcal{J}_{19}q_1q_2\,(\omega-T)\,\epsilon^4}{\omega-2T}+$$
$$\frac{\mathcal{J}_{33}q_1q_2S\,(2\omega-T)\,\epsilon^4}{\omega-2T}+\frac{\mathcal{J}_{31}q_1q_2(S+3T)\epsilon^4}{2\,(\omega-2T)}+\frac{\mathcal{J}_{32}q_1q_2(-TS+S+T)\epsilon^3}{4\,(\omega-2T)}+$$
$$\frac{\mathcal{J}_{35}q_1q_2S\left(\omega(T-1)-T^2\right)\epsilon^3}{\omega-2T}+\frac{\mathcal{J}_{17}q_1q_2\,(T-\omega)\,\epsilon^3}{2\,(\omega-2T)}+$$
$$\frac{\mathcal{J}_{29}q_1q_2S(T-1)\epsilon^3}{6\,(\omega-2T)}+\frac{\mathcal{J}_{30}q_1q_2S(3T-1)\epsilon^3}{6\,(\omega-2T)}+\frac{\mathcal{J}_{23}q_1q_2\left(2\omega^2-2S\omega-S^2\right)\epsilon^3}{(\omega-2S)\,(\omega-2T)}+$$
$$\frac{\mathcal{J}_1q_1q_2\,(11\omega-16S)\,(\epsilon-1)\epsilon^2}{6\,(\omega-2S)\,(\omega-2T)}+\frac{\mathcal{J}_{15}q_1q_2(T-1)\epsilon^2}{8\,(\omega-2T)}+\frac{\mathcal{J}_2\,(1-3\omega)\,q_1q_2S\epsilon^2}{3\,(\omega-S+2)\,(\omega-2T)}+$$
$$\frac{\mathcal{J}_{22}q_1q_2\,(\omega-S-1)\,(7\omega-S)\,\epsilon^2}{6\,(\omega-S+2)\,(\omega-2T)}+\frac{\mathcal{J}_7q_1q_2\left(3\omega^2+\omega+3\,(\omega+1)\,S-10\right)\epsilon^2}{6\,(\omega-S+2)\,(\omega-2T)}+$$
$$\frac{\mathcal{J}_4q_1q_2\,(2\,(\omega+1)\,S-3\omega)\,\epsilon^2}{4\,(\omega-2S)\,(\omega-2T)}+\frac{\mathcal{J}_3q_1q_2(S-1)\,(3\omega-2S)\,\epsilon^2}{8\,(\omega-2S)\,(\omega-2T)}-\frac{\mathcal{J}_{25}q_1q_2\,(\omega+S)\,\epsilon^4}{\omega-2T}-$$
$$\frac{\mathcal{J}_{21}q_1q_2\,((2\omega-2S-3)\,\omega+S)\,\epsilon^3}{(\omega-S+2)\,(\omega-2T)}-\frac{\mathcal{J}_6\,(\omega-1)\,q_1q_2\,(9\omega+3S-10)\,\epsilon^2}{12\,(\omega-S+2)\,(\omega-2T)}-\frac{\mathcal{J}_{16}q_1q_2\epsilon^2}{4\omega-8T}$$

$$\mathcal{G}_{36}=\mathcal{J}_{36}\,(\omega)^{3/2}\,q_1\epsilon^2$$

$$\mathcal{G}_{37} = \mathcal{J}_{36}\epsilon^2\omega^2 - \mathcal{J}_{14}\epsilon^2\omega + \mathcal{J}_{37}\epsilon^2(2\epsilon-1)\omega + \frac{1}{4}\mathcal{J}_6\left(\omega-1\right)\epsilon^2 + \frac{1}{2}\mathcal{J}_7\left(\omega-1\right)\epsilon^2 + \frac{1}{2}\mathcal{J}_1(\epsilon-1)\epsilon^2$$

$$\mathcal{G}_{38} = \mathcal{J}_{38}q_1q_2T\epsilon^2$$

$$\mathcal{G}_{39} = 2\mathcal{J}_{39}\omega\epsilon^4 + \frac{1}{2}\mathcal{J}_{42}\omega\left(\omega+T\right)\epsilon^3 + \frac{2\mathcal{J}_9\omega\left(\omega-T-1\right)\epsilon^3}{\omega-T+2} + \frac{\mathcal{J}_{17}\omega\left(7T-5\omega\right)\epsilon^3}{2\left(\omega-2T\right)} + \mathcal{J}_{14}\omega\epsilon^2 + \mathcal{J}_{38}\omega T\epsilon^2 + \mathcal{J}_{41}\omega T\epsilon^2 + \frac{\mathcal{J}_8\omega T\epsilon^2}{\omega-T+2} + \frac{\mathcal{J}_{10}\omega\left(-\omega+T+1\right)\epsilon^2}{\omega-T+2} + \frac{\mathcal{J}_6\left(\omega-1\right)\left(3\omega+T-2\right)\epsilon^2}{4\left(\omega-T+2\right)} + \frac{\mathcal{J}_{18}\omega\left(-T\omega+\omega+T^2\right)\epsilon^2}{\omega-2T} - \frac{\mathcal{J}_7\left(\left(3\omega-T+5\right)\omega+T-2\right)\epsilon^2}{2\left(\omega-T+2\right)} - \frac{\mathcal{J}_1\left(\omega-T\right)(\epsilon-1)\epsilon^2}{\omega-2T} - \frac{\mathcal{J}_{16}\omega(T-1)\epsilon^2}{2\left(\omega-2T\right)} - \frac{\mathcal{J}_{15}\omega(T-1)\epsilon^2}{4\left(\omega-2T\right)}$$

$$\mathcal{G}_{40} = \mathcal{J}_{42}q_1q_2\left(T-\omega\right)\epsilon^3$$

$$\mathcal{G}_{41} = \mathcal{J}_{39}\left(T-\omega\right)\epsilon^4$$

$$\mathcal{G}_{42} = \mathcal{J}_{40}\left(T-\omega\right)\epsilon^3$$

$$\mathcal{G}_{43} = \mathcal{J}_{43}\left(S-\omega\right)\epsilon^4$$

$$\mathcal{G}_{44} = \frac{\mathcal{J}_{11}q_2ST\epsilon^3}{q_1} + \frac{\mathcal{J}_{44}q_2ST(2\epsilon-1)\epsilon^3}{q_1}$$

$$\mathcal{G}_{45} = \mathcal{J}_{45}\left(S-\omega\right)T\epsilon^4$$

$$\mathcal{G}_{46} = \mathcal{J}_{45}\omega T\epsilon^4 - \mathcal{J}_{31}T\epsilon^4 + \mathcal{J}_{46}T\epsilon^4$$

$$\mathcal{G}_{47} = \frac{\mathcal{J}_{18}q_1\left(\omega(T-1)-T^2\right)\epsilon^2\left(\omega\right)^{3/2}}{\left(\omega-2S\right)\left(\omega-2T\right)} - \frac{\mathcal{J}_{14}q_1\epsilon^2\left(\omega\right)^{3/2}}{\omega-2S} - \frac{\mathcal{J}_{38}q_1T\epsilon^2\left(\omega\right)^{3/2}}{\omega-2S} - \frac{\mathcal{J}_{41}q_1T\epsilon^2\left(\omega\right)^{3/2}}{\omega-2S} - \frac{\mathcal{J}_{42}q_1\left(\omega+T\right)\epsilon^3\left(\omega\right)^{3/2}}{2\left(\omega-2S\right)} + \frac{\mathcal{J}_{46}q_1q_2T\epsilon^4}{\omega-2S} + \frac{\mathcal{J}_{45}q_1q_2\left(2\omega-S\right)T\epsilon^4}{\omega-2S} + \frac{\mathcal{J}_{31}q_1q_2(3S+T)\epsilon^4}{2\left(\omega-2S\right)} + \frac{\mathcal{J}_{43}q_1q_2\left(\omega-S\right)\epsilon^4}{\omega-2S} + \frac{\mathcal{J}_{47}q_1q_2\left(\omega(S-1)-S^2\right)T\epsilon^3}{\omega-2S} + \frac{\mathcal{J}_{12}q_1q_2(S-1)T\epsilon^3}{6\left(\omega-2S\right)} + \frac{\mathcal{J}_{13}q_1q_2(3S-1)T\epsilon^3}{6\left(\omega-2S\right)} + \frac{\mathcal{J}_{32}q_1q_2(-TS+S+T)\epsilon^3}{4\left(\omega-2S\right)} + \frac{\mathcal{J}_{17}q_1q_2\left(2\omega^2-2T\omega-T^2\right)\epsilon^3}{\left(\omega-2S\right)\left(\omega-2T\right)} + \frac{\mathcal{J}_{23}q_1q_2\left(S-\omega\right)\epsilon^3}{2\left(\omega-2S\right)} + \frac{\mathcal{J}_{10}q_1q_2\left(\omega-T-1\right)\left(7\omega-T\right)\epsilon^2}{6\left(\omega-2S\right)\left(\omega-T+2\right)} + \frac{\mathcal{J}_8\left(1-3\omega\right)q_1q_2T\epsilon^2}{3\left(\omega-2S\right)\left(\omega-T+2\right)} + \frac{\mathcal{J}_7q_1q_2\left(3\omega^2+\omega+3\left(\omega+1\right)T-10\right)\epsilon^2}{6\left(\omega-2S\right)\left(\omega-T+2\right)} + \frac{\mathcal{J}_{15}q_1q_2(T-1)\left(3\omega-2T\right)\epsilon^2}{8\left(\omega-2S\right)\left(\omega-2T\right)} + \frac{\mathcal{J}_1q_1q_2\left(11\omega-16T\right)(\epsilon-1)\epsilon^2}{6\left(\omega-2S\right)\left(\omega-2T\right)} + \frac{\mathcal{J}_3q_1q_2(S-1)\epsilon^2}{8\left(\omega-2S\right)} + \frac{\mathcal{J}_{16}q_1q_2\left(2\left(\omega+1\right)T-3\omega\right)\epsilon^2}{4\left(\omega-2S\right)\left(\omega-2T\right)} - \frac{\mathcal{J}_{39}q_1q_2\left(\omega+T\right)\epsilon^4}{\omega-2S} - \frac{\mathcal{J}_4q_1q_2\epsilon^2}{4\omega-8S} - \frac{\mathcal{J}_9q_1q_2\left(\left(2\omega-2T-3\right)\omega+T\right)\epsilon^3}{\left(\omega-2S\right)\left(\omega-T+2\right)} - \frac{\mathcal{J}_6\left(\omega-1\right)q_1q_2\left(9\omega+3T-10\right)\epsilon^2}{12\left(\omega-2S\right)\left(\omega-T+2\right)}$$

$$\mathcal{G}_{48} = \mathcal{J}_{33}\omega S\epsilon^4 + \mathcal{J}_{45}\omega T\epsilon^4 + \mathcal{J}_{48}\omega ST\epsilon^4$$

$$\mathcal{G}_{49} = \mathcal{J}_{49} T \epsilon^2$$
$$\mathcal{G}_{50} = \mathcal{J}_{50} \left(T - \omega\right) \epsilon^3$$
$$\mathcal{G}_{51} = \mathcal{J}_{51} \left(T - \omega\right) \epsilon^3$$
$$\mathcal{G}_{52} = \mathcal{J}_{52} \left(T - \omega\right) \epsilon^3$$
$$\mathcal{G}_{53} = \mathcal{J}_{53} \left(T - \omega\right) \epsilon^3$$
$$\mathcal{G}_{54} = -2\mathcal{J}_{51} \left(\omega - T\right)^2 \epsilon^3 - 2\mathcal{J}_{52} \left(\omega - T\right)^2 \epsilon^3 - 2\mathcal{J}_{53} \left(\omega - T\right)^2 \epsilon^3 + \mathcal{J}_{5} \omega \left(\omega - T\right) \epsilon^2 - \mathcal{J}_{54} \omega \left(\omega - T - 1\right) \left(\omega - T\right) \epsilon^2 + \mathcal{J}_{49} \left(\omega - T\right) T \epsilon^2 + \mathcal{J}_{7} \omega \left(T - \omega\right) \epsilon^2$$
$$\mathcal{G}_{55} = \mathcal{J}_{55} \left(-\omega + S + T\right) \epsilon^4$$
$$\mathcal{G}_{56} = \mathcal{J}_{56} (S - 1) T \epsilon^3$$
$$\mathcal{G}_{57} = \mathcal{J}_{57} \left(T - \omega\right) \epsilon^3$$
$$\mathcal{G}_{58} = \mathcal{J}_{58} \left(T - \omega\right) \epsilon^3$$
$$\mathcal{G}_{59} = \mathcal{J}_{59} T \epsilon^3$$
$$\mathcal{G}_{60} = \frac{3\mathcal{J}_{23} \left(\omega - S\right) \left(\omega - 2T\right) \epsilon^3}{2 \left(\omega - 2S\right)} + \frac{\mathcal{J}_{24} \left(\omega (S - 1) - S^2\right) \left(\omega - 2T\right) \epsilon^2}{\omega - 2S} + \frac{\mathcal{J}_{4} (S - 1) \left(\omega - 2T\right) \epsilon^2}{2 \left(\omega - 2S\right)} + \frac{\mathcal{J}_{3} (S - 1) \left(\omega - 2T\right) \epsilon^2}{4 \left(\omega - 2S\right)} + \frac{\mathcal{J}_{1} \left(\omega - 2T\right) (\epsilon - 1) \epsilon^2}{2 \left(\omega - 2S\right)} - \mathcal{J}_{60} \left(\omega (T - 1) - T^2\right) (2\epsilon - 1) \epsilon^2$$
$$\mathcal{G}_{61} = \mathcal{J}_{61} (-TS + S + T) \epsilon^3$$
$$\mathcal{G}_{62} = -\frac{\mathcal{J}_{62} (T - 1) T \epsilon^2}{T + 1} - \frac{\mathcal{J}_{1} (\epsilon - 1) \epsilon^2}{T + 1} - \frac{3\mathcal{J}_{49} T \epsilon^2}{2(T + 1)}$$
$$\mathcal{G}_{63} = \mathcal{J}_{63} \left(T - \omega\right) \epsilon^3$$
$$\mathcal{G}_{64} = -\frac{\mathcal{J}_{64} (T - 1) T^2 \epsilon^2}{T + 1} - \frac{\mathcal{J}_{8} T \epsilon^2}{T + 1}$$
$$\mathcal{G}_{65} = \mathcal{J}_{65} T \left(T - \omega\right) \epsilon^3$$
$$\mathcal{G}_{66} = \mathcal{J}_{66} T \epsilon^4$$
$$\mathcal{G}_{67} = -\mathcal{J}_{56} q_{8} \epsilon^3 + 2\mathcal{J}_{61} q_{8} \epsilon^3 + \mathcal{J}_{67} q_{8} \epsilon^3$$
$$\mathcal{G}_{68} = -\mathcal{J}_{69} T^2 \epsilon^4 - \mathcal{J}_{68} (T - 1) T \epsilon^4 + \frac{1}{2} \mathcal{J}_{56} \left(\omega - S\right) (T - 1) \epsilon^3 - \frac{1}{2} \mathcal{J}_{67} \left(\omega - S\right) (T - 1) \epsilon^3 - \frac{1}{2} \mathcal{J}_{32} T \epsilon^3 + \mathcal{J}_{61} \left(-T\omega + \omega + S(T - 1) + T\right) \epsilon^3$$
$$\mathcal{G}_{69} = \mathcal{J}_{69} T (-TS + S + T) \epsilon^4$$
$$\mathcal{G}_{70} = \mathcal{J}_{70} T \left(T - \omega\right) \epsilon^4$$
$$\mathcal{G}_{71} = \mathcal{J}_{71} S \epsilon^2$$
$$\mathcal{G}_{72} = -\frac{\mathcal{J}_{72} (S - 1) S \epsilon^2}{S + 1} - \frac{\mathcal{J}_{1} (\epsilon - 1) \epsilon^2}{S + 1} - \frac{3\mathcal{J}_{71} S \epsilon^2}{2(S + 1)}$$
$$\mathcal{G}_{73} = \mathcal{J}_{73} S \epsilon^3$$
$$\mathcal{G}_{74} = \mathcal{J}_{74} S \epsilon^4$$
$$\mathcal{G}_{75} = -\frac{\mathcal{J}_{75} (S - 1) S^2 \epsilon^2}{S + 1} - \frac{\mathcal{J}_{2} S \epsilon^2}{S + 1}$$

$$\mathcal{G}_{76} = \mathcal{J}_{76}\left(S-\omega\right)\epsilon^3$$
$$\mathcal{G}_{77} = \mathcal{J}_{77}\left(S-\omega\right)\epsilon^3$$
$$\mathcal{G}_{78} = \mathcal{J}_{78}\left(-\omega+S+T\right)\epsilon^4$$
$$\mathcal{G}_{79} = \mathcal{J}_{79}S(T-1)\epsilon^3$$
$$\mathcal{G}_{80} = \frac{\mathcal{J}_{81}S(S(T-1)-T)\epsilon^3}{-S\omega+\omega+S^2+S} - \frac{3\mathcal{J}_{73}S^2\epsilon^3}{-S\omega+\omega+S^2+S} -$$
$$\frac{3\mathcal{J}_{17}\left(\omega(S-1)-2S\right)\left(\omega-S\right)\left(\omega-T\right)\epsilon^3}{2\left(\omega(S-1)-S(S+1)\right)\left(\omega-2T\right)} - \frac{\mathcal{J}_{80}\left(\omega-S\right)\left(\omega(S-1)-S^2\right)\left(2\epsilon-1\right)\epsilon^2}{\omega(S-1)-S(S+1)} -$$
$$\frac{\mathcal{J}_{18}\left(\omega(S-1)-2S\right)\left(\omega-S\right)\left(\omega(T-1)-T^2\right)\epsilon^2}{\left(\omega(S-1)-S(S+1)\right)\left(\omega-2T\right)} -$$
$$\frac{\mathcal{J}_{16}\left((S-1)(T-1)\omega^2+S(-TS+S+3)\omega+2S(S(T-1)-T(T+2))\right)\epsilon^2}{2\left(\omega(S-1)-S(S+1)\right)\left(\omega-2T\right)} -$$
$$\frac{\mathcal{J}_{1}\left((S-1)\omega^2-S(S+3)\omega+2S(S+2T)\right)\left(\epsilon-1\right)\epsilon^2}{2\left(\omega(S-1)-S(S+1)\right)\left(\omega-2T\right)} -$$
$$\frac{\mathcal{J}_{15}(T-1)\left((S-1)\omega^2-S(S+3)\omega+2S(S+2T)\right)\epsilon^2}{4\left(\omega(S-1)-S(S+1)\right)\left(\omega-2T\right)}$$
$$\mathcal{G}_{81} = \mathcal{J}_{81}(-TS+S+T)\epsilon^3$$
$$\mathcal{G}_{82} = -\mathcal{J}_{79}q_{11}\epsilon^3 + 2\mathcal{J}_{81}q_{11}\epsilon^3 + \mathcal{J}_{82}q_{11}\epsilon^3$$
$$\mathcal{G}_{83} = \mathcal{J}_{83}S\left(S-\omega\right)\epsilon^3$$
$$\mathcal{G}_{84} = \mathcal{J}_{84}\left(S-\omega\right)\epsilon^4$$
$$\mathcal{G}_{85} = -\mathcal{J}_{86}S^2\epsilon^4 - \mathcal{J}_{85}(S-1)S\epsilon^4 - \frac{1}{2}\mathcal{J}_{32}S\epsilon^3 + \frac{1}{2}\mathcal{J}_{79}(S-1)\left(\omega-T\right)\epsilon^3 -$$
$$\frac{1}{2}\mathcal{J}_{82}(S-1)\left(\omega-T\right)\epsilon^3 + \mathcal{J}_{81}\left(-S\omega+\omega+S+(S-1)T\right)\epsilon^3$$
$$\mathcal{G}_{86} = \mathcal{J}_{86}S(S(T-1)-T)\epsilon^4$$
$$\mathcal{G}_{87} = \mathcal{J}_{87}S\left(S-\omega\right)\epsilon^4$$
$$\mathcal{G}_{88} = \mathcal{J}_{88}\left(S-\omega\right)\epsilon^3$$
$$\mathcal{G}_{89} = \mathcal{J}_{89}\left(S-\omega\right)\epsilon^3$$
$$\mathcal{G}_{90} = \mathcal{J}_{90}(S-1)T\epsilon^3$$
$$\mathcal{G}_{91} = \mathcal{J}_{91}(-TS+S+T)\epsilon^3 - \mathcal{J}_{90}S\epsilon^3$$
$$\mathcal{G}_{92} = \mathcal{J}_{92}S(T-1)\epsilon^3$$
$$\mathcal{G}_{93} = \mathcal{J}_{93}(-TS+S+T)\epsilon^3 - \mathcal{J}_{92}T\epsilon^3$$
$$\mathcal{G}_{94} = \mathcal{J}_{94}\left(-\omega+S+T\right)\epsilon^2$$
$$\mathcal{G}_{95} = 2\mathcal{J}_{96}\epsilon^2 + \mathcal{J}_{95}\left(-\omega+S+T+1\right)\epsilon^2$$
$$\mathcal{G}_{96} = \mathcal{J}_{96}\left(-\omega+S+T\right)\epsilon^2$$
$$\mathcal{G}_{97} = \mathcal{J}_{97}T\left(-\omega+S+T\right)\epsilon^3$$
$$\mathcal{G}_{98} = \mathcal{J}_{99}T\epsilon^3 + \mathcal{J}_{98}T\left(-\omega+S+T+1\right)\epsilon^3$$
$$\mathcal{G}_{99} = \mathcal{J}_{99}T\left(-\omega+S+T\right)\epsilon^3$$
$$\mathcal{G}_{100} = \mathcal{J}_{100}q_1q_2\left(-\omega+S+T\right)\epsilon^2$$

$$\mathcal{G}_{101} = -\frac{6\mathcal{J}_{101}(S+T)\epsilon^3}{S+T+2} + \frac{2\mathcal{J}_{94}\left(-\omega+S+T\right)\epsilon^2}{S+T+2} - \frac{2\mathcal{J}_{6}\left(\omega-1\right)\epsilon^2}{S+T+2} + \frac{2\mathcal{J}_{7}\left(\omega+2\right)\epsilon^2}{S+T+2} - \frac{\mathcal{J}_{102}(S+T-1)(S+T)\epsilon^2}{S+T+2}$$

$$\mathcal{G}_{102} = \mathcal{J}_{101}(S+T)\epsilon^3$$

$$\mathcal{G}_{103} = \frac{3\mathcal{J}_{103}q_1q_2(S+T)\epsilon^3}{2\left(\omega-2(S+T)\right)} + \frac{\mathcal{J}_{104}q_1q_2\left(\omega(S+T-1)-(S+T)^2\right)\epsilon^2}{\omega-2(S+T)} + \frac{\mathcal{J}_{1}q_1q_2(\epsilon-1)\epsilon^2}{2\left(\omega-2(S+T)\right)} + \frac{\mathcal{J}_{96}q_1q_2\left(\omega-S-T-1\right)\epsilon^2}{2\left(\omega-2(S+T)\right)} + \frac{\mathcal{J}_{95}q_1q_2\left(\omega-S-T-1\right)\epsilon^2}{4\left(\omega-2(S+T)\right)}$$

$$\mathcal{G}_{104} = \mathcal{J}_{103}(S+T)\epsilon^3$$

$$\mathcal{G}_{105} = -2\mathcal{J}_{105}\omega\epsilon^4 + \frac{1}{2}\mathcal{J}_{108}\omega\left(-2\omega+S+T\right)\epsilon^3 + \frac{\mathcal{J}_{103}\omega\left(2\omega-7(S+T)\right)\epsilon^3}{2\left(\omega-2(S+T)\right)} - \frac{2\mathcal{J}_{101}\omega(S+T-1)\epsilon^3}{S+T+2} - \mathcal{J}_{14}\omega\epsilon^2 + \mathcal{J}_{100}\omega\left(-\omega+S+T\right)\epsilon^2 + \mathcal{J}_{107}\omega\left(-\omega+S+T\right)\epsilon^2 + \frac{\mathcal{J}_{94}\omega\left(-\omega+S+T\right)\epsilon^2}{S+T+2} + \frac{\mathcal{J}_{6}\left(\omega-1\right)\left(-4\omega+S+T+2\right)\epsilon^2}{4(S+T+2)} + \frac{\mathcal{J}_{104}\omega\left((S+T)^2-\omega(S+T-1)\right)\epsilon^2}{\omega-2(S+T)} + \frac{\mathcal{J}_{7}\left((2\omega+S+T+6)\omega-S-T-2\right)\epsilon^2}{2(S+T+2)} + \frac{\mathcal{J}_{102}\omega(S+T-1)\epsilon^2}{S+T+2} - \frac{\mathcal{J}_{1}(S+T)(\epsilon-1)\epsilon^2}{\omega-2(S+T)} + \frac{\mathcal{J}_{96}\omega\left(-\omega+S+T+1\right)\epsilon^2}{2\left(\omega-2(S+T)\right)} + \frac{\mathcal{J}_{95}\omega\left(-\omega+S+T+1\right)\epsilon^2}{4\left(\omega-2(S+T)\right)}$$

$$\mathcal{G}_{106} = \mathcal{J}_{108}q_1q_2(S+T)\epsilon^3$$

$$\mathcal{G}_{107} = \mathcal{J}_{105}(S+T)\epsilon^4$$

$$\mathcal{G}_{108} = \mathcal{J}_{106}(S+T)\epsilon^3$$

$$\mathcal{G}_{109} = \mathcal{J}_{110}\left(\omega-S-T\right)\epsilon^3 + \mathcal{J}_{109}(T-1)\left(-\omega+S+T\right)\epsilon^3$$

$$\mathcal{G}_{110} = \mathcal{J}_{110}T\left(-\omega+S+T\right)\epsilon^3$$

$$\mathcal{G}_{111} = \mathcal{J}_{111}\left(S-\omega\right)\epsilon^4$$

$$\mathcal{G}_{112} = \mathcal{J}_{112}\left(-T\omega+\omega+T^2+S(T-1)\right)\epsilon^3$$

$$\mathcal{G}_{113} = \mathcal{J}_{113}\left(\omega-T\right)\left(\omega-S-T\right)\epsilon^4$$

$$\mathcal{G}_{114} = -\mathcal{J}_{111}T\epsilon^4 + \mathcal{J}_{113}\omega\left(-\omega+S+T\right)\epsilon^4 + \mathcal{J}_{114}\left(-\omega+S+T\right)\epsilon^4$$

$$\mathcal{G}_{115} = \frac{\mathcal{J}_{108}q_1\left(2\omega-S-T\right)\epsilon^3\left(\omega\right)^{3/2}}{2\left(\omega-2T\right)} + \frac{\mathcal{J}_{104}q_1\left(\omega(S+T-1)-(S+T)^2\right)\epsilon^2\left(\omega\right)^{3/2}}{\left(\omega-2T\right)\left(\omega-2(S+T)\right)} + \frac{\mathcal{J}_{14}q_1\epsilon^2\left(\omega\right)^{3/2}}{\omega-2T} + \frac{\mathcal{J}_{100}q_1\left(\omega-S-T\right)\epsilon^2\left(\omega\right)^{3/2}}{\omega-2T} + \frac{\mathcal{J}_{107}q_1\left(\omega-S-T\right)\epsilon^2\left(\omega\right)^{3/2}}{\omega-2T} + \frac{\mathcal{J}_{105}q_1q_2\left(2\omega-S-T\right)\epsilon^4}{\omega-2T} + \frac{\mathcal{J}_{19}q_1q_2\left(T-\omega\right)\epsilon^4}{\omega-2T} + \frac{\mathcal{J}_{114}q_1q_2\left(-\omega+S+T\right)\epsilon^4}{\omega-2T} + \frac{\mathcal{J}_{101}q_1q_2\left(2(S+T-1)\omega-S-T\right)\epsilon^3}{\left(\omega-2T\right)\left(S+T+2\right)} + \frac{\mathcal{J}_{112}q_1q_2\left((T-1)\omega+S-T(S+T)\right)\epsilon^3}{4\left(\omega-2T\right)} + \frac{\mathcal{J}_{17}q_1q_2\left(\omega-T\right)\epsilon^3}{2\left(\omega-2T\right)} + \frac{\mathcal{J}_{6}\left(\omega-1\right)q_1q_2\left(12\omega-3S-3T-10\right)\epsilon^2}{12\left(\omega-2T\right)\left(S+T+2\right)} +$$

$$\frac{\mathcal{J}_{96}q_1q_2\left(\omega\left(2\omega-2S-2T-1\right)-2(S+T)\right)\epsilon^2}{4\left(\omega-2T\right)\left(\omega-2(S+T)\right)}+$$
$$\frac{\mathcal{J}_{7}q_1q_2\left(\left(-6\omega+3S+3T-4\right)\omega+3S+3T+10\right)\epsilon^2}{6\left(\omega-2T\right)\left(S+T+2\right)}+\frac{\mathcal{J}_{94}\left(3\omega-1\right)q_1q_2\left(\omega-S-T\right)\epsilon^2}{3\left(\omega-2T\right)\left(S+T+2\right)}+$$
$$\frac{\mathcal{J}_{16}q_1q_2\epsilon^2}{4\omega-8T}+\frac{\mathcal{J}_{95}q_1q_2\left(\omega-S-T-1\right)\left(\omega+2(S+T)\right)\epsilon^2}{8\left(\omega-2T\right)\left(\omega-2(S+T)\right)}-$$
$$\frac{\mathcal{J}_{102}q_1q_2(S+T-1)\left(6\omega+S+T\right)\epsilon^2}{6\left(\omega-2T\right)\left(S+T+2\right)}-\frac{\mathcal{J}_{113}q_1q_2\left(2\omega-T\right)\left(\omega-S-T\right)\epsilon^4}{\omega-2T}-$$
$$\frac{\mathcal{J}_{115}q_1q_2\left(\omega-S-T\right)\left(\omega(T-1)-T^2\right)\epsilon^3}{\omega-2T}-\frac{\mathcal{J}_{111}q_1q_2\left(\omega-S+2T\right)\epsilon^4}{2\left(\omega-2T\right)}-$$
$$\frac{\mathcal{J}_{109}q_1q_2\left(\omega-S-T\right)\left(T-1\right)\epsilon^3}{6\left(\omega-2T\right)}-\frac{\mathcal{J}_{110}q_1q_2\left(\omega-S-T\right)\left(3T-1\right)\epsilon^3}{6\left(\omega-2T\right)}-\frac{\mathcal{J}_{15}q_1q_2(T-1)\epsilon^2}{8\left(\omega-2T\right)}-$$
$$\frac{\mathcal{J}_{103}q_1q_2\left(\omega^2-4(S+T)\omega+(S+T)^2\right)\epsilon^3}{\left(\omega-2T\right)\left(\omega-2(S+T)\right)}-\frac{\mathcal{J}_{1}q_1q_2\left(5\omega-16(S+T)\right)\left(\epsilon-1\right)\epsilon^2}{6\left(\omega-2T\right)\left(\omega-2(S+T)\right)}$$

$$\mathcal{G}_{116}=\mathcal{J}_{116}(S+T)\epsilon^4$$

$$\mathcal{G}_{117}=\frac{\mathcal{J}_{97}q_2T\left(-\omega+S+T\right)\epsilon^3}{q_1}+\frac{\mathcal{J}_{117}q_2T\left(-\omega+S+T\right)\left(2\epsilon-1\right)\epsilon^3}{q_1}$$

$$\mathcal{G}_{118}=\mathcal{J}_{118}T(S+T)\epsilon^4$$

$$\mathcal{G}_{119}=\mathcal{J}_{118}\omega T\epsilon^4-\mathcal{J}_{111}T\epsilon^4+\mathcal{J}_{119}T\epsilon^4$$

$$\mathcal{G}_{120}=\frac{\mathcal{J}_{18}q_1\left(\omega(T-1)-T^2\right)\epsilon^2\left(\omega\right)^{3/2}}{\left(\omega-2T\right)\left(\omega-2(S+T)\right)}-\frac{\mathcal{J}_{14}q_1\epsilon^2\left(\omega\right)^{3/2}}{\omega-2(S+T)}-\frac{\mathcal{J}_{38}q_1T\epsilon^2\left(\omega\right)^{3/2}}{\omega-2(S+T)}-$$
$$\frac{\mathcal{J}_{41}q_1T\epsilon^2\left(\omega\right)^{3/2}}{\omega-2(S+T)}-\frac{\mathcal{J}_{42}q_1\left(\omega+T\right)\epsilon^3\left(\omega\right)^{3/2}}{2\left(\omega-2(S+T)\right)}+\frac{\mathcal{J}_{119}q_1q_2T\epsilon^4}{\omega-2(S+T)}+$$
$$\frac{\mathcal{J}_{116}q_1q_2(S+T)\epsilon^4}{\omega-2(S+T)}+\frac{\mathcal{J}_{118}q_1q_2T\left(\omega+S+T\right)\epsilon^4}{\omega-2(S+T)}+\frac{\mathcal{J}_{111}q_1q_2\left(3\omega-3S-2T\right)\epsilon^4}{2\left(\omega-2(S+T)\right)}+$$
$$\frac{\mathcal{J}_{120}q_1q_2T\left(\omega(S+T-1)-(S+T)^2\right)\epsilon^3}{\omega-2(S+T)}+\frac{\mathcal{J}_{112}q_1q_2\left(-T\omega+\omega+T^2+S(T-1)\right)\epsilon^3}{4\left(\omega-2(S+T)\right)}+$$
$$\frac{\mathcal{J}_{98}q_1q_2\left(\omega-S-T-1\right)T\epsilon^3}{6\left(\omega-2(S+T)\right)}+\frac{\mathcal{J}_{99}q_1q_2T\left(3\omega-3S-3T-1\right)\epsilon^3}{6\left(\omega-2(S+T)\right)}+$$
$$\frac{\mathcal{J}_{17}q_1q_2\left(2\omega^2-2T\omega-T^2\right)\epsilon^3}{\left(\omega-2T\right)\left(\omega-2(S+T)\right)}+\frac{\mathcal{J}_{1}q_1q_2\left(11\omega-16T\right)\left(\epsilon-1\right)\epsilon^2}{6\left(\omega-2T\right)\left(\omega-2(S+T)\right)}+$$
$$\frac{\mathcal{J}_{95}q_1q_2\left(\omega-S-T-1\right)\epsilon^2}{8\left(\omega-2(S+T)\right)}+\frac{\mathcal{J}_{8}\left(1-3\omega\right)q_1q_2T\epsilon^2}{3\left(\omega-T+2\right)\left(\omega-2(S+T)\right)}+$$
$$\frac{\mathcal{J}_{10}q_1q_2\left(\omega-T-1\right)\left(7\omega-T\right)\epsilon^2}{6\left(\omega-T+2\right)\left(\omega-2(S+T)\right)}+\frac{\mathcal{J}_{7}q_1q_2\left(3\omega^2+\omega+3\left(\omega+1\right)T-10\right)\epsilon^2}{6\left(\omega-T+2\right)\left(\omega-2(S+T)\right)}+$$
$$\frac{\mathcal{J}_{16}q_1q_2\left(2\left(\omega+1\right)T-3\omega\right)\epsilon^2}{4\left(\omega-2T\right)\left(\omega-2(S+T)\right)}+\frac{\mathcal{J}_{15}q_1q_2(T-1)\left(3\omega-2T\right)\epsilon^2}{8\left(\omega-2T\right)\left(\omega-2(S+T)\right)}-\frac{\mathcal{J}_{39}q_1q_2\left(\omega+T\right)\epsilon^4}{\omega-2(S+T)}-$$
$$\frac{\mathcal{J}_{103}q_1q_2(S+T)\epsilon^3}{2\left(\omega-2(S+T)\right)}-\frac{\mathcal{J}_{96}q_1q_2\epsilon^2}{4\left(\omega-2(S+T)\right)}-\frac{\mathcal{J}_{9}q_1q_2\left(\left(2\omega-2T-3\right)\omega+T\right)\epsilon^3}{\left(\omega-T+2\right)\left(\omega-2(S+T)\right)}-$$
$$\frac{\mathcal{J}_{6}\left(\omega-1\right)q_1q_2\left(9\omega+3T-10\right)\epsilon^2}{12\left(\omega-T+2\right)\left(\omega-2(S+T)\right)}$$

$$\mathcal{G}_{121}=-\mathcal{J}_{118}\omega T\epsilon^4+\mathcal{J}_{113}\omega\left(-\omega+S+T\right)\epsilon^4+\mathcal{J}_{121}\omega T\left(-\omega+S+T\right)\epsilon^4$$

$$\mathcal{G}_{122} = \mathcal{J}_{122} S\epsilon^4$$

$$\mathcal{G}_{123} = \mathcal{J}_{123} T\left(-\omega + S + T + 1\right)\epsilon^3$$

$$\mathcal{G}_{124} = -\frac{3\mathcal{J}_{103}\left(\omega - 2T\right)(S+T)\epsilon^3}{2\left(\omega - 2(S+T)\right)} - \mathcal{J}_{124}\left(\omega(T-1) - T^2\right)(2\epsilon - 1)\epsilon^2 -$$
$$\frac{\mathcal{J}_{104}\left(\omega - 2T\right)\left(\omega(S+T-1) - (S+T)^2\right)\epsilon^2}{\omega - 2(S+T)} - \frac{\mathcal{J}_{96}\left(\omega - 2T\right)\left(\omega - S - T - 1\right)\epsilon^2}{2\left(\omega - 2(S+T)\right)} -$$
$$\frac{\mathcal{J}_{1}\left(\omega - 2T\right)(\epsilon - 1)\epsilon^2}{2\left(\omega - 2(S+T)\right)} - \frac{\mathcal{J}_{95}\left(\omega - 2T\right)\left(\omega - S - T - 1\right)\epsilon^2}{4\left(\omega - 2(S+T)\right)}$$

$$\mathcal{G}_{125} = \mathcal{J}_{125}\left(-T\omega + \omega + T^2 + S(T-1)\right)\epsilon^3$$

$$\mathcal{G}_{126} = -\mathcal{J}_{123} q_{12}\epsilon^3 + 2\mathcal{J}_{125} q_{12}\epsilon^3 + \mathcal{J}_{126} q_{12}\epsilon^3$$

$$\mathcal{G}_{127} = -\mathcal{J}_{128} T^2\epsilon^4 - \mathcal{J}_{127}(T-1)T\epsilon^4 - \frac{1}{2}\mathcal{J}_{112} T\epsilon^3 + \frac{1}{2}\mathcal{J}_{123}(T-1)(S+T)\epsilon^3 -$$
$$\frac{1}{2}\mathcal{J}_{126}(T-1)(S+T)\epsilon^3 - \mathcal{J}_{125}(S(T-1) + (T-2)T)\epsilon^3$$

$$\mathcal{G}_{128} = \mathcal{J}_{128} T\left(-T\omega + \omega + T^2 + S(T-1)\right)\epsilon^4$$

$$\mathcal{G}_{129} = \mathcal{J}_{129} T\left(T - \omega\right)\epsilon^4$$

$$\mathcal{G}_{130} = \mathcal{J}_{130} S\left(-\omega + S + T\right)\epsilon^3$$

$$\mathcal{G}_{131} = \mathcal{J}_{132} S\epsilon^3 + \mathcal{J}_{131} S\left(-\omega + S + T + 1\right)\epsilon^3$$

$$\mathcal{G}_{132} = \mathcal{J}_{132} S\left(-\omega + S + T\right)\epsilon^3$$

$$\mathcal{G}_{133} = \mathcal{J}_{134}\left(\omega - S - T\right)\epsilon^3 + \mathcal{J}_{133}(S-1)\left(-\omega + S + T\right)\epsilon^3$$

$$\mathcal{G}_{134} = \mathcal{J}_{134} S\left(-\omega + S + T\right)\epsilon^3$$

$$\mathcal{G}_{135} = \mathcal{J}_{135}\left(T - \omega\right)\epsilon^4$$

$$\mathcal{G}_{136} = \mathcal{J}_{136}\left(-S\omega + \omega + S^2 + (S-1)T\right)\epsilon^3$$

$$\mathcal{G}_{137} = \mathcal{J}_{137}\left(\omega - S\right)\left(\omega - S - T\right)\epsilon^4$$

$$\mathcal{G}_{138} = -\mathcal{J}_{135} S\epsilon^4 + \mathcal{J}_{137}\omega\left(-\omega + S + T\right)\epsilon^4 + \mathcal{J}_{138}\left(-\omega + S + T\right)\epsilon^4$$

$$\mathcal{G}_{139} = \frac{\mathcal{J}_{108} q_1\left(2\omega - S - T\right)\epsilon^3\left(\omega\right)^{3/2}}{2\left(\omega - 2S\right)} + \frac{\mathcal{J}_{100} q_1\left(\omega - S - T\right)\epsilon^2\left(\omega\right)^{3/2}}{\omega - 2S} +$$
$$\frac{\mathcal{J}_{107} q_1\left(\omega - S - T\right)\epsilon^2\left(\omega\right)^{3/2}}{\omega - 2S} + \frac{\mathcal{J}_{104} q_1\left(\omega(S+T-1) - (S+T)^2\right)\epsilon^2\left(\omega\right)^{3/2}}{\left(\omega - 2S\right)\left(\omega - 2(S+T)\right)} +$$
$$\frac{\mathcal{J}_{14} q_1\epsilon^2\left(\omega\right)^{3/2}}{\omega - 2S} + \frac{\mathcal{J}_{105} q_1 q_2\left(2\omega - S - T\right)\epsilon^4}{\omega - 2S} + \frac{\mathcal{J}_{138} q_1 q_2\left(-\omega + S + T\right)\epsilon^4}{\omega - 2S} +$$
$$\frac{\mathcal{J}_{43} q_1 q_2\left(S - \omega\right)\epsilon^4}{\omega - 2S} + \frac{\mathcal{J}_{133} q_1 q_2(S-1)\left(-\omega + S + T\right)\epsilon^3}{6\left(\omega - 2S\right)} + \frac{\mathcal{J}_{134} q_1 q_2(3S-1)\left(-\omega + S + T\right)\epsilon^3}{6\left(\omega - 2S\right)} +$$
$$\frac{\mathcal{J}_{101} q_1 q_2\left(2(S+T-1)\omega - S - T\right)\epsilon^3}{\left(\omega - 2S\right)\left(S + T + 2\right)} + \frac{\mathcal{J}_{136} q_1 q_2\left((S-1)\omega + T - S(S+T)\right)\epsilon^3}{4\left(\omega - 2S\right)} +$$
$$\frac{\mathcal{J}_{23} q_1 q_2\left(\omega - S\right)\epsilon^3}{2\left(\omega - 2S\right)} + \frac{\mathcal{J}_{6}\left(\omega - 1\right) q_1 q_2\left(12\omega - 3S - 3T - 10\right)\epsilon^2}{12\left(\omega - 2S\right)\left(S + T + 2\right)} +$$
$$\frac{\mathcal{J}_{96} q_1 q_2\left(\omega\left(2\omega - 2S - 2T - 1\right) - 2(S+T)\right)\epsilon^2}{4\left(\omega - 2S\right)\left(\omega - 2(S+T)\right)} +$$

$$\frac{\mathcal{J}_7 q_1 q_2 \left(\left(-6\omega+3S+3T-4\right)\omega+3S+3T+10\right)\epsilon^2}{6\left(\omega-2S\right)\left(S+T+2\right)}+$$
$$\frac{\mathcal{J}_4 q_1 q_2 \epsilon^2}{4\omega-8S}+\frac{\mathcal{J}_{94}\left(3\omega-1\right)q_1 q_2\left(\omega-S-T\right)\epsilon^2}{3\left(\omega-2S\right)\left(S+T+2\right)}+$$
$$\frac{\mathcal{J}_{95} q_1 q_2\left(\omega-S-T-1\right)\left(\omega+2(S+T)\right)\epsilon^2}{8\left(\omega-2S\right)\left(\omega-2(S+T)\right)}-\frac{\mathcal{J}_{137} q_1 q_2\left(2\omega-S\right)\left(\omega-S-T\right)\epsilon^4}{\omega-2S}-$$
$$\frac{\mathcal{J}_{139} q_1 q_2\left(\omega(S-1)-S^2\right)\left(\omega-S-T\right)\epsilon^3}{\omega-2S}-\frac{\mathcal{J}_{135} q_1 q_2\left(\omega+2S-T\right)\epsilon^4}{2\left(\omega-2S\right)}-\frac{\mathcal{J}_3 q_1 q_2(S-1)\epsilon^2}{8\left(\omega-2S\right)}-$$
$$\frac{\mathcal{J}_{102} q_1 q_2(S+T-1)\left(6\omega+S+T\right)\epsilon^2}{6\left(\omega-2S\right)\left(S+T+2\right)}-\frac{\mathcal{J}_{103} q_1 q_2\left(\omega^2-4(S+T)\omega+(S+T)^2\right)\epsilon^3}{\left(\omega-2S\right)\left(\omega-2(S+T)\right)}-$$
$$\frac{\mathcal{J}_1 q_1 q_2\left(5\omega-16(S+T)\right)(\epsilon-1)\epsilon^2}{6\left(\omega-2S\right)\left(\omega-2(S+T)\right)}$$

$$\mathcal{G}_{140}=\frac{\mathcal{J}_{130} q_2 S\left(-\omega+S+T\right)\epsilon^3}{q_1}+\frac{\mathcal{J}_{140} q_2 S\left(-\omega+S+T\right)(2\epsilon-1)\epsilon^3}{q_1}$$

$$\mathcal{G}_{141}=\mathcal{J}_{141} S(S+T)\epsilon^4$$

$$\mathcal{G}_{142}=\mathcal{J}_{141}\omega S\epsilon^4-\mathcal{J}_{135} S\epsilon^4+\mathcal{J}_{142} S\epsilon^4$$

$$\mathcal{G}_{143}=\frac{\mathcal{J}_{24} q_1\left(\omega(S-1)-S^2\right)\epsilon^2\left(\omega\right)^{3/2}}{\left(\omega-2S\right)\left(\omega-2(S+T)\right)}-\frac{\mathcal{J}_{14} q_1\epsilon^2\left(\omega\right)^{3/2}}{\omega-2(S+T)}-\frac{\mathcal{J}_{20} q_1 S\epsilon^2\left(\omega\right)^{3/2}}{\omega-2(S+T)}-$$
$$\frac{\mathcal{J}_{27} q_1 S\epsilon^2\left(\omega\right)^{3/2}}{\omega-2(S+T)}-\frac{\mathcal{J}_{28} q_1\left(\omega+S\right)\epsilon^3\left(\omega\right)^{3/2}}{2\left(\omega-2(S+T)\right)}+\frac{\mathcal{J}_{142} q_1 q_2 S\epsilon^4}{\omega-2(S+T)}+\frac{\mathcal{J}_{116} q_1 q_2(S+T)\epsilon^4}{\omega-2(S+T)}+$$
$$\frac{\mathcal{J}_{141} q_1 q_2 S\left(\omega+S+T\right)\epsilon^4}{\omega-2(S+T)}+\frac{\mathcal{J}_{135} q_1 q_2\left(3\omega-2S-3T\right)\epsilon^4}{2\left(\omega-2(S+T)\right)}+$$
$$\frac{\mathcal{J}_{143} q_1 q_2 S\left(\omega(S+T-1)-(S+T)^2\right)\epsilon^3}{\omega-2(S+T)}+\frac{\mathcal{J}_{136} q_1 q_2\left(-S\omega+\omega+S^2+(S-1)T\right)\epsilon^3}{4\left(\omega-2(S+T)\right)}+$$
$$\frac{\mathcal{J}_{131} q_1 q_2 S\left(\omega-S-T-1\right)\epsilon^3}{6\left(\omega-2(S+T)\right)}+\frac{\mathcal{J}_{132} q_1 q_2 S\left(3\omega-3S-3T-1\right)\epsilon^3}{6\left(\omega-2(S+T)\right)}+$$
$$\frac{\mathcal{J}_{23} q_1 q_2\left(2\omega^2-2S\omega-S^2\right)\epsilon^3}{\left(\omega-2S\right)\left(\omega-2(S+T)\right)}+\frac{\mathcal{J}_1 q_1 q_2\left(11\omega-16S\right)(\epsilon-1)\epsilon^2}{6\left(\omega-2S\right)\left(\omega-2(S+T)\right)}+$$
$$\frac{\mathcal{J}_{95} q_1 q_2\left(\omega-S-T-1\right)\epsilon^2}{8\left(\omega-2(S+T)\right)}+\frac{\mathcal{J}_2\left(1-3\omega\right)q_1 q_2 S\epsilon^2}{3\left(\omega-S+2\right)\left(\omega-2(S+T)\right)}+$$
$$\frac{\mathcal{J}_{22} q_1 q_2\left(\omega-S-1\right)\left(7\omega-S\right)\epsilon^2}{6\left(\omega-S+2\right)\left(\omega-2(S+T)\right)}+$$
$$\frac{\mathcal{J}_7 q_1 q_2\left(3\omega^2+\omega+3\left(\omega+1\right)S-10\right)\epsilon^2}{6\left(\omega-S+2\right)\left(\omega-2(S+T)\right)}+\frac{\mathcal{J}_4 q_1 q_2\left(2\left(\omega+1\right)S-3\omega\right)\epsilon^2}{4\left(\omega-2S\right)\left(\omega-2(S+T)\right)}+$$
$$\frac{\mathcal{J}_3 q_1 q_2(S-1)\left(3\omega-2S\right)\epsilon^2}{8\left(\omega-2S\right)\left(\omega-2(S+T)\right)}-\frac{\mathcal{J}_{25} q_1 q_2\left(\omega+S\right)\epsilon^4}{\omega-2(S+T)}-$$
$$\frac{\mathcal{J}_{103} q_1 q_2(S+T)\epsilon^3}{2\left(\omega-2(S+T)\right)}-\frac{\mathcal{J}_{96} q_1 q_2\epsilon^2}{4\left(\omega-2(S+T)\right)}-$$
$$\frac{\mathcal{J}_{21} q_1 q_2\left(\left(2\omega-2S-3\right)\omega+S\right)\epsilon^3}{\left(\omega-S+2\right)\left(\omega-2(S+T)\right)}-\frac{\mathcal{J}_6\left(\omega-1\right)q_1 q_2\left(9\omega+3S-10\right)\epsilon^2}{12\left(\omega-S+2\right)\left(\omega-2(S+T)\right)}$$

$$\mathcal{G}_{144}=-\mathcal{J}_{141}\omega S\epsilon^4+\mathcal{J}_{137}\omega\left(-\omega+S+T\right)\epsilon^4+\mathcal{J}_{144}\omega S\left(-\omega+S+T\right)\epsilon^4$$

$$\mathcal{G}_{145}=\mathcal{J}_{145} T\epsilon^4$$

$$\mathcal{G}_{146} = \mathcal{J}_{146} S \left(-\omega + S + T + 1\right) \epsilon^3$$

$$\mathcal{G}_{147} = -\mathcal{J}_{147} \left(\omega - S\right) \epsilon^3 (2\epsilon - 1)$$

$$\mathcal{G}_{148} = \mathcal{J}_{148} \left(-S\omega + \omega + S^2 + (S-1)T\right) \epsilon^3$$

$$\mathcal{G}_{149} = -\mathcal{J}_{146} q_7 \epsilon^3 + 2\mathcal{J}_{148} q_7 \epsilon^3 + \mathcal{J}_{149} q_7 \epsilon^3$$

$$\mathcal{G}_{150} = -\mathcal{J}_{151} S^2 \epsilon^4 - \mathcal{J}_{150}(S-1) S \epsilon^4 - \frac{1}{2}\mathcal{J}_{136} S \epsilon^3 + \frac{1}{2}\mathcal{J}_{146}(S-1)(S+T)\epsilon^3 -$$
$$\frac{1}{2}\mathcal{J}_{149}(S-1)(S+T)\epsilon^3 - \mathcal{J}_{148}(S(S+T-2) - T)\epsilon^3$$

$$\mathcal{G}_{151} = \mathcal{J}_{151} S \left(-S\omega + \omega + S^2 + (S-1)T\right) \epsilon^4$$

$$\mathcal{G}_{152} = \mathcal{J}_{152} S \left(S - \omega\right) \epsilon^4$$

$$\mathcal{G}_{153} = \mathcal{J}_{153} S \epsilon^4$$

$$\mathcal{G}_{154} = \mathcal{J}_{154}(S+T)\epsilon^4$$

$$\mathcal{G}_{155} = \mathcal{J}_{155} T \epsilon^4$$

$$\mathcal{G}_{156} = \mathcal{J}_{156} \left(S\omega + T - S(S+T)\right) \epsilon^3$$

$$\mathcal{G}_{157} = \mathcal{J}_{157} S \epsilon^4$$

$$\mathcal{G}_{158} = \mathcal{J}_{158} \left(S(T-1) + T\left(T - \omega\right)\right) \epsilon^3$$

$$\mathcal{G}_{159} = \mathcal{J}_{159} q_{10} q_3 \epsilon^4$$

$$\mathcal{G}_{160} = \frac{3\mathcal{J}_{135} \left(\omega - T\right)^2 \epsilon^4}{4S} + \frac{1}{2}\mathcal{J}_{153} \left(\omega - T\right) \epsilon^4 - \frac{1}{2}\mathcal{J}_{159} \left(\omega - 2T\right) \left(\omega - S - T\right) \epsilon^4 +$$
$$\frac{1}{2}\mathcal{J}_{157} \left(T - \omega\right) \epsilon^4 + \mathcal{J}_{160} \left(T - \omega\right) \epsilon^4 + \frac{\mathcal{J}_{116} \left(\omega - T\right) \left(S + T\right) \epsilon^4}{2S} +$$
$$\frac{\mathcal{J}_{31} \left(3T^2 + 3\left(S - \omega\right) T + S\left(\omega + 4S\right)\right) \epsilon^4}{4S} - \frac{\mathcal{J}_{19} \left(\omega - T\right)^2 \epsilon^4}{2S} + \frac{\mathcal{J}_{17} \left(\omega - T\right)^2 \epsilon^3}{4S} +$$
$$\frac{\mathcal{J}_{32} \left(\omega - T\right) \left(S(T-1) - T\right) \epsilon^3}{8S} + \frac{\mathcal{J}_{136} \left(\omega - T\right) \left(-S\omega + \omega + S^2 + (S-1)T\right) \epsilon^3}{8S} -$$
$$\frac{\mathcal{J}_{103} \left(\omega - T\right) \left(S + T\right) \epsilon^3}{4S} + \frac{\mathcal{J}_{16} \left(\omega - T\right) \epsilon^2}{8S} + \frac{\mathcal{J}_{15} (T-1) \left(T - \omega\right) \epsilon^2}{16S} + \frac{\mathcal{J}_{96} \left(T - \omega\right) \epsilon^2}{8S}$$
$$- \frac{\mathcal{J}_{95} \left(\omega - T\right) \left(-\omega + S + T + 1\right) \epsilon^2}{16S}$$

$$\mathcal{G}_{161} = \frac{\mathcal{J}_{153} q_1 \left(\omega - T\right) \epsilon^4}{q_2} + \frac{\mathcal{J}_{157} q_1 \left(T - \omega\right) \epsilon^4}{q_2} +$$
$$\frac{2\mathcal{J}_{160} q_1 \left(T - \omega\right) \epsilon^4}{q_2} + \frac{\mathcal{J}_{116} q_1 \left(\omega - T\right) \left(S + T\right) \epsilon^4}{q_2 S} + \frac{\mathcal{J}_{31} q_1 \left(\omega - T\right) \left(S - 3T\right) \epsilon^4}{2q_2 S} +$$
$$\frac{\mathcal{J}_{135} q_1 \left(\omega - T\right) \left(3\omega - 2S - 3T\right) \epsilon^4}{2q_2 S} - \frac{\mathcal{J}_{19} q_1 \left(\omega - T\right)^2 \epsilon^4}{q_2 S} +$$
$$\frac{\mathcal{J}_{17} q_1 \left(\omega - T\right) \left(\omega - 2S - T\right) \epsilon^3}{2q_2 S} + \frac{\mathcal{J}_{158} q_1 q_2 \left(-TS + S + \left(\omega - T\right) T\right) \epsilon^3}{2\left(\omega - 2\right)} +$$
$$\epsilon^3 \mathcal{J}_{136}\, q_1 \left(\frac{\left(\left(-S\omega + \omega + S^2 - 2\right)\omega + 4S\right)\omega + \left(\omega - \left(\omega + 2\right) S - 2\right) T^2}{4\left(\omega - 2\right) q_2 S} + \right.$$
$$\left. \frac{\left(-2\left(\omega - 2\right)\omega - \left(\omega + 2\right) S^2 + 2\left(\omega^2 + \omega - 2\right) S\right) T}{4\left(\omega - 2\right) q_2 S} \right) +$$

$$\epsilon^3 \mathcal{J}_{32}\, q_1 \left(\frac{S\left(-\omega+2S+2\right)\omega+\left(\omega-\left(\omega+2\right)S-2\right)T^2}{4\left(\omega-2\right)q_2 S}+ \right.$$
$$\left. \frac{\left(\omega\left((S-1)\omega+S(3-2S)+2\right)-2S\right)T}{4\left(\omega-2\right)q_2 S} \right) + \frac{\mathcal{J}_{161} q_1 \left(S\omega^2-4(S+T)\omega+4T(S+T)\right)\epsilon^3}{2\left(\omega-2\right)q_2}+$$
$$\frac{\mathcal{J}_{159} q_1 \left((S+2T)\omega-2\left(\omega^2-(2S+3T+2)\omega+2(T+1)(S+T)\right)\epsilon\omega-2T(S+T)\right)\epsilon^3}{2\left(\omega-2\right)q_2}-$$
$$\frac{\mathcal{J}_{103} q_1 \left(\omega-T\right)(S+T)\epsilon^3}{2q_2 S}+\frac{\mathcal{J}_{16} q_1\left(\omega-2S-T\right)\epsilon^2}{4q_2 S}+\frac{\mathcal{J}_{96} q_1\left(T-\omega\right)\epsilon^2}{4q_2 S}+$$
$$\frac{\mathcal{J}_{15} q_1 (T-1)\left(-\omega+2S+T\right)\epsilon^2}{8q_2 S}+\frac{\mathcal{J}_7 q_1 \epsilon^2}{2q_2}-\frac{\mathcal{J}_6\left(\omega-1\right)q_1\epsilon^2}{4q_2}-$$
$$\frac{\mathcal{J}_{95} q_1\left(\omega-T\right)\left(-\omega+S+T+1\right)\epsilon^2}{8q_2 S}$$

$$\mathcal{G}_{162} = \mathcal{J}_{162} T \epsilon^4$$

$$\mathcal{G}_{163} = -\mathcal{J}_{163} q_5 (S+T)^{3/2}\epsilon^4$$

$$\mathcal{G}_{164} = \mathcal{J}_{164} q_4 q_9 \epsilon^4$$

$$\mathcal{G}_{165} = \frac{1}{2}\mathcal{J}_{162}\left(\omega-S\right)\epsilon^4+\frac{1}{2}\mathcal{J}_{155}\left(S-\omega\right)\epsilon^4+\mathcal{J}_{165}\left(S-\omega\right)\epsilon^4-$$
$$\frac{1}{2}\mathcal{J}_{164}\left(\omega-2S\right)\left(\omega-S-T\right)\epsilon^4+\frac{\mathcal{J}_{116}\left(\omega-S\right)(S+T)\epsilon^4}{2T}+$$
$$\frac{\mathcal{J}_{31}\left(7T^2+(\omega+6S)T+3S\left(S-\omega\right)\right)\epsilon^4}{4T}-\frac{\mathcal{J}_{43}\left(\omega-S\right)^2\epsilon^4}{2T}+\frac{3\mathcal{J}_{111}\left(\omega-S\right)^2\epsilon^4}{4T}+$$
$$\frac{\mathcal{J}_{23}\left(\omega-S\right)^2\epsilon^3}{4T}-\frac{\mathcal{J}_{103}\left(\omega-S\right)(S+T)\epsilon^3}{4T}+\frac{\mathcal{J}_{32}\left(\omega-S\right)(S(T-1)-T)\epsilon^3}{8T}-$$
$$\frac{\mathcal{J}_{112}\left(\omega-S\right)\left((T-1)\omega+S-T(S+T)\right)\epsilon^3}{8T}+\frac{\mathcal{J}_4\left(\omega-S\right)\epsilon^2}{8T}+\frac{\mathcal{J}_{96}\left(S-\omega\right)\epsilon^2}{8T}+$$
$$\frac{\mathcal{J}_3(S-1)\left(S-\omega\right)\epsilon^2}{16T}+\frac{\mathcal{J}_{95}\left(\omega-S\right)\left(\omega-S-T-1\right)\epsilon^2}{16T}$$

$$\mathcal{G}_{166} = \frac{\mathcal{J}_{162} q_1\left(\omega-S\right)\epsilon^4}{q_2}+\frac{\mathcal{J}_{155} q_1\left(S-\omega\right)\epsilon^4}{q_2}+$$
$$\frac{2\mathcal{J}_{165} q_1\left(S-\omega\right)\epsilon^4}{q_2}+\frac{\mathcal{J}_{116} q_1\left(\omega-S\right)(S+T)\epsilon^4}{q_2 T}+\frac{\mathcal{J}_{111} q_1\left(\omega-S\right)(3\omega-3S-2T)\epsilon^4}{2q_2 T}-$$
$$\frac{\mathcal{J}_{43} q_1\left(\omega-S\right)^2\epsilon^4}{q_2 T}-\frac{\mathcal{J}_{31} q_1\left(\omega-S\right)(3S-T)\epsilon^4}{2q_2 T}+\frac{\mathcal{J}_{23} q_1\left(\omega-S\right)\left(\omega-S-2T\right)\epsilon^3}{2q_2 T}+$$
$$\frac{\mathcal{J}_{112} q_1\left(\left(\omega-2\right)\left(\omega-S\right)^2-\left(\omega+2\right)\left(\omega-S-2\right)T\left(\omega-S\right)+\left(\omega^2-\left(\omega+2\right)S\right)T^2\right)\epsilon^3}{4\left(\omega-2\right)q_2 T}+$$
$$\frac{\mathcal{J}_{32} q_1\left(-2\omega(S-1)T^2+\left(\omega-S\right)\left(-\omega+\left(\omega+2\right)S+2\right)T+\left(\omega-2\right)S\left(S-\omega\right)\right)\epsilon^3}{4\left(\omega-2\right)q_2 T}+$$
$$\frac{\mathcal{J}_{166} q_1\left(T\omega^2-4(S+T)\omega+4S(S+T)\right)\epsilon^3}{2\left(\omega-2\right)q_2}+\frac{\mathcal{J}_{156} q_1 q_2\left(S\omega+T-S(S+T)\right)\epsilon^3}{2\left(\omega-2\right)}+$$
$$\frac{\mathcal{J}_{164} q_1\left((2S+T)\omega-2\left(\omega^2-(3S+2T+2)\omega+2(S+1)(S+T)\right)\epsilon\omega-2S(S+T)\right)\epsilon^3}{2\left(\omega-2\right)q_2}-$$
$$\frac{\mathcal{J}_{103} q_1\left(\omega-S\right)(S+T)\epsilon^3}{2q_2 T}+\frac{\mathcal{J}_3 q_1(S-1)\left(-\omega+S+2T\right)\epsilon^2}{8q_2 T}+\frac{\mathcal{J}_4 q_1\left(\omega-S-2T\right)\epsilon^2}{4q_2 T}+$$

$$\frac{\mathcal{J}_7 q_1 \epsilon^2}{2q_2} - \frac{\mathcal{J}_6 (\omega-1) q_1 \epsilon^2}{4q_2} + \frac{\mathcal{J}_{96} q_1 (S-\omega)\epsilon^2}{4q_2 T} + \frac{\mathcal{J}_{95} q_1 (\omega-S)(\omega-S-T-1)\epsilon^2}{8q_2 T}$$

$$\mathcal{G}_{167} = \mathcal{J}_{154}\omega\epsilon^4 + \mathcal{J}_{170}(-\omega+S+T)\epsilon^4 + \frac{\mathcal{J}_{159}\omega S(-\omega+S+T)\epsilon^4}{S+T} + \frac{\mathcal{J}_{162} T(-\omega+S+T)\epsilon^4}{S+T} + \frac{2\mathcal{J}_{169} T(-\omega+S+T)\epsilon^4}{S+T} + \frac{\mathcal{J}_{113} T(T-\omega)(-\omega+S+T)\epsilon^4}{S+T} + \frac{\mathcal{J}_{153} S(2\omega+S+T)\epsilon^4}{2(S+T)} + \frac{\mathcal{J}_{168} T(-\omega+S+T)(S-2T)\epsilon^4}{S+T} + \frac{1}{4}\mathcal{J}_{31}\left(\frac{8(S-T)\omega}{S+T} - S + 3T\right)\epsilon^4 + \frac{\mathcal{J}_{135}\left(6\omega^2 + 7(S+T)\omega - 4S^2 - 13T^2 - 11ST\right)\epsilon^4}{4(S+T)} + \frac{\mathcal{J}_{164}(\omega-S-T)T(\omega-2(S+T))\epsilon^4}{S+T} + \frac{\mathcal{J}_{163}(-\omega+S+T)\left(-((S+3T)\omega) + 2S^2 + T^2 + 5ST\right)\epsilon^4}{2(S+T)} + \frac{1}{2}\mathcal{J}_{116}\left(3S + T\left(\frac{4\omega}{S+T} - 1\right)\right)\epsilon^4 + \frac{\mathcal{J}_{43}(\omega-S)^2\epsilon^4}{S+T} - \frac{4\mathcal{J}_{105}\omega T\epsilon^4}{S+T} + \frac{\mathcal{J}_{155}(\omega-S-T)T\epsilon^4}{S+T} + \frac{2\mathcal{J}_{165}(\omega-S-T)T\epsilon^4}{S+T} + \frac{\mathcal{J}_{137}(\omega-S)(\omega-S-T)T\epsilon^4}{S+T} - \frac{\mathcal{J}_{167}(S(T-1)-T)T(-\omega+S+T)\epsilon^4}{S+T} - \frac{\mathcal{J}_{160} S(2\omega+S+T)\epsilon^4}{S+T} - \frac{\mathcal{J}_{157} S(2\omega+S+T)\epsilon^4}{2(S+T)} - \frac{3\mathcal{J}_{111}(\omega-S)(\omega-S-2T)\epsilon^4}{2(S+T)} - \frac{\mathcal{J}_{19}\left(2\omega^2 + S\omega - 2S^2 + T^2 - 3(\omega+S)T\right)\epsilon^4}{2(S+T)} + \frac{3}{8}\mathcal{J}_{32}(S(T-1)-T)\epsilon^3 - \mathcal{J}_{106} T\epsilon^3 + \frac{\mathcal{J}_{108}\omega T(-2\omega+S+T)\epsilon^3}{S+T} + \frac{\mathcal{J}_{133}(S-1)T(-\omega+S+T)\epsilon^3}{3(S+T)} + \frac{\mathcal{J}_{109}(T-1)T(-\omega+S+T)\epsilon^3}{3(S+T)} + \frac{\mathcal{J}_{136}(2\omega+S+3T)\left(-S\omega+\omega+S^2+(S-1)T\right)\epsilon^3}{8(S+T)} + \frac{\mathcal{J}_{112}(-\omega+S+2T)\left(-T\omega+\omega+T^2+S(T-1)\right)\epsilon^3}{4(S+T)} - \frac{\mathcal{J}_{23}(\omega-S)^2\epsilon^3}{2(S+T)} + \frac{\mathcal{J}_{110}(\omega-S-T)T\epsilon^3}{3(S+T)} + \frac{\mathcal{J}_{134}(\omega-S-T)T\epsilon^3}{3(S+T)} + \frac{\mathcal{J}_{17}(\omega-T)(2\omega+S-T)\epsilon^3}{4(S+T)} - \frac{2\mathcal{J}_{101} T\left(2(S+T-1)\omega + (S+T-5)(S+T)\right)\epsilon^3}{(S+T)(S+T+2)} - \frac{\mathcal{J}_{103}\left(8T\omega^2 - (S+T)(3S+43T)\omega + 6(S+T)^2(S+5T)\right)\epsilon^3}{4(S+T)\left(2(S+T)-\omega\right)} + \frac{2\mathcal{J}_{100}\omega T(-\omega+S+T)\epsilon^2}{S+T} + \frac{2\mathcal{J}_{107}\omega T(-\omega+S+T)\epsilon^2}{S+T} + \frac{\mathcal{J}_7 T\left((6\omega-3S-3T-8)\omega+6S+6T-16\right)\epsilon^2}{3(S+T)(S+T+2)} + \frac{\mathcal{J}_{94} T(-\omega+S+T)(6\omega+9S+9T+4)\epsilon^2}{3(S+T)(S+T+2)} + \frac{\mathcal{J}_{102} T(S+T-1)(6\omega+7(S+T))\epsilon^2}{3(S+T)(S+T+2)} + \frac{2\mathcal{J}_{104}\omega T\left((S+T)^2 - \omega(S+T-1)\right)\epsilon^2}{(S+T)(\omega-2(S+T))} + \frac{\mathcal{J}_{96}\left(-16T\omega^2 + (T(64T-25)+S(64T+3))\omega - 2(S+T)(3S(8T+1)+T(24T-17))\right)\epsilon^2}{8(S+T)\left(2(S+T)-\omega\right)} + \frac{\mathcal{J}_1 T(\omega+4(S+T))(\epsilon-1)\epsilon^2}{3(S+T)\left(2(S+T)-\omega\right)} - \frac{2\mathcal{J}_{14}\omega T\epsilon^2}{S+T} + \frac{\mathcal{J}_4(S-\omega)\epsilon^2}{4(S+T)} + \frac{\mathcal{J}_3(\omega-S)(S-1)\epsilon^2}{8(S+T)} +$$

$$\frac{\mathcal{J}_{16}\left(2\omega+S-T\right)\epsilon^2}{8(S+T)}+\frac{\mathcal{J}_{15}(T-1)\left(-2\omega-S+T\right)\epsilon^2}{16(S+T)}-\frac{\mathcal{J}_{6}\left(\omega-1\right)T\left(6\omega+3S+3T-8\right)\epsilon^2}{3(S+T)(S+T+2)}-$$
$$\frac{\mathcal{J}_{95}\left(-\omega+S+T+1\right)\left((25T-3S)\omega+2(S+T)(3S-17T)\right)\epsilon^2}{16(S+T)\left(2(S+T)-\omega\right)}$$

$$\mathcal{G}_{168}=-\frac{1}{2}\mathcal{J}_{159}S\left(-\omega+S+T\right)\epsilon^4+\frac{1}{2}\mathcal{J}_{163}(S-T)\left(-\omega+S+T\right)\epsilon^4-$$
$$\frac{1}{2}\mathcal{J}_{168}(S-T)\left(-\omega+S+T\right)\epsilon^4+\mathcal{J}_{167}(S(T-1)-T)\left(-\omega+S+T\right)\epsilon^4-$$
$$\frac{1}{2}\mathcal{J}_{164}T\left(-\omega+S+T\right)\epsilon^4$$

$$\mathcal{G}_{169}=\frac{3}{4}\mathcal{J}_{111}\left(\omega-S\right)\epsilon^4+\frac{1}{2}\mathcal{J}_{153}S\epsilon^4-\frac{1}{2}\mathcal{J}_{157}S\epsilon^4-$$
$$\mathcal{J}_{160}S\epsilon^4+\frac{1}{2}\mathcal{J}_{43}\left(S-\omega\right)\epsilon^4+\frac{3}{4}\mathcal{J}_{135}\left(\omega-T\right)\epsilon^4+\frac{1}{2}\mathcal{J}_{163}\left(\omega-2S\right)\left(\omega-S-T\right)\epsilon^4-$$
$$\frac{1}{2}\mathcal{J}_{155}T\epsilon^4+\frac{1}{2}\mathcal{J}_{162}T\epsilon^4-\mathcal{J}_{165}T\epsilon^4+\frac{1}{2}\mathcal{J}_{19}\left(T-\omega\right)\epsilon^4-$$
$$\frac{1}{2}\mathcal{J}_{31}(S+T)\epsilon^4+\mathcal{J}_{169}\left(-\omega+S+T\right)\epsilon^4+\frac{1}{2}\mathcal{J}_{159}S\left(-\omega+S+T\right)\epsilon^4+$$
$$\frac{1}{2}\mathcal{J}_{168}(S-T)\left(-\omega+S+T\right)\epsilon^4+\frac{1}{2}\mathcal{J}_{164}T\left(-\omega+S+T\right)\epsilon^4+\mathcal{J}_{116}\left(\omega+S+T\right)\epsilon^4+$$
$$\frac{1}{4}\mathcal{J}_{23}\left(\omega-S\right)\epsilon^3+\frac{1}{4}\mathcal{J}_{17}\left(\omega-T\right)\epsilon^3+\frac{1}{4}\mathcal{J}_{32}(S(T-1)-T)\epsilon^3-\frac{1}{2}\mathcal{J}_{103}(S+T)\epsilon^3+$$
$$\frac{1}{8}\mathcal{J}_{136}\left(-S\omega+\omega+S^2+(S-1)T\right)\epsilon^3+\frac{1}{8}\mathcal{J}_{112}\left(-T\omega+\omega+T^2+S(T-1)\right)\epsilon^3+\frac{\mathcal{J}_{16}\epsilon^2}{8}+$$
$$\frac{\mathcal{J}_{4}\epsilon^2}{8}-\frac{1}{16}\mathcal{J}_{3}(S-1)\epsilon^2+\frac{1}{8}\mathcal{J}_{95}\left(\omega-S-T-1\right)\epsilon^2-\frac{1}{16}\mathcal{J}_{15}(T-1)\epsilon^2-\frac{\mathcal{J}_{96}\epsilon^2}{4}$$

$$\mathcal{G}_{170}=\mathcal{J}_{163}\omega q_5q_6\epsilon^4+\mathcal{J}_{159}q_5q_6S\epsilon^4-\mathcal{J}_{164}q_5q_6T\epsilon^4+\mathcal{J}_{168}q_5q_6\left(-\omega+S+T\right)\epsilon^4$$

$$\mathcal{G}_{171}=-\mathcal{J}_{171}(S-1)S\epsilon^4$$

$$\mathcal{G}_{172}=\mathcal{J}_{172}S\epsilon^4$$

$$\mathcal{G}_{173}=\frac{1}{2}\mathcal{J}_{159}S\left(2(S+T)-\omega\right)\epsilon^4+\mathcal{J}_{174}\left(-S\omega+\omega+S^2+(S-1)T\right)(2\epsilon-1)\epsilon^4+$$
$$\frac{1}{2}\mathcal{J}_{146}\left(-S\omega+\omega+S^2+(S-1)T\right)\epsilon^3+\mathcal{J}_{81}\left(-S\omega+\omega+S^2+(S-1)T\right)\epsilon^3+$$
$$\frac{1}{2}\mathcal{J}_{82}\left(-S\omega+\omega+S^2+(S-1)T\right)\epsilon^3+\mathcal{J}_{148}\left((S-1)\omega+T-S(S+T)\right)\epsilon^3+$$
$$\frac{1}{2}\mathcal{J}_{149}\left((S-1)\omega+T-S(S+T)\right)\epsilon^3+\frac{1}{2}\mathcal{J}_{79}\left((S-1)\omega+T-S(S+T)\right)\epsilon^3$$

$$\mathcal{G}_{174}=\frac{1}{2}\mathcal{J}_{159}\omega S\epsilon^4-\mathcal{J}_{145}S\epsilon^4-\frac{1}{2}\mathcal{J}_{153}S\epsilon^4+\frac{1}{2}\mathcal{J}_{157}S\epsilon^4+$$
$$\mathcal{J}_{160}S\epsilon^4+\frac{1}{2}\mathcal{J}_{19}\left(\omega-T\right)\epsilon^4+\frac{3}{4}\mathcal{J}_{135}\left(T-\omega\right)\epsilon^4-\frac{1}{2}\mathcal{J}_{116}(S+T)\epsilon^4-$$
$$\frac{1}{4}\mathcal{J}_{31}(S-3T)\epsilon^4+\mathcal{J}_{174}S(2\epsilon-1)\epsilon^4+\mathcal{J}_{175}S(2\epsilon-1)\epsilon^4+$$
$$\frac{1}{4}\mathcal{J}_{17}\left(T-\omega\right)\epsilon^3+\frac{1}{4}\mathcal{J}_{103}(S+T)\epsilon^3+\frac{1}{8}\mathcal{J}_{32}(-TS+S+T)\epsilon^3+$$
$$\frac{\mathcal{J}_{146}S\left(\left(-\omega+S+1\right)S^2+\left(\left(-\omega+S+2\right)\omega-2S+2\right)TS+\left((S-1)\omega-3S+1\right)T^2\right)\epsilon^3}{2S^2\left(-\omega+S+1\right)^2+2(S-1)^2T^2+4S\left(-S\omega+\omega+S^2+1\right)T}+$$

$$\frac{\mathcal{J}_{148}S\left(\left(\omega-S-1\right)S^2+\left(\omega^2-(S+2)\omega+2(S-1)\right)TS+\left(-S\omega+\omega+3S-1\right)T^2\right)\epsilon^3}{S^2\left(-\omega+S+1\right)^2+(S-1)^2T^2+2S\left(-S\omega+\omega+S^2+1\right)T}+$$
$$\frac{\mathcal{J}_{149}S\left(\left(\omega-S-1\right)S^2+\left(\omega^2-(S+2)\omega+2(S-1)\right)TS+\left(-S\omega+\omega+3S-1\right)T^2\right)\epsilon^3}{2S^2\left(-\omega+S+1\right)^2+2(S-1)^2T^2+4S\left(-S\omega+\omega+S^2+1\right)T}+$$
$$\frac{1}{8}\mathcal{J}_{136}\left((S-1)\omega+T-S(S+T)\right)\epsilon^3+$$
$$\epsilon^3\mathcal{J}_{81}\left(\frac{\omega^3-\left(S^2+((S-3)S+3)T\right)\omega^2+\left(S^3+(4S-5)TS^2-(S-1)((S-3)S+3)T^2\right)\omega}{\omega^2+2(S-1)T\omega+T\left((T-4)S^2-2TS+T\right)}+\right.$$
$$\left.\frac{T\left(-3S^4+S^3+(S-3)(S-2)TS^2+(S-1)^3T^2\right)}{\omega^2+2(S-1)T\omega+T\left((T-4)S^2-2TS+T\right)}\right)+$$
$$\epsilon^3\mathcal{J}_{82}\left(\frac{\omega^3-\left(S^2+((S-3)S+3)T\right)\omega^2+\left(S^3+(4S-5)TS^2-(S-1)((S-3)S+3)T^2\right)\omega}{2\left(\omega^2+2(S-1)T\omega+T\left((T-4)S^2-2TS+T\right)\right)}+\right.$$
$$\left.\frac{T\left(-3S^4+S^3+(S-3)(S-2)TS^2+(S-1)^3T^2\right)}{2\left(\omega^2+2(S-1)T\omega+T\left((T-4)S^2-2TS+T\right)\right)}\right)+$$
$$\epsilon^3\mathcal{J}_{79}\left(\frac{-(S-1)^3T^3+\left(\omega(S-1)((S-3)S+3)-(S-3)(S-2)S^2\right)T^2}{2\left(\omega^2+2(S-1)T\omega+T\left((T-4)S^2-2TS+T\right)\right)}+\right.$$
$$\left.\frac{\left(((S-3)S+3)\omega^2+S^2(5-4S)\omega+S^3(3S-1)\right)T-\omega\left(\omega^2-S^2\omega+S^3\right)}{2\left(\omega^2+2(S-1)T\omega+T\left((T-4)S^2-2TS+T\right)\right)}\right)+$$
$$\frac{\mathcal{J}_{96}\epsilon^2}{8}+\frac{1}{16}\mathcal{J}_{15}(T-1)\epsilon^2+\frac{1}{16}\mathcal{J}_{95}\left(-\omega+S+T+1\right)\epsilon^2-\frac{\mathcal{J}_{16}\epsilon^2}{8}$$

$$\mathcal{G}_{175}=\mathcal{J}_{172}(S-1)T\epsilon^4-\frac{1}{2}\mathcal{J}_{159}\left(\left(\omega-2\right)S-2T\right)\epsilon^4+$$
$$\mathcal{J}_{174}(-TS+S+T)(2\epsilon-1)\epsilon^4+\mathcal{J}_{173}(S-1)(-TS+S+T)(2\epsilon-1)\epsilon^4+$$
$$2\mathcal{J}_{148}(S(T-1)-T)\epsilon^3+\frac{1}{2}\mathcal{J}_{149}(S(T-1)-T)\epsilon^3+\frac{1}{2}\mathcal{J}_{136}(-TS+S+T)\epsilon^3+$$
$$\frac{1}{2}\mathcal{J}_{146}(-TS+S+T)\epsilon^3-\frac{1}{2}\mathcal{J}_{79}(-TS+S+T)\epsilon^3+\mathcal{J}_{81}(-TS+S+T)\epsilon^3+\frac{1}{2}\mathcal{J}_{82}(-TS+S+T)\epsilon^3$$

$$\mathcal{G}_{176}=-\mathcal{J}_{176}(T-1)T\epsilon^4$$

$$\mathcal{G}_{177}=\mathcal{J}_{177}T\epsilon^4$$

$$\mathcal{G}_{178}=\frac{1}{2}\mathcal{J}_{164}\left(\omega-2S\right)T\epsilon^4+\mathcal{J}_{179}(-TS+S+T)(2\epsilon-1)\epsilon^4+\frac{1}{2}\mathcal{J}_{123}(S(T-1)-T)\epsilon^3+$$
$$\mathcal{J}_{61}(S(T-1)-T)\epsilon^3+\frac{1}{2}\mathcal{J}_{67}(S(T-1)-T)\epsilon^3+\mathcal{J}_{125}(-TS+S+T)\epsilon^3+$$
$$\frac{1}{2}\mathcal{J}_{126}(-TS+S+T)\epsilon^3+\frac{1}{2}\mathcal{J}_{56}(-TS+S+T)\epsilon^3$$

$$\mathcal{G}_{179}=\frac{1}{2}\mathcal{J}_{116}\left(S-\omega\right)\epsilon^4-\mathcal{J}_{55}T\epsilon^4+\mathcal{J}_{179}T(2\epsilon-1)\epsilon^4+$$
$$\mathcal{J}_{180}T(2\epsilon-1)\epsilon^4+\frac{\mathcal{J}_{165}\left(\omega-S\right)T\epsilon^4}{S+T}+\frac{\mathcal{J}_{43}\left(\omega-S\right)^2\epsilon^4}{2(S+T)}+$$
$$\frac{\mathcal{J}_{164}\omega\left(\omega-S\right)T\epsilon^4}{2(S+T)}+\frac{\mathcal{J}_{155}\left(\omega-S\right)T\epsilon^4}{2(S+T)}+$$
$$\frac{\mathcal{J}_{162}\left(S-\omega\right)T\epsilon^4}{2(S+T)}-\frac{\mathcal{J}_{111}\left(\omega-S\right)\left(3\omega-3S-2T\right)\epsilon^4}{4(S+T)}-$$

$$\frac{\mathcal{J}_{31}\left(2T^2+(\omega+S)\,T+3S\,(S-\omega)\right)\epsilon^4}{4(S+T)}+\frac{1}{4}\mathcal{J}_{103}\,(\omega-S-2T)\,\epsilon^3+$$
$$\frac{\mathcal{J}_{61}T\left((\omega-1)\,(\omega-S)^2+(\omega(S-1)-3S)\,T\,(\omega-S)-(\omega-4)\,ST^2\right)\epsilon^3}{(\omega-S)^2+2ST\,(\omega-S)+(S-4)ST^2}+$$
$$\frac{\mathcal{J}_{67}T\left((\omega-1)\,(\omega-S)^2+(\omega(S-1)-3S)\,T\,(\omega-S)-(\omega-4)\,ST^2\right)\epsilon^3}{2\left((\omega-S)^2+2ST\,(\omega-S)+(S-4)ST^2\right)}+$$
$$\frac{\mathcal{J}_{112}\,(\omega-S-2T)\,((T-1)\omega+S-T(S+T))\,\epsilon^3}{8(S+T)}+$$
$$\epsilon^3\mathcal{J}_{123}\left(\frac{S^3(T-1)^3-T^3\,(-\omega+T+1)^2+S^2T\,(((5-2T)T-3)\omega+T(2(T-2)T+3)-3)}{2\left(S^2(T-1)^2+T^2\,(-\omega+T+1)^2+2ST\,(-T\omega+\omega+T^2+1)\right)}+\right.$$
$$\left.\frac{ST^2\,((T-2)\omega^2-2(T-2)T\omega+\omega+(T-3)\,(T^2+T+1))}{2\left(S^2(T-1)^2+T^2\,(-\omega+T+1)^2+2ST\,(-T\omega+\omega+T^2+1)\right)}\right)+$$
$$\epsilon^3\mathcal{J}_{125}\left(\frac{-S^3(T-1)^3+T^3\,(-\omega+T+1)^2+S^2T\,((T-1)(2T-3)\omega+T(-2(T-2)T-3)+3)}{S^2(T-1)^2+T^2\,(-\omega+T+1)^2+2ST\,(-T\omega+\omega+T^2+1)}-\right.$$
$$\left.\frac{ST^2\,((T-2)\omega^2-2(T-2)T\omega+\omega+(T-3)\,(T^2+T+1))}{S^2(T-1)^2+T^2\,(-\omega+T+1)^2+2ST\,(-T\omega+\omega+T^2+1)}\right)+$$
$$\epsilon^3\mathcal{J}_{126}\left(\frac{-S^3(T-1)^3+T^3\,(-\omega+T+1)^2+S^2T\,((T-1)(2T-3)\omega+T(-2(T-2)T-3)+3)}{2\left(S^2(T-1)^2+T^2\,(-\omega+T+1)^2+2ST\,(-T\omega+\omega+T^2+1)\right)}-\right.$$
$$\left.\frac{ST^2\,((T-2)\omega^2-2(T-2)T\omega+\omega+(T-3)\,(T^2+T+1))}{2\left(S^2(T-1)^2+T^2\,(-\omega+T+1)^2+2ST\,(-T\omega+\omega+T^2+1)\right)}\right)-$$
$$\frac{\mathcal{J}_{23}\,(\omega-S)\,(\omega-S-2T)\,\epsilon^3}{4(S+T)}-\frac{\mathcal{J}_{32}\,(\omega-S-2T)\,(S(T-1)-T)\epsilon^3}{8(S+T)}+$$
$$\frac{\mathcal{J}_{56}T\left(-\left((\omega-1)\,(\omega-S)^2\right)-(\omega(S-1)-3S)\,T\,(\omega-S)+(\omega-4)\,ST^2\right)\epsilon^3}{2\left((\omega-S)^2+2ST\,(\omega-S)+(S-4)ST^2\right)}+$$
$$\frac{\mathcal{J}_4\,(-\omega+S+2T)\,\epsilon^2}{8(S+T)}+\frac{\mathcal{J}_{96}\,(\omega-S-2T)\,\epsilon^2}{8(S+T)}-$$
$$\frac{\mathcal{J}_{95}\,(\omega-S-2T)\,(\omega-S-T-1)\,\epsilon^2}{16(S+T)}-\frac{\mathcal{J}_3(S-1)\,(-\omega+S+2T)\,\epsilon^2}{16(S+T)}$$

$$\mathcal{G}_{180}=-\mathcal{J}_{177}\left(-T\omega+\omega+T^2+S(T-1)\right)\epsilon^4+\mathcal{J}_{164}\,(\omega-S(T+1))\,\epsilon^4+$$
$$\mathcal{J}_{178}(T-1)\left(-T\omega+\omega+T^2+S(T-1)\right)(2\epsilon-1)\epsilon^4+\mathcal{J}_{179}\left(-T\omega+\omega+T^2+T\right)(2\epsilon-1)\epsilon^4-$$
$$\frac{1}{2}\mathcal{J}_{123}\left(-T\omega+\omega+T^2+T\right)\epsilon^3+\mathcal{J}_{125}\left(-T\omega+\omega+T^2+T\right)\epsilon^3+$$
$$\frac{1}{2}\mathcal{J}_{126}\left(-T\omega+\omega+T^2+T\right)\epsilon^3+\frac{1}{2}\mathcal{J}_{32}\left(-T\omega+\omega+T^2+T\right)\epsilon^3+$$
$$\frac{1}{2}\mathcal{J}_{56}\left(-T\omega+\omega+T^2+T\right)\epsilon^3-2\mathcal{J}_{61}\left(-T\omega+\omega+T^2+T\right)\epsilon^3+$$
$$\frac{1}{2}\mathcal{J}_{67}\,(\omega(T-1)-T(T+1))\,\epsilon^3,$$

where $\{q_i\}$ are the following square roots:

$$q_1 = \sqrt{4-\omega} \tag{C.92}$$
$$q_2 = \sqrt{\omega} \tag{C.93}$$
$$q_3 = \sqrt{S} \tag{C.94}$$
$$q_4 = \sqrt{T} \tag{C.95}$$
$$q_5 = \sqrt{-S-T+4} \tag{C.96}$$
$$q_6 = \sqrt{S+T} \tag{C.97}$$
$$q_7 = \sqrt{2ST\left(-\omega S+\omega+S^2+1\right)+S^2(-\omega+S+1)^2+(S-1)^2T^2} \tag{C.98}$$
$$q_8 = \sqrt{2ST(\omega-S)+(\omega-S)^2+(S-4)ST^2} \tag{C.99}$$
$$q_9 = \sqrt{4(\omega-S)(S+T)-\omega^2T} \tag{C.100}$$
$$q_{10} = \sqrt{4(\omega-T)(S+T)-\omega^2S} \tag{C.101}$$
$$q_{11} = \sqrt{\omega^2+2\omega ST-2\omega T+S^2T^2-4S^2T-2ST^2+T^2} \tag{C.102}$$
$$q_{12} = \sqrt{2ST\left(-\omega T+\omega+T^2+1\right)+T^2(-\omega+T+1)^2+S^2(T-1)^2}. \tag{C.103}$$

Bibliography

[1] G. A. *et al.* (ATLAS), *Observation of a new particle in the search for the Standard Model Higgs boson with the ATLAS detector at the LHC*, *Physics Letters B* **716** (2012) 1–29.

[2] G. Heinrich, *Collider Physics at the Precision Frontier*, *Phys. Rept.* **922** (2021) 1–69, [2009.00516].

[3] J.-H. Zhang, *On the two-loop hexagon wilson loop remainder function in n=4 sym*, *Physics Letters B* **697** (2011) 370–377.

[4] M. Becchetti, R. Bonciani, L. Cieri, F. Coro and F. Ripani, *Two-loop form factors for diphoton production in quark annihilation channel with heavy quark mass dependence*, 2308.11412.

[5] M. Becchetti, R. Bonciani, L. Cieri, F. Coro and F. Ripani, *Full top-quark mass dependence in diphoton production at nnlo in qcd*, *Physics Letters B* **848** (2024) 138362.

[6] OpenLoops 2 collaboration, F. Buccioni, J.-N. Lang, J. M. Lindert, P. Maierhöfer, S. Pozzorini, H. Zhang et al., *OpenLoops 2*, *Eur. Phys. J. C* **79** (2019) 866, [1907.13071].

[7] S. Actis, A. Denner, L. Hofer, J.-N. Lang, A. Scharf and S. Uccirati, *R e c o l a—recursive computation of one-loop amplitudes*, *Computer Physics Communications* **214** (May, 2017) 140–173.

[8] J. Alwall, R. Frederix, S. Frixione, V. Hirschi, F. Maltoni, O. Mattelaer et al., *The automated computation of tree-level and next-to-leading order differential cross sections, and their matching to parton shower simulations*, *Journal of High Energy Physics* **2014** (July, 2014) .

[9] T. Peraro, *Ninja: Automated integrand reduction via laurent expansion for one-loop amplitudes*, *Computer Physics Communications* **185** (Oct., 2014) 2771–2797.

[10] K. G. Chetyrkin, A. L. Kataev and F. V. Tkachov, *Higher Order Corrections to Sigma-t (e+ e- —> Hadrons) in Quantum Chromodynamics*, *Phys. Lett. B* **85** (1979) 277–279.

[11] K. G. Chetyrkin and F. V. Tkachov, *Integration by Parts: The Algorithm to Calculate beta Functions in 4 Loops*, *Nucl. Phys. B* **192** (1981) 159–204.

[12] S. Laporta, *High precision calculation of multiloop Feynman integrals by difference equations*, *Int.J.Mod.Phys.* **A15** (2000) 5087–5159, [hep-ph/0102033].

[13] A. V. Kotikov, *Differential equations method: New technique for massive Feynman diagrams calculation*, *Phys. Lett. B* **254** (1991) 158–164.

[14] A. V. Kotikov, *Differential equation method: The Calculation of N point Feynman diagrams*, *Phys. Lett. B* **267** (1991) 123–127.

[15] Z. Bern, L. J. Dixon and D. A. Kosower, *Dimensionally regulated pentagon integrals*, *Nucl. Phys. B* **412** (1994) 751–816, [hep-ph/9306240].

[16] E. Remiddi, *Differential equations for Feynman graph amplitudes*, *Nuovo Cim. A* **110** (1997) 1435–1452, [hep-th/9711188].

[17] T. Gehrmann and E. Remiddi, *Differential equations for two loop four point functions*, *Nucl. Phys. B* **580** (2000) 485–518, [hep-ph/9912329].

[18] M. Argeri and P. Mastrolia, *Feynman Diagrams and Differential Equations*, *Int. J. Mod. Phys. A* **22** (2007) 4375–4436, [0707.4037].

[19] J. M. Henn, *Multiloop integrals in dimensional regularization made simple*, *Phys. Rev. Lett.* **110** (2013) 251601, [1304.1806].

[20] J. M. Henn, *Lectures on differential equations for Feynman integrals*, *J. Phys. A* **48** (2015) 153001, [1412.2296].

[21] E. REMIDDI and J. A. M. VERMASEREN, *Harmonic polylogarithms*, *International Journal of Modern Physics A* **15** (2000) 725–754.

[22] A. B. Goncharov, *Multiple polylogarithms, cyclotomy and modular complexes*, 2011.

[23] A. B. Goncharov, *Multiple polylogarithms and mixed tate motives*, 2001.

[24] J. Vollinga and S. Weinzierl, *Numerical evaluation of multiple polylogarithms*, *Computer Physics Communications* **167** (2005) 177–194.

[25] C. Duhr and F. Dulat, *PolyLogTools — polylogs for the masses*, *JHEP* **08** (2019) 135, [1904.07279].

[26] E. Panzer, *Algorithms for the symbolic integration of hyperlogarithms with applications to feynman integrals*, *Computer Physics Communications* **188** (Mar., 2015) 148–166.

[27] C. Bauer, A. Frink and R. Kreckel, *Introduction to the ginac framework for symbolic computation within the c++ programming language*, 2001.

[28] M. Delto, C. Duhr, L. Tancredi and Y. J. Zhu, *Two-loop qed corrections to the scattering of four massive leptons*, *Phys. Rev. Lett.* **132** (Jun, 2024) 231904.

[29] R. Bonciani, V. Del Duca, H. Frellesvig, J. Henn, M. Hidding, L. Maestri et al., *Evaluating a family of two-loop non-planar master integrals for higgs + jet production with full heavy-quark mass dependence*, *Journal of High Energy Physics* **2020** (Jan., 2020) .

[30] H. Frellesvig, R. Morales and M. Wilhelm, *Classifying post-Minkowskian geometries for gravitational waves via loop-by-loop Baikov*, *JHEP* **08** (2024) 243, [2405.17255].

[31] S. Borowka, G. Heinrich, S. Jahn, S. Jones, M. Kerner, J. Schlenk et al., *pysecdec: A toolbox for the numerical evaluation of multi-scale integrals*, *Computer Physics Communications* **222** (Jan., 2018) 313–326.

[32] F. Moriello, *Generalised power series expansions for the elliptic planar families of Higgs + jet production at two loops*, *JHEP* **01** (2020) 150, [1907.13234].

[33] M. Hidding, *DiffExp, a Mathematica package for computing Feynman integrals in terms of one-dimensional series expansions*, *Comput. Phys. Commun.* **269** (2021) 108125, [2006.05510].

[34] T. Armadillo, R. Bonciani, S. Devoto, N. Rana and A. Vicini, *Evaluation of Feynman integrals with arbitrary complex masses via series expansions*, *Comput. Phys. Commun.* **282** (2023) 108545, [2205.03345].

[35] P. Maierhöfer, J. Usovitsch and P. Uwer, *Kira—A Feynman integral reduction program*, *Comput. Phys. Commun.* **230** (2018) 99–112, [1705.05610].

[36] J. Klappert, F. Lange, P. Maierhöfer and J. Usovitsch, *Integral reduction with Kira 2.0 and finite field methods*, *Comput. Phys. Commun.* **266** (2021) 108024, [2008.06494].

[37] C. Anastasiou and A. Lazopoulos, *Automatic integral reduction for higher order perturbative calculations*, *JHEP* **07** (2004) 046, [hep-ph/0404258].

[38] C. Studerus, *Reduze-Feynman Integral Reduction in C++*, *Comput.Phys.Commun.* **181** (2010) 1293–1300, [0912.2546].

[39] A. von Manteuffel and C. Studerus, *Reduze 2 - Distributed Feynman Integral Reduction*, 1201.4330.

[40] R. N. Lee, *Presenting LiteRed: a tool for the Loop InTEgrals REDuction*, 1212.2685.

[41] R. N. Lee, *LiteRed 1.4: a powerful tool for reduction of multiloop integrals*, *J. Phys. Conf. Ser.* **523** (2014) 012059, [1310.1145].

[42] A. V. Smirnov, *Algorithm FIRE – Feynman Integral REduction*, *JHEP* **10** (2008) 107, [0807.3243].

[43] A. V. Smirnov, *FIRE5: a C++ implementation of Feynman Integral REduction*, *Comput. Phys. Commun.* **189** (2014) 182–191, [1408.2372].

[44] T. Peraro, *FiniteFlow: multivariate functional reconstruction using finite fields and dataflow graphs*, *JHEP* **07** (2019) 031, [1905.08019].

[45] Z. Wu, J. Boehm, R. Ma, H. Xu and Y. Zhang, *Neatibp 1.0, a package generating small-size integration-by-parts relations for feynman integrals*, 2024.

[46] J. M. Henn, *Multiloop integrals in dimensional regularization made simple*, *Physical Review Letters* **110** (June, 2013) .

[47] K.-T. Chen, *Iterated path integrals*, *Bull. Am. Math. Soc.* **83** (1977) 831–879.

[48] F. Brown and C. Duhr, *A double integral of dlog forms which is not polylogarithmic*, 2020.

[49] L. Görges, C. Nega, L. Tancredi and F. J. Wagner, *On a procedure to derive ϵ-factorised differential equations beyond polylogarithms*, 2305.14090.

[50] C. Meyer, *Algorithmic transformation of multi-loop master integrals to a canonical basis with canonica*, *Computer Physics Communications* **222** (Jan., 2018) 295–312.

[51] M. Becchetti and R. Bonciani, *Two-Loop Master Integrals for the Planar QCD Massive Corrections to Di-photon and Di-jet Hadro-production*, *JHEP* **01** (2018) 048, [1712.02537].

[52] E. REMIDDI and J. A. M. VERMASEREN, *Harmonic polylogarithms*, *International Journal of Modern Physics A* **15** (Feb., 2000) 725–754.

[53] X. Liu and Y.-Q. Ma, *AMFlow: A mathematica package for feynman integrals computation via auxiliary mass flow*, *Computer Physics Communications* **283** (feb, 2023) 108565.

[54] M. Becchetti, R. Bonciani, V. Del Duca, V. Hirschi, F. Moriello and A. Schweitzer, *Next-to-leading order corrections to light-quark mixed QCD-EW contributions to Higgs boson production*, *Phys. Rev. D* **103** (2021) 054037, [2010.09451].

[55] R. Bonciani, L. Buonocore, M. Grazzini, S. Kallweit, N. Rana, F. Tramontano et al., *Mixed Strong-Electroweak Corrections to the Drell-Yan Process*, *Phys. Rev. Lett.* **128** (2022) 012002, [2106.11953].

[56] R. Bonciani, V. Del Duca, H. Frellesvig, M. Hidding, V. Hirschi, F. Moriello et al., *Next-to-leading-order QCD corrections to Higgs production in association with a jet*, *Phys. Lett. B* **843** (2023) 137995, [2206.10490].

[57] ATLAS collaboration, G. Aad et al., *Measurement of the production cross section of pairs of isolated photons in pp collisions at 13 TeV with the ATLAS detector*, *JHEP* **11** (2021) 169, [2107.09330].

[58] ATLAS collaboration, M. Aaboud et al., *Measurements of integrated and differential cross sections for isolated photon pair production in pp collisions at $\sqrt{s} = 8$ TeV with the ATLAS detector*, *Phys. Rev. D* **95** (2017) 112005, [1704.03839].

[59] CMS collaboration, S. Chatrchyan et al., *Measurement of differential cross sections for the production of a pair of isolated photons in pp collisions at $\sqrt{s} = 7$ TeV*, *Eur. Phys. J. C* **74** (2014) 3129, [1405.7225].

[60] ATLAS collaboration, G. Aad et al., *Measurement of isolated-photon pair production in pp collisions at $\sqrt{s} = 7$ TeV with the ATLAS detector*, *JHEP* **01** (2013) 086, [1211.1913].

[61] ATLAS collaboration, G. Aad et al., *Search for periodic signals in the dielectron and diphoton invariant mass spectra using 139 fb^{-1} of pp collisions at $\sqrt{s} = 13$ TeV with the ATLAS detector*, 2305.10894.

[62] ATLAS collaboration, G. Aad et al., *Search in diphoton and dielectron final states for displaced production of Higgs or Z bosons with the ATLAS detector in s=13 TeV pp collisions*, *Phys. Rev. D* **108** (2023) 012012, [2304.12885].

[63] ATLAS collaboration, G. Aad et al., *Search for boosted diphoton resonances in the 10 to 70 GeV mass range using 138 fb^{-1} of 13 TeV pp collisions with the ATLAS detector*, *JHEP* **07** (2023) 155, [2211.04172].

[64] CMS collaboration, A. M. Sirunyan et al., *Search for supersymmetry using Higgs boson to diphoton decays at $\sqrt{s} = 13$ TeV*, *JHEP* **11** (2019) 109, [1908.08500].

[65] CMS collaboration, V. Khachatryan et al., *Search for high-mass diphoton resonances in proton–proton collisions at 13 TeV and combination with 8 TeV search*, *Phys. Lett. B* **767** (2017) 147–170, [1609.02507].

[66] ATLAS collaboration, M. Aaboud et al., *Search for new phenomena in high-mass diphoton final states using 37 fb^{-1} of proton–proton collisions collected at $\sqrt{s} = 13$ TeV with the ATLAS detector*, *Phys. Lett. B* **775** (2017) 105–125, [1707.04147].

[67] ATLAS collaboration, G. Aad et al., *Measurements of the Higgs boson inclusive and differential fiducial cross-sections in the diphoton decay channel with pp collisions at $\sqrt{s}$ = 13 TeV with the ATLAS detector*, *JHEP* **08** (2022) 027, [2202.00487].

[68] CMS collaboration, A. Tumasyan et al., *Measurement of the Higgs boson inclusive and differential fiducial production cross sections in the diphoton decay channel with pp collisions at $\sqrt{s} = 13$ TeV*, *JHEP* **07** (2023) 091, [2208.12279].

[69] CMS collaboration, A. M. Sirunyan et al., *Measurements of Higgs boson production cross sections and couplings in the diphoton decay channel at $\sqrt{s} = 13$ TeV*, *JHEP* **07** (2021) 027, [2103.06956].

[70] CMS collaboration, A. M. Sirunyan et al., *A measurement of the Higgs boson mass in the diphoton decay channel*, *Phys. Lett. B* **805** (2020) 135425, [2002.06398].

[71] ATLAS collaboration, M. Aaboud et al., *Measurements of Higgs boson properties in the diphoton decay channel with 36 fb^{-1} of pp collision data at $\sqrt{s} = 13$ TeV with the ATLAS detector*, *Phys. Rev. D* **98** (2018) 052005, [1802.04146].

[72] CMS collaboration, V. Khachatryan et al., *Observation of the Diphoton Decay of the Higgs Boson and Measurement of Its Properties*, *Eur. Phys. J. C* **74** (2014) 3076, [1407.0558].

[73] ATLAS collaboration, G. Aad et al., *Measurement of Higgs boson production in the diphoton decay channel in pp collisions at center-of-mass energies of 7 and 8 TeV with the ATLAS detector*, *Phys. Rev. D* **90** (2014) 112015, [1408.7084].

[74] ATLAS collaboration, G. Aad et al., *Measurements of fiducial and differential cross sections for Higgs boson production in the diphoton decay channel at $\sqrt{s} = 8$ TeV with ATLAS*, *JHEP* **09** (2014) 112, [1407.4222].

[75] ATLAS collaboration, G. Aad et al., *Observation of a new particle in the search for the Standard Model Higgs boson with the ATLAS detector at the LHC*, *Phys. Lett. B* **716** (2012) 1–29, [1207.7214].

[76] CMS collaboration, S. Chatrchyan et al., *Observation of a New Boson at a Mass of 125 GeV with the CMS Experiment at the LHC*, *Phys. Lett. B* **716** (2012) 30–61, [1207.7235].

[77] S. Catani, L. Cieri, D. de Florian, G. Ferrera and M. Grazzini, *Diphoton production at hadron colliders: a fully-differential QCD calculation at NNLO*, *Phys. Rev. Lett.* **108** (2012) 072001, [1110.2375].

[78] J. M. Campbell, R. K. Ellis, Y. Li and C. Williams, *Predictions for diphoton production at the LHC through NNLO in QCD*, *JHEP* **07** (2016) 148, [1603.02663].

[79] S. Catani, L. Cieri, D. de Florian, G. Ferrera and M. Grazzini, *Diphoton production at the LHC: a QCD study up to NNLO*, *JHEP* **04** (2018) 142, [1802.02095].

[80] R. Schuermann, X. Chen, T. Gehrmann, E. W. N. Glover, M. Höfer and A. Huss, *NNLO Photon Production with Realistic Photon Isolation*, *PoS* **LL2022** (2022) 034, [2208.02669].

[81] L. Ametller, E. Gava, N. Paver and D. Treleani, *Role of the QCD Induced Gluon - Gluon Coupling to Gauge Boson Pairs in the Multi - Tev Region*, *Phys. Rev. D* **32** (1985) 1699.

[82] S. J. Parke and T. R. Taylor, *An Amplitude for n Gluon Scattering*, *Phys. Rev. Lett.* **56** (1986) 2459.

[83] D. A. Dicus and S. S. D. Willenbrock, *Photon Pair Production and the Intermediate Mass Higgs Boson*, *Phys. Rev. D* **37** (1988) 1801.

[84] V. D. Barger, T. Han, J. Ohnemus and D. Zeppenfeld, *Pair Production of $W^{\pm}$, γ and Z in Association With Jets*, *Phys. Rev. D* **41** (1990) 2782.

[85] M. L. Mangano and S. J. Parke, *Multiparton amplitudes in gauge theories*, *Phys. Rept.* **200** (1991) 301–367, [hep-th/0509223].

[86] Z. Bern, L. J. Dixon and D. A. Kosower, *One loop corrections to two quark three gluon amplitudes*, *Nucl. Phys. B* **437** (1995) 259–304, [hep-ph/9409393].

[87] A. Signer, *One loop corrections to five parton amplitudes with external photons*, *Phys. Lett. B* **357** (1995) 204–210, [hep-ph/9507442].

[88] C. Balazs, E. L. Berger, S. Mrenna and C. P. Yuan, *Photon pair production with soft gluon resummation in hadronic interactions*, *Phys. Rev. D* **57** (1998) 6934–6947, [hep-ph/9712471].

[89] V. Del Duca, W. B. Kilgore and F. Maltoni, *Multiphoton amplitudes for next-to-leading order QCD*, *Nucl. Phys. B* **566** (2000) 252–274, [hep-ph/9910253].

[90] C. Anastasiou, E. W. N. Glover and M. E. Tejeda-Yeomans, *Two loop QED and QCD corrections to massless fermion boson scattering*, *Nucl. Phys. B* **629** (2002) 255–289, [hep-ph/0201274].

[91] V. Del Duca, F. Maltoni, Z. Nagy and Z. Trocsanyi, *QCD radiative corrections to prompt diphoton production in association with a jet at hadron colliders*, *JHEP* **04** (2003) 059, [hep-ph/0303012].

[92] F. Caola, A. Chakraborty, G. Gambuti, A. von Manteuffel and L. Tancredi, *Three-loop helicity amplitudes for quark-gluon scattering in QCD*, *JHEP* **12** (2022) 082, [2207.03503].

[93] H. A. Chawdhry, M. Czakon, A. Mitov and R. Poncelet, *Two-loop leading-color helicity amplitudes for three-photon production at the LHC*, *JHEP* **06** (2021) 150, [2012.13553].

[94] B. Agarwal, F. Buccioni, A. von Manteuffel and L. Tancredi, *Two-loop leading colour QCD corrections to $q\bar{q} \to \gamma\gamma g$ and $qg \to \gamma\gamma q$*, *JHEP* **04** (2021) 201, [2102.01820].

[95] H. A. Chawdhry, M. Czakon, A. Mitov and R. Poncelet, *Two-loop leading-colour QCD helicity amplitudes for two-photon plus jet production at the LHC*, *JHEP* **07** (2021) 164, [2103.04319].

[96] B. Agarwal, F. Buccioni, A. von Manteuffel and L. Tancredi, *Two-Loop Helicity Amplitudes for Diphoton Plus Jet Production in Full Color*, *Phys. Rev. Lett.* **127** (2021) 262001, [2105.04585].

[97] S. Badger, T. Gehrmann, M. Marcoli and R. Moodie, *Next-to-leading order QCD corrections to diphoton-plus-jet production through gluon fusion at the LHC*, *Phys. Lett. B* **824** (2022) 136802, [2109.12003].

[98] Z. Bern, A. De Freitas and L. J. Dixon, *Two loop amplitudes for gluon fusion into two photons*, *JHEP* **09** (2001) 037, [hep-ph/0109078].

[99] H. A. Chawdhry, M. Czakon, A. Mitov and R. Poncelet, *NNLO QCD corrections to diphoton production with an additional jet at the LHC*, *JHEP* **09** (2021) 093, [2105.06940].

[100] M. Chiesa, N. Greiner, M. Schönherr and F. Tramontano, *Electroweak corrections to diphoton plus jets*, *JHEP* **10** (2017) 181, [1706.09022].

[101] L. Cieri and G. Sborlini, *Exploring QED Effects to Diphoton Production at Hadron Colliders*, *Symmetry* **13** (2021) 994.

[102] L. J. Dixon and M. S. Siu, *Resonance continuum interference in the diphoton Higgs signal at the LHC*, *Phys. Rev. Lett.* **90** (2003) 252001, [hep-ph/0302233].

[103] S. P. Martin, *Shift in the LHC Higgs diphoton mass peak from interference with background*, *Phys. Rev.* **D86** (2012) 073016, [1208.1533].

[104] D. de Florian, N. Fidanza, R. J. Hernandez-Pinto, J. Mazzitelli, Y. Rotstein Habarnau and G. F. R. Sborlini, *A complete $O(\alpha_S^2)$ calculation of the signal-background interference for the Higgs diphoton decay channel*, *Eur. Phys. J.* **C73** (2013) 2387, [1303.1397].

[105] S. P. Martin, *Interference of Higgs diphoton signal and background in production with a jet at the LHC*, *Phys. Rev.* **D88** (2013) 013004, [1303.3342].

[106] L. J. Dixon and Y. Li, *Bounding the Higgs Boson Width Through Interferometry*, *Phys. Rev. Lett.* **111** (2013) 111802, [1305.3854].

[107] J. Campbell, M. Carena, R. Harnik and Z. Liu, *Interference in the $gg \to h \to \gamma\gamma$ On-Shell Rate and the Higgs Boson Total Width*, *Phys. Rev. Lett.* **119** (2017) 181801, [1704.08259].

[108] L. Cieri, F. Coradeschi, D. de Florian and N. Fidanza, *Transverse-momentum resummation for the signal-background interference in the $H \to \gamma\gamma$ channel at the LHC*, *Phys. Rev.* **D96** (2017) 054003, [1706.07331].

[109] P. Bargiela, F. Buccioni, F. Caola, F. Devoto, A. von Manteuffel and L. Tancredi, *Signal-background interference effects in Higgs-mediated diphoton production beyond NLO*, *Eur. Phys. J. C* **83** (2023) 174, [2212.06287].

[110] L. Cieri, F. Coradeschi and D. de Florian, *Diphoton production at hadron colliders: transverse-momentum resummation at next-to-next-to-leading logarithmic accuracy*, *JHEP* **06** (2015) 185, [1505.03162].

[111] T. Becher and T. Neumann, *Fiducial q_T resummation of color-singlet processes at N^3LL+NNLO*, *JHEP* **03** (2021) 199, [2009.11437].

[112] S. R. Dugad, P. Jain, S. Mitra, P. Sanyal and R. K. Verma, *The top threshold effect in the $\gamma\gamma$ production at the LHC*, *Eur. Phys. J.* **C78** (2018) 715, [1605.07360].

[113] S. Kawabata and H. Yokoya, *Top-quark mass from the diphoton mass spectrum*, *Eur. Phys. J.* **C77** (2017) 323, [1607.00990].

[114] F. Maltoni, M. K. Mandal and X. Zhao, *Top-quark effects in diphoton production through gluon fusion at next-to-leading order in QCD*, *Phys. Rev. D* **100** (2019) 071501, [1812.08703].

[115] L. Chen, G. Heinrich, S. Jahn, S. P. Jones, M. Kerner, J. Schlenk et al., *Photon pair production in gluon fusion: Top quark effects at NLO with threshold matching*, *JHEP* **04** (2020) 115, [1911.09314].

[116] M. Becchetti, R. Bonciani, L. Cieri, F. Coro and F. Ripani, *Full top-quark mass dependence in diphoton production at nnlo in qcd*, 2023.

[117] T. Peraro and L. Tancredi, *Tensor decomposition for bosonic and fermionic scattering amplitudes*, *Phys. Rev. D* **103** (2021) 054042, [2012.00820].

[118] S. Caron-Huot and J. M. Henn, *Iterative structure of finite loop integrals*, *JHEP* **06** (2014) 114, [1404.2922].

[119] R. Bonciani, P. Mastrolia and E. Remiddi, *Vertex diagrams for the QED form-factors at the two loop level*, *Nucl. Phys. B* **661** (2003) 289–343, [hep-ph/0301170].

[120] U. Aglietti and R. Bonciani, *Master integrals with 2 and 3 massive propagators for the 2 loop electroweak form-factor - planar case*, *Nucl. Phys. B* **698** (2004) 277–318, [hep-ph/0401193].

[121] R. Bonciani, P. Mastrolia and E. Remiddi, *Master integrals for the two loop QCD virtual corrections to the forward backward asymmetry*, *Nucl. Phys. B* **690** (2004) 138–176, [hep-ph/0311145].

[122] R. Bonciani, A. Ferroglia and A. A. Penin, *Heavy-flavor contribution to Bhabha scattering*, *Phys. Rev. Lett.* **100** (2008) 131601, [0710.4775].

[123] R. Bonciani, A. Ferroglia and A. A. Penin, *Calculation of the Two-Loop Heavy-Flavor Contribution to Bhabha Scattering*, *JHEP* **02** (2008) 080, [0802.2215].

[124] A. B. Goncharov, *Multiple polylogarithms and mixed Tate motives*, math/0103059.

[125] A. B. Goncharov, *Multiple polylogarithms, cyclotomy and modular complexes*, *Math. Res. Lett.* **5** (1998) 497–516, [1105.2076].

[126] A. Goncharov, *Multiple polylogarithms and mixed Tate motives*, math/0103059.

[127] E. Remiddi and J. A. M. Vermaseren, *Harmonic polylogarithms*, *Int. J. Mod. Phys. A* **15** (2000) 725–754, [hep-ph/9905237].

[128] J. Vollinga and S. Weinzierl, *Numerical evaluation of multiple polylogarithms*, *Comput. Phys. Commun.* **167** (2005) 177, [hep-ph/0410259].

[129] L. Adams, E. Chaubey and S. Weinzierl, *Simplifying Differential Equations for Multiscale Feynman Integrals beyond Multiple Polylogarithms*, *Phys. Rev. Lett.* **118** (2017) 141602, [1702.04279].

[130] F. C. S. Brown and A. Levin, *Multiple elliptic polylogarithms*, 2013.

[131] J. Broedel, C. R. Mafra, N. Matthes and O. Schlotterer, *Elliptic multiple zeta values and one-loop superstring amplitudes*, *JHEP* **07** (2015) 112, [1412.5535].

[132] J. Broedel, C. Duhr, F. Dulat and L. Tancredi, *Elliptic polylogarithms and iterated integrals on elliptic curves. Part I: general formalism*, *JHEP* **05** (2018) 093, [1712.07089].

[133] Y. I. Manin, *Iterated integrals of modular forms and noncommutative modular symbols*, in *Algebraic geometry and number theory*, vol. 253 of *Progr. Math.*, (Boston), pp. 565–597, Birkhäuser Boston, 2006. math/0502576.

[134] F. Brown, *Multiple modular values and the relative completion of the fundamental group of* $\mathcal{M}_{1,1}$, 1407.5167v4.

[135] L. Adams, C. Bogner and S. Weinzierl, *The two-loop sunrise graph in two space-time dimensions with arbitrary masses in terms of elliptic dilogarithms*, *J. Math. Phys.* **55** (2014) 102301, [1405.5640].

[136] H. Frellesvig, *On epsilon factorized differential equations for elliptic Feynman integrals*, *JHEP* **03** (2022) 079, [2110.07968].

[137] H. Frellesvig and S. Weinzierl, *On ε-factorised bases and pure Feynman integrals*, 2301.02264.

[138] C. Duhr, A. Klemm, F. Loebbert, C. Nega and F. Porkert, *Yangian-Invariant Fishnet Integrals in Two Dimensions as Volumes of Calabi-Yau Varieties*, *Phys. Rev. Lett.* **130** (2023) 041602, [2209.05291].

[139] C. Duhr, A. Klemm, C. Nega and L. Tancredi, *The ice cone family and iterated integrals for Calabi-Yau varieties*, *JHEP* **02** (2023) 228, [2212.09550].

[140] J. L. Bourjaily et al., *Functions Beyond Multiple Polylogarithms for Precision Collider Physics*, in *Snowmass 2021*, 3, 2022. 2203.07088.

[141] S. Abreu, M. Becchetti, C. Duhr and M. A. Ozcelik, *Two-loop master integrals for pseudo-scalar quarkonium and leptonium production and decay*, *JHEP* **09** (2022) 194, [2206.03848].

[142] S. Abreu, M. Becchetti, C. Duhr and M. A. Ozcelik, *Two-loop form factors for pseudo-scalar quarkonium production and decay*, *JHEP* **02** (2023) 250, [2211.08838].

[143] S. Pozzorini and E. Remiddi, *Precise numerical evaluation of the two loop sunrise graph master integrals in the equal mass case*, *Comput. Phys. Commun.* **175** (2006) 381–387, [hep-ph/0505041].

[144] U. Aglietti, R. Bonciani, L. Grassi and E. Remiddi, *The Two loop crossed ladder vertex diagram with two massive exchanges*, *Nucl. Phys. B* **789** (2008) 45–83, [0705.2616].

[145] R. Bonciani, G. Degrassi, P. P. Giardino and R. Gröber, *A Numerical Routine for the Crossed Vertex Diagram with a Massive-Particle Loop*, *Comput. Phys. Commun.* **241** (2019) 122–131, [1812.02698].

[146] R. N. Lee, A. V. Smirnov and V. A. Smirnov, *Solving differential equations for Feynman integrals by expansions near singular points*, *JHEP* **03** (2018) 008, [1709.07525].

[147] M. K. Mandal and X. Zhao, *Evaluating multi-loop Feynman integrals numerically through differential equations*, *JHEP* **03** (2019) 190, [1812.03060].

[148] R. Bonciani, V. Del Duca, H. Frellesvig, J. M. Henn, M. Hidding, L. Maestri et al., *Evaluating a family of two-loop non-planar master integrals for Higgs + jet production with full heavy-quark mass dependence*, *JHEP* **01** (2020) 132, [1907.13156].

[149] T. Hahn, *Generating Feynman diagrams and amplitudes with FeynArts 3*, *Comput. Phys. Commun.* **140** (2001) 418–431, [hep-ph/0012260].

[150] U. Aglietti, R. Bonciani, G. Degrassi and A. Vicini, *Analytic Results for Virtual QCD Corrections to Higgs Production and Decay*, *JHEP* **01** (2007) 021, [hep-ph/0611266].

[151] C. Anastasiou, S. Beerli, S. Bucherer, A. Daleo and Z. Kunszt, *Two-loop amplitudes and master integrals for the production of a Higgs boson via a massive quark and a scalar-quark loop*, *JHEP* **01** (2007) 082, [hep-ph/0611236].

[152] A. von Manteuffel and L. Tancredi, *A non-planar two-loop three-point function beyond multiple polylogarithms*, *JHEP* **06** (2017) 127, [1701.05905].

[153] T. Ahmed, E. Chaubey, M. Kaur and S. Maggio, *Two-loop non-planar four-point topology with massive internal loop*, 2024.

[154] S. Catani and M. Grazzini, *An NNLO subtraction formalism in hadron collisions and its application to Higgs boson production at the LHC*, *Phys. Rev. Lett.* **98** (2007) 222002, [hep-ph/0703012].

[155] S. Catani, L. Cieri, D. de Florian, G. Ferrera and M. Grazzini, *Universality of transverse-momentum resummation and hard factors at the NNLO*, *Nucl. Phys. B* **881** (2014) 414–443, [1311.1654].

[156] G. Bozzi, S. Catani, D. de Florian and M. Grazzini, *Transverse-momentum resummation and the spectrum of the Higgs boson at the LHC*, *Nucl. Phys. B* **737** (2006) 73–120, [hep-ph/0508068].

[157] F. Caola, A. von Manteuffel and L. Tancredi, *Diphoton amplitudes in three-loop quantum chromodynamics*, *Physical Review Letters* **126** (Mar., 2021) .

[158] J. Kuipers, T. Ueda, J. A. M. Vermaseren and J. Vollinga, *FORM version 4.0*, *Comput. Phys. Commun.* **184** (2013) 1453–1467, [1203.6543].

[159] B. Ruijl, T. Ueda and J. Vermaseren, *FORM version 4.2*, 1707.06453.

[160] P. Bärnreuther, M. Czakon and P. Fiedler, *Virtual amplitudes and threshold behaviour of hadronic top-quark pair-production cross sections*, *JHEP* **02** (2014) 078, [1312.6279].

[161] D. J. Broadhurst, J. Fleischer and O. V. Tarasov, *Two loop two point functions with masses: Asymptotic expansions and Taylor series, in any dimension*, *Z. Phys. C* **60** (1993) 287–302, [hep-ph/9304303].

[162] K. Melnikov and T. v. Ritbergen, *The Three loop relation between the MS-bar and the pole quark masses*, *Phys. Lett. B* **482** (2000) 99–108, [hep-ph/9912391].

[163] A. Mitov and S. Moch, *The Singular behavior of massive QCD amplitudes*, *JHEP* **05** (2007) 001, [hep-ph/0612149].

[164] J. Broedel, C. Duhr, F. Dulat, B. Penante and L. Tancredi, *Elliptic polylogarithms and Feynman parameter integrals*, *JHEP* **05** (2019) 120, [1902.09971].

[165] A. B. Goncharov, M. Spradlin, C. Vergu and A. Volovich, *Classical Polylogarithms for Amplitudes and Wilson Loops*, *Phys. Rev. Lett.* **105** (2010) 151605, [1006.5703].

[166] C. Duhr, H. Gangl and J. R. Rhodes, *From polygons and symbols to polylogarithmic functions*, *JHEP* **10** (2012) 075, [1110.0458].

[167] M. Becchetti, F. Coro, C. Nega, L. Tancredi and F. J. Wagner, *In preparation...*, .

[168] J. M. Henn, *Lectures on differential equations for feynman integrals*, *Journal of Physics A: Mathematical and Theoretical* **48** (mar, 2015) 153001.

[169] X. Liu, Y.-Q. Ma and C.-Y. Wang, *A Systematic and Efficient Method to Compute Multi-loop Master Integrals*, *Phys. Lett. B* **779** (2018) 353–357, [1711.09572].

[170] X. Liu and Y.-Q. Ma, *Multiloop corrections for collider processes using auxiliary mass flow*, *Phys. Rev. D* **105** (2022) L051503, [2107.01864].

[171] H. Frellesvig and C. G. Papadopoulos, *Cuts of Feynman Integrals in Baikov representation*, *JHEP* **04** (2017) 083, [1701.07356].

[172] M. Harley, F. Moriello and R. M. Schabinger, *Baikov-Lee Representations Of Cut Feynman Integrals*, *JHEP* **06** (2017) 049, [1705.03478].

[173] P. A. Baikov, *Explicit solutions of n loop vacuum integral recurrence relations*, hep-ph/9604254.

[174] C. Dlapa, *Algorithms and techniques for finding canonical differential equations of Feynman integrals*. PhD thesis, Munich U., 2022. 10.5282/edoc.29769.

[175] F. Cascioli, P. Maierhofer and S. Pozzorini, *Scattering Amplitudes with Open Loops*, *Phys. Rev. Lett.* **108** (2012) 111601, [1111.5206].

[176] M. Zoller, F. Buccioni, J.-N. Lang, S. Pozzorini and H. Zhang, *On-the-fly reduction of open loops*, *PoS* **LL2018** (2018) 045, [1807.10713].

[177] A. van Hameren, C. G. Papadopoulos and R. Pittau, *Automated one-loop calculations: A Proof of concept*, *JHEP* **09** (2009) 106, [0903.4665].

[178] A. van Hameren, *OneLOop: For the evaluation of one-loop scalar functions*, *Comput. Phys. Commun.* **182** (2011) 2427–2438, [1007.4716].

[179] A. Denner, S. Dittmaier and L. Hofer, *Collier: a fortran-based Complex One-Loop LIbrary in Extended Regularizations*, *Comput. Phys. Commun.* **212** (2017) 220–238, [1604.06792].

[180] M. Grazzini, S. Kallweit and M. Wiesemann, *Fully differential NNLO computations with MATRIX*, *Eur. Phys. J. C* **78** (2018) 537, [1711.06631].

[181] S. Camarda et al., *DYTurbo: Fast predictions for Drell-Yan processes*, *Eur. Phys. J. C* **80** (2020) 251, [1910.07049].

[182] S. Camarda, L. Cieri and G. Ferrera, *Drell–Yan lepton-pair production: qT resummation at N3LL accuracy and fiducial cross sections at N3LO*, *Phys. Rev. D* **104** (2021) L111503, [2103.04974].

[183] NNPDF collaboration, R. D. Ball et al., *Parton distributions from high-precision collider data*, *Eur. Phys. J. C* **77** (2017) 663, [1706.00428].

[184] A. Buckley, J. Ferrando, S. Lloyd, K. Nordström, B. Page, M. Rüfenacht et al., *LHAPDF6: parton density access in the LHC precision era*, *Eur. Phys. J. C* **75** (2015) 132, [1412.7420].

[185] S. Frixione, *Isolated photons in perturbative QCD*, *Phys. Lett. B* **429** (1998) 369–374, [hep-ph/9801442].

[186] S. Frixione and W. Vogelsang, *Isolated photon production in polarized pp collisions*, *Nucl. Phys. B* **568** (2000) 60–92, [hep-ph/9908387].

[187] S. Catani et al., *QCD*, in *Workshop on Standard Model Physics (and more) at the LHC (First Plenary Meeting)*, 5, 2000. hep-ph/0005025. DOI.

[188] M. A. Ebert and F. J. Tackmann, *Impact of isolation and fiducial cuts on q_T and N-jettiness subtractions*, *JHEP* **03** (2020) 158, [1911.08486].

[189] S. Camarda, L. Cieri and G. Ferrera, *Fiducial perturbative power corrections within the $\mathbf{q}_T$ subtraction formalism*, *Eur. Phys. J. C* **82** (2022) 575, [2111.14509].

[190] L. Buonocore, S. Kallweit, L. Rottoli and M. Wiesemann, *Linear power corrections for two-body kinematics in the qT subtraction formalism*, *Phys. Lett. B* **829** (2022) 137118, [2111.13661].

[191] S. C. *et al.* (CMS), *Observation of a new boson at a mass of 125 GeV with the CMS experiment at the LHC*, *Physics Letters B* **716** (2012) 30–61.

[192] R. V. Harlander and T. Neumann, *Probing the nature of the Higgs-gluon coupling*, *Phys. Rev. D* **88** (Oct, 2013) 074015.

[193] M. Grazzini, A. Ilnicka, M. Spira and M. Wiesemann, *Modeling BSM effects on the Higgs transverse-momentum spectrum in an EFT approach*, *Journal of High Energy Physics* **2017** (Mar., 2017) .

[194] A. Azatov, C. Grojean, A. Paul and E. Salvioni, *Resolving gluon fusion loops at current and future hadron colliders*, *Journal of High Energy Physics* **2016** (Sept., 2016) .

[195] U. Langenegger, M. Spira and I. Strebel, *Testing the Higgs Boson Coupling to Gluons*, 2015.

[196] S. Dawson, I. M. Lewis and M. Zeng, *Usefulness of effective field theory for boosted Higgs production*, *Phys. Rev. D* **91** (Apr, 2015) 074012.

[197] D. Ghosh and M. Wiebusch, *Dimension-six triple gluon operator in* Higgs + jet *observables*, *Phys. Rev. D* **91** (Feb, 2015) 031701.

[198] M. Buschmann, D. Gonçalves, S. Kuttimalai, M. Schönherr, F. Krauss and T. Plehn, *Mass effects in the Higgs-gluon coupling: boosted vs. off-shell production*, *Journal of High Energy Physics* **2015** (Feb., 2015) .

[199] S. Dawson, I. M. Lewis and M. Zeng, *Effective field theory for Higgs boson plus jet production*, *Phys. Rev. D* **90** (Nov, 2014) 093007.

[200] M. Buschmann, C. Englert, D. Gonçalves, T. Plehn and M. Spannowsky, *Resolving the Higgs-gluon coupling with jets*, *Phys. Rev. D* **90** (Jul, 2014) 013010.

[201] M. Schlaffer, M. Spannowsky, M. Takeuchi, A. Weiler and C. Wymant, *Boosted Higgs shapes*, *The European Physical Journal C* **74** (Oct., 2014) .

[202] C. Grojean, E. Salvioni, M. Schlaffer and A. Weiler, *Very boosted Higgs in gluon fusion*, *Journal of High Energy Physics* **2014** (May, 2014) .

[203] A. Azatov and A. Paul, *Probing Higgs couplings with high p_T Higgs production*, *Journal of High Energy Physics* **2014** (Jan., 2014) .

[204] A. Banfi, A. Martin and V. Sanz, *Probing top-partners in Higgs+jets*, *Journal of High Energy Physics* **2014** (Aug., 2014) .

[205] H. M. Georgi, S. L. Glashow, M. E. Machacek and D. V. Nanopoulos, *Higgs Bosons from Two-Gluon Annihilation in Proton-Proton Collisions*, *Phys. Rev. Lett.* **40** (Mar, 1978) 692–694.

[206] D. Graudenz, M. Spira and P. M. Zerwas, *QCD corrections to Higgs-boson production at proton-proton colliders*, *Phys. Rev. Lett.* **70** (Mar, 1993) 1372–1375.

[207] M. Spira, A. Djouadi, D. Graudenz and R. Zerwas, *Higgs boson production at the LHC*, *Nuclear Physics B* **453** (1995) 17–82.

[208] R. V. Harlander and W. B. Kilgore, *Next-to-Next-to-Leading Order Higgs Production at Hadron Colliders*, *Phys. Rev. Lett.* **88** (May, 2002) 201801.

[209] C. Anastasiou and K. Melnikov, *Higgs boson production at hadron colliders in NNLO QCD*, *Nuclear Physics B* **646** (2002) 220–256.

[210] V. Ravindran, J. Smith and W. van Neerven, *NNLO corrections to the total cross section for Higgs boson production in hadron–hadron collisions*, *Nuclear Physics B* **665** (2003) 325–366.

[211] C. Anastasiou, C. Duhr, F. Dulat, F. Herzog and B. Mistlberger, *Higgs Boson Gluon-Fusion Production in QCD at Three Loops*, *Phys. Rev. Lett.* **114** (May, 2015) 212001.

[212] B. Mistlberger, *Higgs boson production at hadron colliders at N^3LO in QCD*, *Journal of High Energy Physics* **2018** (May, 2018) .

[213] U. Aglietti, R. Bonciani, G. Degrassi and A. Vicini, *Two-loop light fermion contribution to Higgs production and decays*, *Physics Letters B* **595** (2004) 432–441.

[214] U. Aglietti, R. Bonciani, G. Degrassi and A. Vicini, *Master integrals for the two-loop light fermion contributions to $gg \to H$ and $H \to \gamma\gamma$*, *Physics Letters B* **600** (2004) 57–64.

[215] G. Degrassi and F. Maltoni, *Two-loop electroweak corrections to Higgs production at hadron colliders*, *Physics Letters B* **600** (2004) 255–260.

[216] M. Bonetti, K. Melnikov and L. Tancredi, *Two-loop electroweak corrections to Higgs–gluon couplings to higher orders in the dimensional regularization parameter*, *Nuclear Physics B* **916** (2017) 709–726.

[217] C. Anastasiou, C. Duhr, F. Dulat, E. Furlan, T. Gehrmann, F. Herzog et al., *High precision determination of the gluon fusion Higgs boson cross-section at the LHC*, 2016.

[218] S. Actis, G. Passarino, C. Sturm and S. Uccirati, *Nlo electroweak corrections to higgs boson production at hadron colliders*, *Physics Letters B* **670** (Dec., 2008) 12–17.

[219] V. Del Duca, W. Kilgore, C. Oleari, C. Schmidt and D. Zeppenfeld, *Production of a higgs boson accompanied by two jets via gluon fusion*, *Phys. Rev. Lett.* **87** (Aug, 2001) 122001.

[220] L. Budge, J. M. Campbell, G. De Laurentis, R. K. Ellis and S. Seth, *The one-loop amplitudes for higgs + 4 partons with full mass effects*, *Journal of High Energy Physics* **2020** (May, 2020) .

[221] R. V. Harlander, M. Prausa and J. Usovitsch, *The light-fermion contribution to the exact higgs-gluon form factor in qcd*, *Journal of High Energy Physics* **2019** (Oct., 2019) .

[222] M. Czakon and M. Niggetiedt, *Exact quark-mass dependence of the higgs-gluon form factor at three loops in qcd*, *Journal of High Energy Physics* **2020** (May, 2020) .

[223] M. Niggetiedt and J. Usovitsch, *The higgs-gluon form factor at three loops in qcd with three mass scales*, *Journal of High Energy Physics* **2024** (Feb., 2024) .

[224] S. Jones, M. Kerner and G. Luisoni, *Next-to-leading-order qcd corrections to higgs boson plus jet production with full top-quark mass dependence*, *Physical Review Letters* **120** (Apr., 2018) .

[225] M. Czakon, R. Harlander, J. Klappert and M. Niggetiedt, *Exact top-quark mass dependence in hadronic higgs production*, *Physical Review Letters* **127** (Oct., 2021) .

[226] R. Bonciani, V. Del Duca, H. Frellesvig, M. Hidding, V. Hirschi, F. Moriello et al., *Next-to-leading-order qcd corrections to higgs production in association with a jet*, *Physics Letters B* **843** (Aug., 2023) 137995.

[227] M. Czakon, F. Eschment, M. Niggetiedt, R. Poncelet and T. Schellenberger, *Top-bottom interference contribution to fully inclusive higgs production*, *Physical Review Letters* **132** (May, 2024) .

[228] V. Hirschi, S. Lionetti and A. Schweitzer, *One-loop weak corrections to Higgs production*, *Journal of High Energy Physics* **2019** (May, 2019) .

[229] M. Bonetti, K. Melnikov and L. Tancredi, *Three-loop mixed QCD-electroweak corrections to Higgs boson gluon fusion*, *Physical Review D* **97** (Feb., 2018) .

[230] M. Bonetti, K. Melnikov and L. Tancredi, *Higher order corrections to mixed QCD-EW contributions to Higgs boson production in gluon fusion*, *Physical Review D* **97** (Mar., 2018) .

[231] C. Anastasiou, V. Del Duca, E. Furlan, B. Mistlberger, F. Moriello, A. Schweitzer et al., *Mixed QCD-electroweak corrections to Higgs production via gluon fusion in the small mass approximation*, *Journal of High Energy Physics* **2019** (Mar., 2019) .

[232] M. Bonetti, E. Panzer, V. A. Smirnov and L. Tancredi, *Two-loop mixed qcd-ew corrections to $gg \to hg$*, *Journal of High Energy Physics* **2020** (Nov., 2020) .

[233] M. Becchetti, R. Bonciani, V. Del Duca, V. Hirschi, F. Moriello and A. Schweitzer, *Next-to-leading order corrections to light-quark mixed qcd-ew contributions to higgs boson production*, *Physical Review D* **103** (Mar., 2021) .

[234] M. Bonetti, E. Panzer and L. Tancredi, *Two-loop mixed QCD-EW corrections to $q\bar{q} \to Hg$, $qg \to Hq$, and $\bar{q}g \to H\bar{q}$*, *Journal of High Energy Physics* **2022** (June, 2022) .

[235] G. 't Hooft and M. Veltman, *Regularization and renormalization of gauge fields*, *Nuclear Physics B* **44** (1972) 189–213.

[236] D. Kreimer, *The $\gamma(5)$ Problem and Anomalies: A Clifford Algebra Approach*, *Phys. Lett. B* **237** (1990) 59–62.

[237] J. G. Korner, D. Kreimer and K. Schilcher, *A Practicable gamma(5) scheme in dimensional regularization*, *Z. Phys. C* **54** (1992) 503–512.

[238] P. Nogueira, *Automatic feynman graph generation*, *Journal of Computational Physics* **105** (1993) 279–289.

[239] S. Catani, *The singular behaviour of qcd amplitudes at two-loop order*, *Physics Letters B* **427** (1998) 161–171.

[240] M. Becchetti, R. Bonciani, V. Casconi, V. Del Duca and F. Moriello, *Planar master integrals for the two-loop light-fermion electroweak corrections to higgs plus jet production*, *Journal of High Energy Physics* **2018** (Dec., 2018) .